Title
Electrostatic Sensing for Underwater Object Detection and Localization

Author
Herman, Henry Edward

Publication Date
2013

Peer reviewed|Thesis/dissertation

University of California
Los Angeles

Electrostatic Sensing for Underwater Object Detection and Localization

A thesis submitted in partial satisfaction
of the requirements for the degree
Master of Science in Electrical Engineering

by

Henry Edward Herman III

2013

Abstract of the Thesis

Electrostatic Sensing for Underwater Object Detection and Localization

by

Henry Edward Herman III

Master of Science in Electrical Engineering

University of California, Los Angeles, 2013

Professor Mani Srivastava, Chair

Essential to all autonomous creatures is the ability to sense the surrounding environment. Evolution has developed complicated sensory structures to help organisms gain knowledge about the physical state of the world. Creatures lacking in advanced sensory systems are more likely at to fall victim to the harsh reality of nature. One of the hallmarks of the advanced lifeforms are highly evolved sensory systems. Sensory receptors are diverse and vary within species and environments. Of the possible sensing modalities, one is of primary use to creatures living in aqueous environments: electrorecption. Their are two classes of creatures that sense electric fields, those that sense passive electric fields and those that actively emit and then detect their own electric field. Some examples of animals with passive electric field sensing abilities include species like skates, sharks, and rays as well as mammals such dolphins and platypuses. Passive electric field sensors are sensitive enough to detect the tiny voltage potentials disturbance from muscle contractions and heart beats. These signal can betray the presence of prey and predators. Creatures with this remarkable sense consequently have an advantage in environments where optical and chemical sensors may fail.

The term active sensory system refers to the need for a creature to emit some form of signal into the environment using its own energy store. One familiar example is the echolocation ability of bats, where the bat emits a ultrasonic pressure wave that reflects off of nearby objects and can be used for hunting small prey. In contrast to passive electrosense which requires the target to generate an electric field, species that use active electrosense generate their own electric fields, normally some order of magnitude larger. Active electrosense has the distinct advantage that the target object need only have a different physical composition from the surrounding fluid. Contrast is generated from the spatial differences in impedance when a target object enters the field. Consequently active electrosense can be used to identify non-living matter. Active electrosense is an example of convergent evolution. Two separate groups of freshwater fish, the Gymnotiformes(South America) and the Mormyridae(Africa) have been shown to actively generate electric fields. We will look to these species for design inspiration.

In this work we will engineer a system to mimic the ability of weakly electric fish to detect, identify and locate objects in the nearby vicinity. In general electrosense has a shorter range than acoustical sensing such as sonar, but applications can be found for navigating in confined spaces and obstacle detection and avoidance. Specifically, we propose and fabricate the design for a complete electrosense system capable of being mounted on an underwater remotely operated vehicle. We then propose ways of processing the sensory data, with the intention of identifying and locating nearby anomalies.

The thesis of Henry Edward Herman III is approved.

Michael Van Dam

William Kaiser

Mani Srivastava, Committee Chair

University of California, Los Angeles

2013

Table of Contents

List of Figures

List of Tables

CHAPTER 1

Introduction

Humans have multiple passive senses. At the earliest age children are taught about the five sense, seeing, hearing, smelling, tasting and touching. In fact, we humans have additional senses rarely mentioned, senses that while less obvious, are often no less important. A more complete list might be as follows:

- Vision (Sight)
- Auditory (Hearing)
- Olfaction and Gustation (Smell and Taste)
- Mechanoreception (Touch and Pressure Sensing)
- Equilibrium and Balance
- Acceleration
- Thermoreception (Temperature)
- Chronoreception (Time)

Our senses evolved to meet our needs and in the environments we most commonly inhabit they do quite a satisfactory job of informing us about our world. However, there is no doubt our human senses have distinct limitations. Our eyes our only capable of perceiving light in a fairly small range of wavelengths. Our

ears amplify mechanical waves, but again they are only capable of detecting a narrow range of frequency. Similarly, the chemicals our noses are sensitive too are fewer than other species.

In the comparatively short time we call modern history humans have also extended our own sensory systems through technological advancement. Before we developed physics and engineering to construct completely artificial sensor system, we first looked to nature. It was clear that other species could *sense* environmental signals we could not. A wolf was clearly more sensitive to smells and sounds, and to harness this ability humans devised methods of training and *domesticating* this species. In this way, while we ourselves could not sense and track a prey source simply from the chemical remnants it left behind, we could rely upon other species for their heightened capabilities.

It was not till somewhat later that it became evident that some species had special sensory abilities we as a species had no analog for, and in many ways this was acceptable until we began to venture in environments that our own senses were not as well adapted.

A few notable examples of unique sensing modalities we as a species are incapable of sensing include:

- Echolocation
- Magnetorecepetion
- Electroreception

Even more interesting, their are some *sensing* abilities we developed technologically on our own, without realizing that nature had, through millions of years of evolution, *discovered* first. The humble compass might be the clearest

example of just such a discovered sensor. The first navigation compass was likely invented by the Chinese as early as the 9th century, and it came into great use as man began exploring distant shores by ocean travel[Nee86]. It was not until 1975 when when it was recognized that some species of bacteria could orient themselves using iron particles, clearly bacteria *figured it out first* [Bla75]. Since then multiple species have been identified as being sensitive to magnetic fields, including homing pigeons and small rodents[MB81] [Wal96].

Echolocation is used by countless species for navigation. Dolphins and bats are well known for their prowess at locating food sources and avoiding obstacles. This "active" sensory system clearly gives a significant advantage. Active and passive sonar give a very similar capability to ocean bound vessels.

Clearly we can learn from these unique species. Which leads directly to the topic of this thesis, to explore electrosense and electrolocation as a modality for underwater navigation; specifically looking to species of fish that use similar detections schemes for "bio-inspiration". Many aquatic species such as fish make their home in aqueous environments where electrical fields strength and range can be stronger by orders of magnitude. Additionally, for species living in murky rivers, lakes and oceans where photons can be scattered by highly dispersive medium, and light receptors have less use, active sonar can give away position, and chemical sensing has much slower response times, electric field sensing abilities can be essential to identifying and locating food sources, avoiding predators, and communicating with mates and competitors. Lissman and Machin were able to demonstrate first that Gymnarchus niloticus used its own electrostatic sensor for prey localization[LM58].

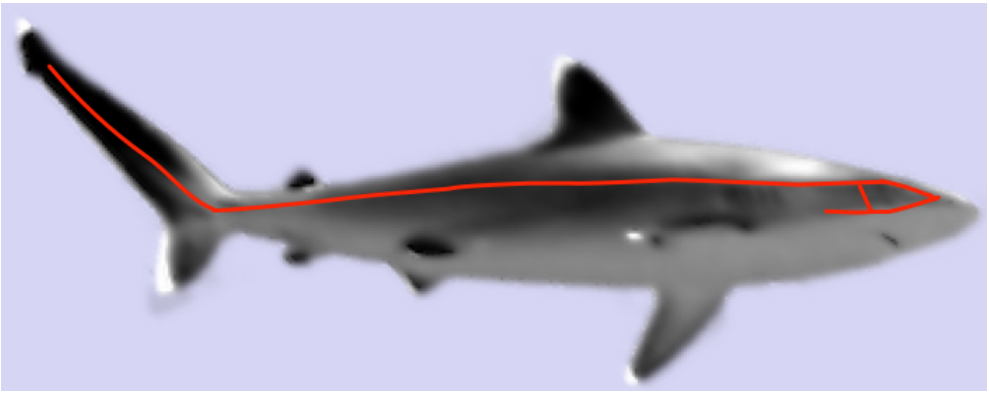

Figure 1.1: Sketch of a shark showing the location of the lateral line organs; the sensory system used by aquatic vertebrate species to detect motion and movement. The organ is composed of tiny hair cells that convert fluidic motion into electrical signals that are then processed by the animals neurological system. This organ is used by many species of fish for schooling behavior and prey tracking.

1.1 Electrosense in Nature

The lateral line organs developed in aquatic vertebrate fish to detect nearby motion and pressure. It is composed of tiny hair cells similar to those found in our own ears for acoustical sound transduction[Pa76]. Movement of these tiny hair cells generates electric pulses that then get transmitted to the nervous system for processing[Pa12]. The adjacent pressure variations can arise from fluctuation in ocean currents, relative animal motion or nearby movement of other animals. This sense plays a primary capability in the schooling capability fish. Figure 1.1 shows the location of the lateral line sense organs along the side of a white tip reef shark.

In some species the hair cells along the lateral line further evolved to sense spatial electrical potential. It is fascinating to note that these electroreceptors still closely morphologically resemble their precursor mechanotransductor hair

cells. The evolution of electroreceptors has evolved multiple times independently in geographical distant locations. This is referred to as convergent evolution; where two separate species with different ancestors develop analogous structures to fill similar ecological niches.

1.2 Passive vs Active Electrosense

1.2.1 Elasmobranchii

The subclass Elasmobranchii contains many familiar species, including sharks and skates. Except for a few notable exception of the order, Torpediniformes (e.g., Torpedo ray or electric ray), the rest of the Elasmobranchii subclass uses passive electric receptors. In fact several species of sharks are known to be able to detect field changes changes as small as 5 nV/m. These sensors are purely passive, consequently these species of fish rely upon outside electrical stimulus. The primary source of these electrical stimuli being the contraction of muscles and the firing of neuron action potentials from other near by animals. Many elasmobranchs are able to measure nano-volt adjacent voltage potentials. They do this by using an organelle discovered by Stefano Lorenzini in 1678. Figure 1.2 shows the configuration of this organ, known as ampullae lorenzini. The skin resistance of elasmobranchs often matches closely with the resistance of the water. The ampullae itself contains tiny pores and tubes or canals lined with cells of very high resistance, the canal is filled with a jelly like substance of very low resistance. This low resistance canal allows the voltage at the surface of the ampullae to match closely with the voltage at the base where there exists a sensory epithelium with cells sensitive to voltage differentials. Many ampullae may be grouped together as depicted in Figure 1.2 allowing for a differential

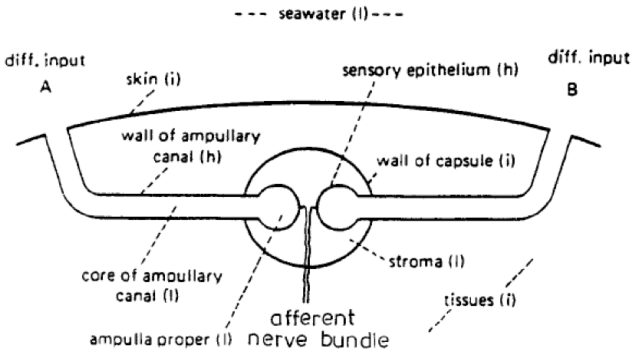

Figure 1.2: Ampullae of Lorenzini is a tiny organelle consisting of a pore and canal lined with cells of high resistance. The contents of the canal are filled with a gel of low resistance. The base of the canal is lined with electroreceptors, tiny hair like cells, that generate an action potential when a voltage potential greater than the cells threshold is placed across it. They are often found in bundles allowing for a measurement of differential voltages. Sensitivity can be in the nano volts (Source: [Kra96]).

mode of measurement. The resulting signal consequently has a large common mode rejection allowing the animal to sense small external voltage gradients even in the presence of its own self generated potentials [Kra96].

The body of marine fish is lined with a skin that is equal or lower resistance than the surround ocean. Marine fish must do this to maintain equal osmotic pressure. If the fish had skin that impeded the flow of ions it would result in the net flow of water out of the fish to relieve the osmotic pressure. The result is a body that is conductive. Of course voltage potentials measured across small distances of a conductive medium will often be small since they have little resistance. Marine fish thus developed long canals lined with high impedance cells, 6 $M\Omega \cdot \text{cm}^2$, and filled with very low impedance gel, 25 - 31 $\Omega \cdot \text{cm}^2$ [Kal58]. The sensory cells are located at the base of the canals. These long canals increase

the distance between the point of measurement and the reference point inside the fish, resulting in larger variations in potentials. The bottom graphic in figure 1.3 shows the common configuration in marine fish in comparison with the configuration in freshwater fish, on top [Kra96].

1.2.2 Teleostei

The weakly electric fish belong to the family Teleostei. Most bony fish belong to this family. Electroreceptors and electric discharge organs evolved separately in two distinct teleostei subfamilies: the *Gymnotiformes* and the *Mormyridae*.

Gymnotiformes are native to south america. This subfamily includes the notorious electric eel; a fish that is capable of using electric discharge for stunning prey. Aside from the electric eel, the rest of the Gymnotiformes use their electric discharge organs (EO) and electroreceptors purely for sensing and communication. Gymnotiformes are generally long slender fish with rigid bodies. They keep the sensory system fixed and swim using the their anal fins [Fer96]. It is postulated that the rigid body of Gymnotiformes plays an important role in the fishes ability to electrolocate; as it prevents changes in body geometry from affecting the received sensory inputs from the environment. The *black knife ghost fish* is one of the most commonly studied species of Gymnotiforme.

Mormyridae developed their elecrosense capabilities completely separate from the Gymnotiformes, through a process known commonly as convergent evolution. Mormyridae are native to Africa, making their home in fresh water such as streams and lakes. Mormyridae can be recognized by the elongated proboscis [Fer96]. The peter's elephant nose fish or Gnathonemus petersii, is a common aquarium fish and member of the Gymnotiformes; its image is shown in figure 1.5

What is interesting about these two is species is their similar morphology,

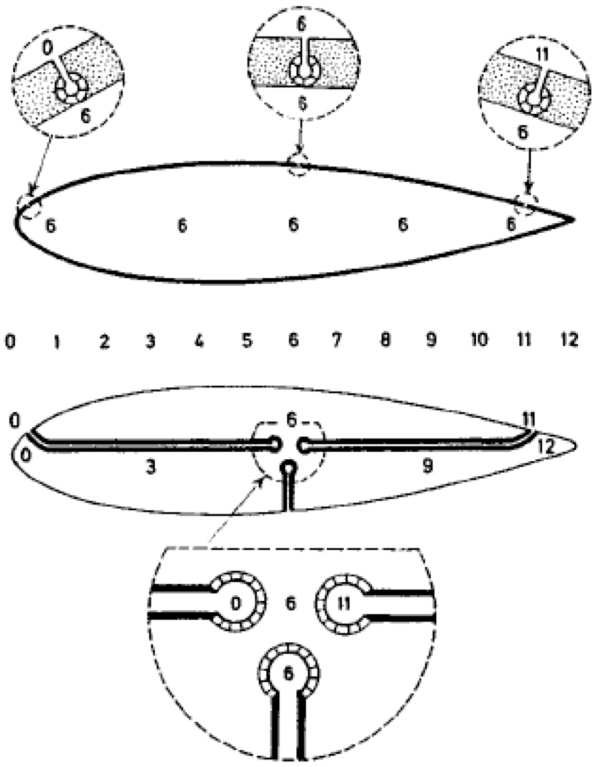

Figure 1.3: Ampullae of Lorenzini of marine fish differ from freshwater fish electroreceptors. Fresh water fish *top*; have electroreceptors with short canals. Marine fish *bottom* have longer canals. The canals are lined with cells of high resistance. Marine fishes bodies often have impedance closely matching or even lower than the surround aqueous medium. The ampullae then can maximize the voltage measured by using long canals, since the voltage magnitudes will vary across longer distances. In freshwater fish the body remains at an iso-potential (Source: [Kra96]).

including the similarities in the electrosensory systems. Fresh water teleosts, as they are called, differ from saltwater fish in that they have a high resistance skin.

Figure 1.4: Gnathonemus petersii is a common freshwater aquarium fish and member of Mormyridae family. Its electrical discharged can be heard by placing a differential amplifier in the tank in which it resides (Source: [Fie]).

In Gymnotiformes it is often on the order of $50\text{k}\Omega \cdot \text{cm}^2$ [Ben71]. This skin is important since it prevents the fish from losing the necessary ions through osmotic flow out of the body. As a direct result of reduced skin conductance the inside of fresh water skin is maintained at an iso-potential. The sensed voltages are thus measure directly across shallow pores in the skin. *Tuberous Electroreceptors* as they are known in weakly electric fish have specially evolved to sense the voltages generated from the fishes own *electric organ*. Like the Ampullae of Lorenzini, special voltage sensitive cell form a boundary between the bottom surface of the pore and the internal body of the fish. The canals that lead into the pores may be short but they are also lined with high impedance cells. This prevents current from returning from anywhere but through the sensory cells. The upper graphic in figure 1.3 shows the common configuration of tuberous electroreceptor. Note the iso-potential maintained in the body of the fish. Voltages are generated by current returning across the electroreceptors, these voltages then generate the action potentials that are propagated through the fishes nervous system for further processing in the fishes brain [Kra96].

Weakly electric fish will generate a voltage using their electric organ, as a result the electric field resembles a dipole as in figure 1.5. Equal potential lines

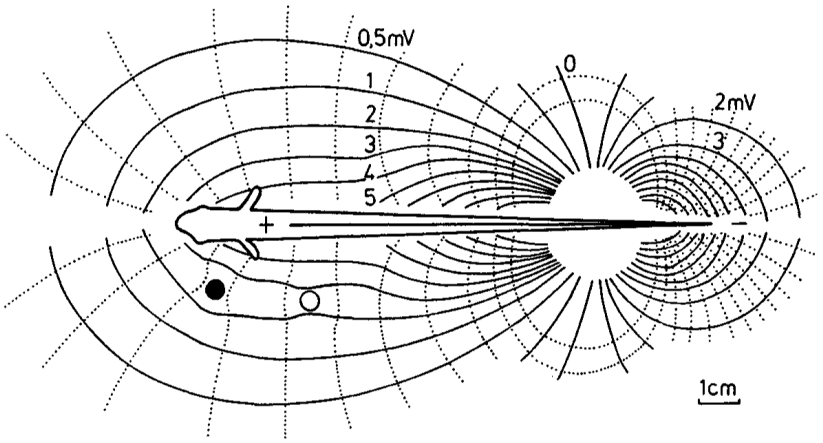

Figure 1.5: Weakly electric fish use their *electric organ* to generate an electric field by polarizing the special cells. Since the aqueous medium in which they inhabit is conductive, current flows and returns through electroreceptors along the skin of the fish. In this figure the voltage at the electric organ is set to zero. The dark, solid lines are the equal potential lines (iso-potential) showing the magnitude of the electric field along each contour. The electric field lines are shown as dotted lines. The field resembles a classic dipole. The current across the skin is proportional to the voltage at each point. The dark sphere represents a conductor acting to *short* the electric field in the vicinity, while the light sphere is a insulator and cause the electric field to spread out (Source: [Kra96]).

are shown in the figure allowing the visualization of the voltage gradients across the surface of the fishes skin. Note that the internal body of the fish is kept at iso-potential, meaning the current that returns across the electroreceptors is proportional to the voltage measured at the surface. Objects that enter the field, such as the black and white spheres create changes in the electric field, changing the voltages present at the skin of the fish, resulting in changes in the relative current returning through each receptor.

1.3 Electrical Resistive Tomography

Electrical Resistive Tomography also known is *Electrical Resistive Imaging* is a common technique used in geology and prospecting to locate underground spatial anomalies that could identify regions and layers of particular interest or value. Electrical resistive tomography work on the same principle as electrolocation in weakly electric fish, consequently it could be said nature *discovered* it first. The technique has been documented being used since the 1930's when it was used to identify layers to target for prospecting. It was first proposed by Conrad Schlumberger in 1912. Since then it has become significantly more advanced thanks to advances in solving the *inverse problem* [Tik63]. It can now be used in generating 2D, 3D tomographic images of conductivity. Contrast is generated by regions with different resistance. Minerals and ores often have vary different electrical properties and can be identified. Electrical resistive tomography can be used in the tracking of ground water and thus is used to search for suitable locations for wells [Da92].

In electric resistive tomography a known electrical current is applied through electrodes into the ground. Since the ground is non-homogenous, the spatial electrical properties cause varying voltage potentials to be generated. A typical electrode configuration is shown in figure 1.6, here electrodes C1 and C2 source and sink current in to the medium. Electrodes P1 and P2 are measurement electrodes that record the voltage potential. Often multiple reading are required to determine the complete boundary conditions and solve the inverse problem, therefore either the positions of the electrodes are varied or additional electrodes are spaced out on the surface. With enough measurement the complete spatial electrical properties of the geological region may be determined. In long-electrode electrical resistive tomography long bore holes are drilled into the earth, and elec-

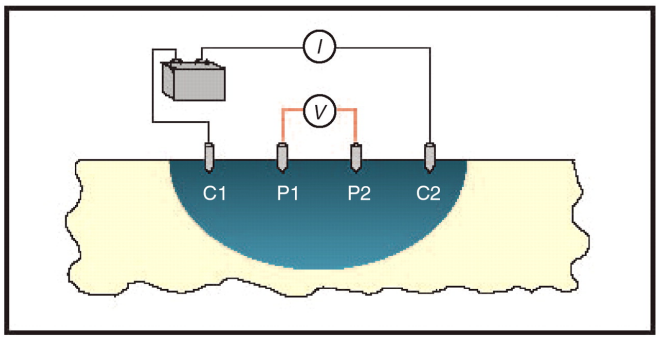

Figure 1.6: Depiction of an electrical resistive tomography experiment. A current I is passed through electrodes C1 and C2. The current results a the generation of spatial varying electrical field. Voltage potential measurements are taken between electrodes P1 and P2. The magnitude of this measured electric potential relates directly to the spatial varying conductivity of the earth. Multiple measurements may be taken and the a multidimensional conductivity map may be generated by solving the *inverse problem* (Source: [SS09]).

trodes are placed within the holes, current is injected using one pair of electrodes while all the other electrodes record voltage potentials; then a different pair of electrodes is used to inject current, additional measurements are taken and the process repeats till all combinations of interest have been measured. Figure 1.7 shows a typical configuration for a long-electrode electrical resistive tomography setup. The long electrodes provide better depth information. Again current is injected from some sub-set of electrodes, while voltage measurements are recorded from the remaining electrodes.

1.4 Electrical Impedance Tomography

The field of *electrical impedance tomography* can be attributed to the J.G. Webster and R.P. Hendersen, who in 1978 published a paper on using a novel *impedance*

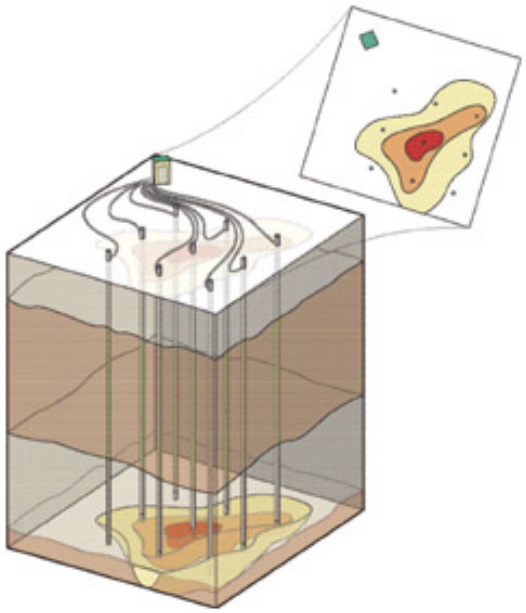

Figure 1.7: Often multiple electrodes are used in electrical resistive tomography. Schematic of a long-electrode electrical resistive tomography experiment is shown. Using a known current allows the calculation of the resistive properties of the earth from the multiple measured electric potentials (Source: [Fri]).

camera to develop images or spatial maps of a patients torso admittance. It was implied that they could measure lung ventilation and respiration levels in patient. One of the key advantages of electrical impedance is the lack of ionizing radiation, and the ability to provided near realtime lung perfusion measurements [BB84]. Figure 1.8 shows the experimental and instrument setup. A known voltage source was applied to one side of the patient, an array of 144 current sensing electrodes were placed on the opposite side of the patient. The current measurement were multiplexed and digitally sampled. These samples could be multiplexed and processed in a computer. The resulting processed signal was then output to a screen as a raster scan of the patients spatial impedance properties. It it important to take note of the distortion caused by large objects of different impedance in the

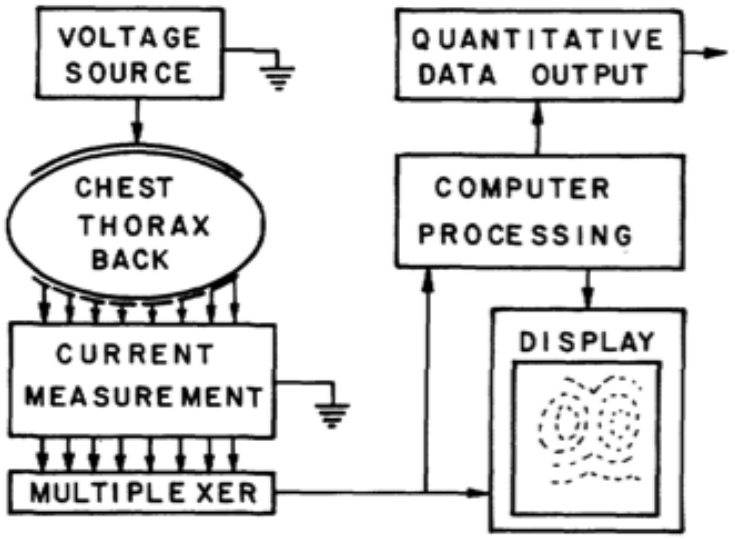

Figure 1.8: The first documented use of impedance imaging for medical applications was conducted by Ross P. Hendersen and John G Webster. Their *impedance camera* was capable of generating 100 spatial measurements at 32 frames per second. In their configuration they applied a known voltage and measured the resulting currents at the remaing electrodes. Current measurements were multiplexed to an data acquisition unit and further processed on a computer and output to a display (Source: [BB84]).

torso. As a result, the current no longer takes a direct root resulting in significant non-linearities in the solution. In the work [BB84], these non-linearites were ignored, consequently image quality was effected. Figure 1.9 shows the effects of a large object on electric field lines.

While the work by Webster et al. showed in principle impedance imaging could be used clinically it was D.C. Barber and B. H. Brown who considered the non-linearities involved in electrical impedance tomography and posed it as a reconstruction problem [HW78]. In their work they proposed a system for measuring the the boundary voltages that result when a known current distribution

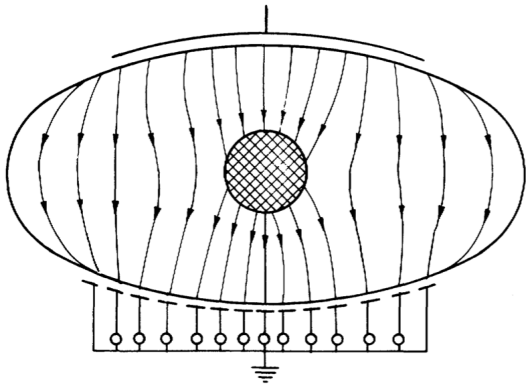

Figure 1.9: Regions of varying conductance cause distortion in electrical field lines. Here the effects on the electric field are shown when a cylinder object with a impedance different from the surround tissue is placed in the homogenous torso (Source: [BB84]).

in applied. They suggested solutions for solving the forward and inverse problem, that is, using the boundary measurements to make approximations of the volumes conductive properties.

Additionally, factors such as the impedance of the electrodes must be considered, as it was shown to cause significant errors in measurement in electrical impedance tomography. Frequency is also a consideration in tissue imaging. While in theory one could use DC voltages or DC currents, they both can lead to ionization of tissue. To avoid this all systems use low frequency AC waveforms, normally sine waves. Frequencies from 1kHz to 100kHz are considered optimal since tissue has little capacitance in these lower frequencies, being considered *mostly resistive*. Also, capacitance is less likely to be introduced via cabling at these lower frequencies.

The system first proposed by [HW78] can be considered a two electrode system. In such a system the contact impedance of the electrode with the surface of the skin must not be neglected without introducing significant errors. Later four

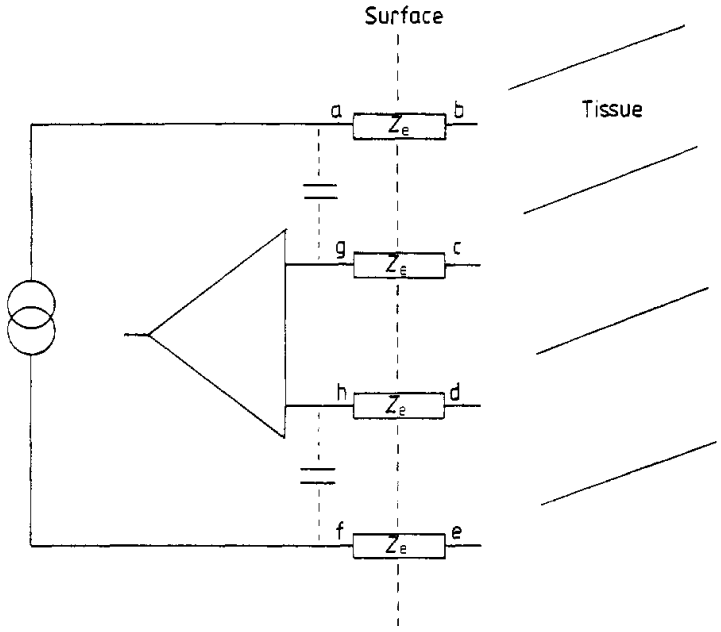

Figure 1.10: Typical configuration for a 4 electrode electrical impedance tomography system. A known current is applied across electrodes a and f. The electrode contact impedance is modeled as Z_e and is present across nodes a and b, g and c, h and d and across f and e (Source: [HW78]).

electrodes systems were introduced. These four electrode configuration is nearly identical with the configuration of the standard electrical resistive tomography system used for geological prospecting and research as in figure 1.6 . Figure 1.10 shows the proposed 4 electrode configuration as applied to tissue. Note the contact impedance modeled as Z_e and the stray cable capacitance that exists in between the lead wires.

CHAPTER 2

Physics of Electrostatics and Impedance Sensing

While the problem of solving for the spatial impedance of medium using only the boundary measurements is non-linear it is possible to solve for the electric field resulting from a current injection or the current density given a applied potential, if the geometry is fairly simple. In the case where the geometry is not simple it is still possible to determine a *good* answer using numerical methods such as *finite element analysis*. Finite element analysis is discussed in the next chapter.

To best develop an intuition for how the current and voltage interact in the aqueous medium of the tank we will start our discussion of the math in the absence of current flow, this is the case when the medium it self is non-conducting. This is, of course, an extreme over simplification. Later we relax this requirement, and explore the changes required to use current in electrostatics instead of charge. We will see that very few changes are needed at all.

2.1 Coulomb's Law

Coulomb was a french physicist in the late 18^{th} century. His *Coulomb's Law* is really an experiment observation. Later we will discuss how it falls directly out of one of Maxwell's equations. The law given by equation 2.1 is an inverse square law for the forces acting on two particles containing excess charge q and q'. The unit vector between the charged particles is given by r_1 while r is the

magnitude of the distance between them. ϵ is the *permeability* or *capacitivity* of the space [Smy89]. Note the medium here does not carry a current, since it is non-conductive. This is often called the electrostatic regime. While current may flow in electrostatic problems, it must be static, i.e. not fluctuate.

$$F = \frac{qq'}{4\pi\epsilon \mathrm{r}^2} r_1 \tag{2.1}$$

2.2 Electrical Intensity

We can step beyond the case of for two charged particles to a more general statement. Instead of a force as in section 2.1 we describe the electric intensity as the magnitude of a field generated by the existence of a charged particle. Equation-2.2 show the normalized version of equation 2.1, obtained by dividing the force by the magnitude of our test charge. The summation arises from the superposition principle, where the electric intensity can arise from multiple charged particles. This quantity, the electric intensity, which conceptually only makes sense for as single point can be extended and all points can be considered, in the case this leads directly to the concept of an the *electric field*.

$$E_p = -\frac{1}{4\pi\epsilon} \sum_{i=1}^{n} \frac{q_i}{r_i^2} r_i \tag{2.2}$$

2.3 Electric Field of a Dipole

The weakly electric fish to a first approximation generates a dipole, using its electric organ to selectively pump ions, or charged carriers. While the field itself varies with time, and current flows, we temporarily neglect these behaviors and

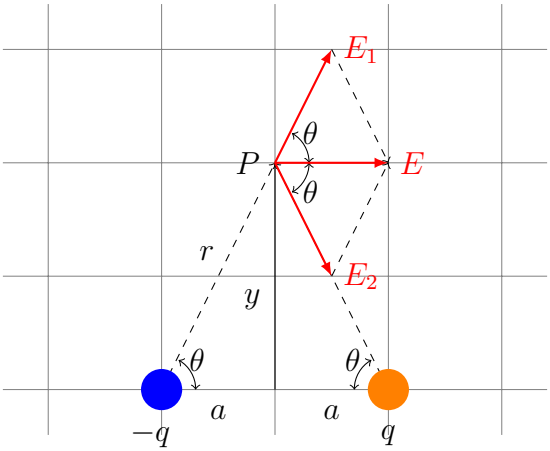

Figure 2.1: Calculating the electric field resulting from a dipole. Charges $+q$ and $-q$ are place at distance of $2a$ apart. The measurement point is placed a distance of r from each charge. θ is the resulting angle between the components of the electric field resulting from each charge. E_1 and E_2 are the components of the electric field as a result of charge $+q$ and $-q$ respectively[Smy89].

instead assume a non-conductive environment with a dielectric constant of ϵ and a constant charge. Just such a dipole is shown in figure 2.1, here the two charged $+q$ and $-q$ are separated by a distance of $2a$. The point of field measurement is placed at point P. The angle that results between the resulting field and the two separate component fields is θ. The radius between point P and the charges q and $-q$ is r. The electric field generated from each charge, E_1 and E_2 are generated from charges q and $-q$ respectively. Due to the superposition principle the resulting field intensity at point P is E and can be calculate using the electric intensity equation from above 2.2 [SB00].

$$E_1 = E_2 = \frac{1}{4\pi\epsilon}\frac{q}{r^2} = \frac{1}{4\pi\epsilon}\frac{q}{y^2 + a^2} \tag{2.3}$$

The geometry selected, with the point P perfectly center between q and $-q$ allows us to cancel both the y components of E_1 and E_2. The total field is then

the summation of the two components and is shown in equation 2.4.

$$E = E_{1x} + E_{2x} \tag{2.4}$$

We can solve for the x components of the each individual field using simple trigonometry, $E_{1x} = E_{1x} = E_1 \cos\theta$. Again trigonometry allows us to substitute $\cos\theta = \frac{a}{\sqrt{y^2+a^2}}$. Equation 2.5 shows the result of making this substitutions into equation 2.4.

$$E = 2\frac{1}{4\pi\epsilon}\frac{q}{y^2+a^2}\frac{a}{\sqrt{y^2+a^2}} \tag{2.5}$$

Further simplification of the equation 2.5 results in 2.6.

$$E = \frac{2}{4\pi\epsilon}\frac{qa}{(y^2+a^2)^{3/2}} \tag{2.6}$$

Finally if we let y get large, it dominates the denominator of equation 2.6. That is $y >> a$, results in equation 2.7. Unlike in the case when we have a single point charge where the electric field varies as a function of $\frac{1}{r^2}$, in the case of a dipole the electric field varies as a function of $\frac{1}{r^3}$. This explains the limited distance range that is seen in electrostatic sensing, as the amount of energy required to generate a strong field at a distance is very large. Intuitively this result is satisfying, as from a very large distance away two equal but opposite charges separated by a distance some order of magnitude smaller will *cancel* each other out. It is important to note the effect of the separation distance a has on the electric field strength. The separation distance, a, appears in both the denominator and numerator of equation 2.6. A larger separation distance can adversely effect the electric field strength. If we are in a situation where the distance $y >> a$, equation 2.7 applies and increasing a linearly increases field

strength.

$$E \approx 2\frac{1}{4\pi\epsilon}\frac{qa}{y^3} \tag{2.7}$$

2.4 Voltage and Potential

2.4.1 Potential From a Point Charge

A point charge produces an electric field that continues on to infinity. As discussed above the intensity of that electric field falls off as a function of $\frac{1}{r^2}$. The concept of a field is a convenience, allowing a calculation of the quantity of energy required to move an object in presence of the charge. Often we deal with the concept of a voltage potential, or the work a system is capable of performing. This is especially important as it applies to weakly electric fish and the field they generate by creating voltage using their electric organs. We will now look at the definition of the electrostatic potential to gain some insight into the relation between the electric field and the voltage potential.

Figure 2.2 shows a point charge at q. The electric field, a vector, resulting from the charge q is shown as E. It is important to note that the electric field is spatially varying, and therefore must be recalculated at each point we move in the space. Assuming we place a object or point charge at O, we can move said object from O to P following the curved path. The path itself can be broken into tiny sub-paths ds. The vector r_o is the starting position of our test charge. As we move it, each tiny ds we generate a new r vector and continue moving it till we reach the destination P at vector r_p. The work W or potential V can be calculated using the equation $dW = -E \cdot ds$, or the dot product of the path vector ds and the electric field vector E. Of course the dot product of two vector $a \cdot b$ can be written as $|a||b|\cos\theta$ where θ is the angle between the vectors and a and b.

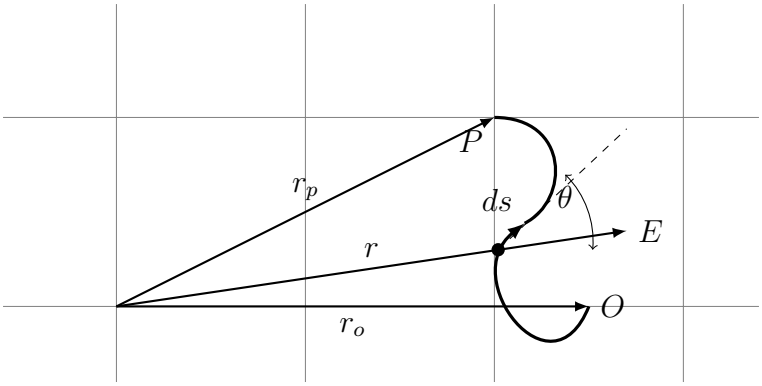

Figure 2.2: Calculating the work from moving a charge in an electric field and an introduction to voltage potentials. Here we have point charge q. Another charged point is placed at O and is moved to P. The path is composed of small movements ds. The electric field vector E is shown as well as the angle θ formed between the vectors ds and E [Smy89].

The result is $dV = |E||ds|\cos\theta$, substituting the results we found above for the electric intensity E, equation 2.2 we arrive at the result shown in equation 2.8. Using $dr = \mathrm{ds}\ \cos\theta$ and taking the path integral from moving the point from r_o to r_p we arrive at equation 2.9 which allows to calculate the electric potential required to move a test point from O to P in the presence of a point charge q. The concept of electric potential or *voltage* only makes sense in the context of moving between two points. This is clear from equation 2.9, where we *sum* the tiny dV along the path to determine the total voltage. This therefore requires integration. The path taken is arbitrary, and the voltage potential between two points is the same regardless of route.

$$dV = -\frac{\mathrm{q}\ \cos\theta}{4\pi\epsilon \mathrm{r}^2} ds \tag{2.8}$$

$$\int_0^{V_p} dV = -\frac{q}{4\pi\epsilon \mathrm{r}^2} \int_{r_o}^{r_p} \frac{dr}{r^2} \tag{2.9}$$

Integration of equation 2.9 results in equation 2.10 if we assume r_o is at infinity.

$$V_p = \frac{q}{4\pi\epsilon r_p} \tag{2.10}$$

2.4.2 Electrostatic Potential From Multiple Charges

Due to the principle of superposition it is possible to generate an equivalent expression for multiple charges simply by conducting a sum over all charges placed in the field. Unfortunately except for fairly simple geometries this so difficult to do in reality, but it does assist in building intuition.

$$V_p = \frac{1}{4\pi\epsilon} \sum_{i=1}^{n} \frac{q_i}{r_i} \tag{2.11}$$

2.5 Electric Field Lines, Equal Potential Lines and Visualizing an Electric Field

Unfortunately it is impossible to visualize an electric field in reality, this led to development of two techniques for visualizing the electric field in calculations. First to visualize the electric field a map is generated, where by all points of in the field with unit vectors pointing in then same direction are connected. Mathematically this means solving $ds = \lambda E$ given some fixed λ. A second technique is to connect all points on the image with the same potential. This can be done by letting $V = \mathrm{C}$, where C is a constant. These lines are of course referred to as the equal potential lines. Any point along an equal potential line will have the

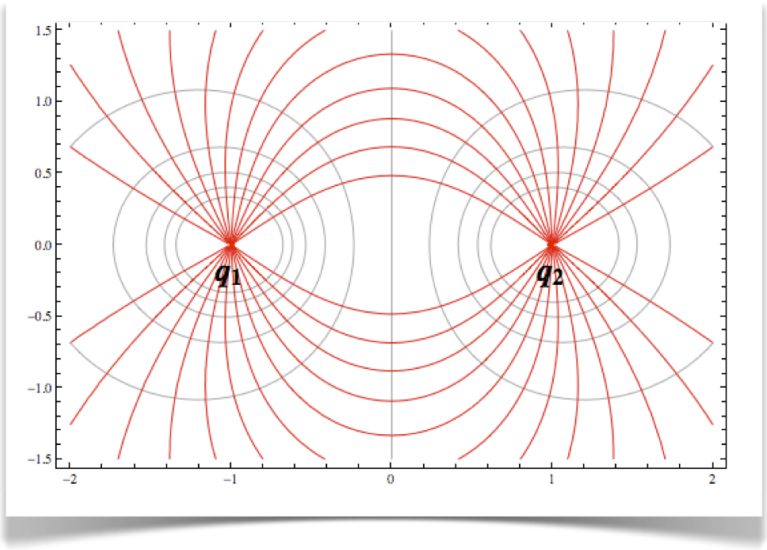

Figure 2.3: Electric dipole. Equal potential lines are shown in grey. Electric field lines are visible in red. q_1 and q_2 represent two charges of the same magnitude but different polarity.

same voltage as any other point on the line, relative to some reference voltage. Figure 2.3 shows a plot of the electric field lines and the equal potential ones for two equal but opposite point charges q_1 and q_2. The redlines are the electric field lines and the grey lines are the equal potential lines. It is interesting to note that the equal potential lines are always tangent to the electric field lines, which leads us to discuss their relation.

2.6 Revisiting the Electric Field and Voltage Relation in Multiple Dimensions

It is important to take into account additional dimensions, especially as we move to exploring simulations in 2 dimensions and finally tank experiments in 3 dimensions. Our equation for the work done by moving a charge in an electric

field was $dW = -E \cdot ds$, this was discussed in section 2.4.1 . Note that dW is a scalar, while E and ds are vector quantities. We can substitute voltage (V) for W realizing the potential and the work on synonymous terms. Rearranging we arrive at $\frac{dV}{ds} = -E$. This is the classic definition relationship between voltage and the electric field in one dimension. When we move to 3 dimensions, the result is similar and shown in equations 2.12 and 2.13 . These equations will be used later as we arrive at Poisson's equation.

$$E = -\nabla V \tag{2.12}$$

$$E = -\frac{\partial V}{\partial x} - \frac{\partial V}{\partial y} - \frac{\partial V}{\partial z} \tag{2.13}$$

2.7 Gauss's Flux Theroem

It would be impossible to continue discussing the physics and mathematics of electrostatics without introducing Gauss's Law, also known as Gauss's Flux Theorem. This theorem has two forms, an integral form and a derivative form. Both are important, yet the derivative form is used more often specifically as we move to simulation. In general simulation is required to solve any non-symmetric geometries.

2.7.1 Integral Form of Guass's Flux Theorem

Up to now, everything we have done has made the assumption of our charged elements being points. In some ways we continue to model everything as points, except advance our notion to include a notion of a distribution of charges. Interesting Guass's Law is in many ways equivalent to Coulomb's law and can be

derived directly from it [Smy89].

The general integral form of Gauss' Law is given in equation 2.14. If ϵ was constant, i.e. we were dealing with a homogenous medium, we could divide Q by ϵ to arrive at a term called the electric flux, $\phi = \frac{Q}{\epsilon}$. The relation then mean the electric flux, or the number of electric field lines leaving a closed surface, as defined by he surface integral is proportional to the total charge divide by the permeability constant.

$$\oiint_s \epsilon E \cdot dA = Q \tag{2.14}$$

2.7.2 Derivative Form of Guass's Flux Theorem

Gauss Law also has an equivalent derivative form. Instead of charge Q as in equation 2.14 we now introduce the charge density, ρ. In contrast to summing over the surface of an enclosed space using the surface integral we use divergence, which is a measurement of the outward flux from a single point. Again, the electric flux is proportional to the charge density at an infinitesimal point, shown in equation 2.15.

$$\nabla \cdot D = \nabla \cdot \epsilon E = \frac{dQ}{dv} = \rho \tag{2.15}$$

2.8 Derivation of Poisson's Equation

It is finally possible to introduce Poisson's equation, which can be considered one of the most important equation in applied mathematics. This equations is an integral part of electrostatics as it defines the relationship between the measured boundary voltages and the material properties of the medium under observation.

2.8.1 Poisson's Equation for a non-homogenous dielectric

From above we now have an equation relating the electric field to the charge density, equation 2.15, as well as an equation relating the electric field to the electric potential, equation 2.12. This last relation is essential, since we generally measure voltage (electric potentials), when we are exploring the physical electrical properties of a substance. We can substitute for the electric field as shown, by plugging equation 2.12 into equation 2.15, resulting in equation 2.17. One small modification was required, scaling the electric field E by ϵ the permeability constant as in equation 2.16. Poission's equation simplifies to Laplace's equation in the case where ρ is zero.

$$D = \epsilon E = -\epsilon \nabla V \tag{2.16}$$

$$\nabla \cdot (\epsilon \nabla V) = -\rho \tag{2.17}$$

2.8.2 Rectangular form of Poisson's Equation

In rectangular coordinates we can expand equation 2.17 above to include the partial derivative from all three dimensions, $x, y,$ and z. This expanded form is shown in equation 2.18.

$$-\frac{\partial}{\partial x}(\epsilon \frac{\partial V}{\partial x}) - \frac{\partial}{\partial y}(\epsilon \frac{\partial V}{\partial y}) - \frac{\partial}{\partial z}(\epsilon \frac{\partial V}{\partial z}) = \rho \tag{2.18}$$

2.9 Extending Our Results to the Case of Electric Current Flow

Up to this point we have been assuming no current flow, that is the medium in which we are placing our charges are themselves non-conducting. While this type

of approximation is fine when we are doing electrostatics in air, where very little current can flow, it does not apply if we are generating electric fields underwater.

2.9.1 Applying Direct Current

We start by assuming our excitation signal is a direct current signal. The assumption is not how electrolocation is done in practice, but if we limit ourselves to low frequencies can be used with confidence. In the cases of electrical impedance tomography, electrical resistive tomography, and even in the case of the weakly electric fish, the excitation is an alternating signal. There are of course several reasons for this, maybe the most important being that a direct current signal tends to ionize the medium, changing its electrical properties. For a fish an AC signal also allows the fish to relax, instead of continuously driving current into the water, consequently saving energy.

Just as in the case for a non-conducting medium the relationship between the potential V and the electric field E is $\nabla V = -E$. We can now introduce a new term J which we deem the *current density*. The current density is the flux of current flowing through a unit area. It can be imagined as the flow of charges through an area. There is a relationship between the electric field and the current flux, one that any engineer would normally immediately recognize, if we used it in its normal form, instead we introduce it in a continuum form, equation 2.19.

$$J = \sigma E \tag{2.19}$$

In equation 2.19 the term σ is the conductivity of the material. In its macroscopic form equation 2.19 becomes $V = IR$ or ohm's law. Because we are working with infinitesimal small points we will use the continuum form.

Just as ohm's law has a continuum based version, we can generate a continuum based version of Kirchoff's current law. In the macro, lump circuit model we say the sum of all currents into a node is zero. This really ends up being a equation describing the conservation of charge, as the current must be zero or else accumulation of charge would occur at the node. In the continuum case, we apply the same law's of conservation to a infinitesimal small point. The divergence operator, $\nabla\cdot$, is really a measurement of the quantity of "stuff" entering or leaving a tiny region, we can say the divergence of the current flux is zero. The result is shown in equation 2.20.

$$\nabla \cdot J = 0 \tag{2.20}$$

Combining equation 2.16 ,equation 2.19 and equation 2.20 yields equation , known as Laplace's equation.

$$\nabla \cdot (\sigma \nabla V) = 0 \tag{2.21}$$

Laplace's equation is often referred to as the potential equation, since any particle placed in a field, either gravitational or electric in nature must satisfy it. When solving the laplace equation there are two versions of the problem. The Dirichlet problem, where the boundary values must take on defined values. In impedance sensing this is equivalent to fixing the boundary voltages and recording the resulting current. The other version of the problem is the Neumann problem, where the values of the normal derivative are defined, this would be equivalent to injecting a current. The laplace equation ends up defining the relationship between the spatial varying conductance σ, the measured voltage V, and the current density J. While solutions do exist for very simple symmetric geometries complicated geometries like we will expect to see in our tank environment really

require simulation via numerical methods. The next chapter will introduce some of these concepts, as well as present simulations of our expected tank results.

CHAPTER 3

Finite Element Analysis and Simulation

The electrostatic field generated by a weakly electric fish, satisfies Laplace's equation 2.21. Since we are dealing with *statics*, there is no time dependence, and instead we must deal with boundary conditions on the surface of the region being explored. Laplace's equation is a second order differential equation, which requires knowledge of of all boundary conditions to completely solve.

There are two ways of describing the boundary conditions, one is to specify the voltage. This would be equivalent to completely surrounding the body under investigation with electrodes and controlling the excitation voltages. This form of the problem is often call the Dirichlet Problem. The alternative method is to define the rate of change of voltage in the direction of the normal to the boundary, or equivalently controlling the current applied to each boundary electrode. This problem is known as the Neumann problem. In electrical resistive tomography, as it is applied to geological survey experiments, the practice is to apply and control a voltage [SB01]. In contrast, in the case of electrical impedance tomography the alternative is far more common, that is applying a known current and recording the boundary voltages. In the case of electrical impedance tomography, it is clear why current is applied instead of voltage; excess current through tissue can causes damage, and large excess currents can even cause death. This is why electrical impedance tomography systems generally use a howland current pump, and never exceed 5 mA of applied current. It is important to make this distinction as we

move to simulating an impedance measurement system, especially since the tools we will use were designed for electrical impedance tomography.

The solution of the Laplace equation as it is presented in electrical impedance tomography is referred to as the inverse problem. Difficulties in solving two dimensional and three dimensional electrical impedance problems comes from the nature of the laplace equation, and physics of electrical statics. These types of problems are ill-posed and non-linear. Since computation has greatly improved since the 1980's when electrical impedance tomography was first introduced it is now possible to generate solutions using advanced finite element analysis. The inverse problems have become common enough to necessitate the development of a toolset for solving them.

The *Electrical Impedance and Diffuse Optical Reconstruction Software* Project, or EIDORs was developed as a MATLAB toolkit specifically to give researchers in the field of electrical impedance measurement and diffuse optics a tool for modeling and solving both the forward and inverse problem and developing new algorithms to improve simulation and reconstruction. In the case of the forward problem, it allows researchers to model a body or environment along with all of its electrical properties then apply a simulated current and solve for the expected voltage potentials at the boundary. It also comes with numerous visual tools to assist in understanding the current and voltage distributions [PL02]. Since we will be defining the the materials composition and geometry of our simulation and solving for the boundary voltage given a current excitation it is possible to use only the forward solver. EIDORs constructs a system matrix from the supplied fine element mesh and the electrode positions, then uses either the Cholesky method or the LU method so solve [PL02]. The forward solver was adequate for development of our simulations.

While are sensor system will not have knowledge of the complete boundary conditions as normal torso based electrical impedance systems we can still use EIDORs to explore the effects of distance, lateral position, object composition, and object size. on the voltage measurements on a linear array and these will inform our decisions on the physical design.

3.1 Simulation Setup

The EIDORs library is written in MATLAB, therefore all simulations were written as scripts, the configuration parameters can be found in the source code. The listing of the source code is available in appendix .1.

3.1.1 Tank Configuration

The simulation will take place in a salt water tank. We will match the dimensions of the tank used in our physical experiments. The physical tank is 30 inches wide by 30 inches long, and it was a depth of just under 24 inches. While EIDORs has the capability of solving the forward inverse problem in 3 dimensions, 2 dimensions will be enough to give insight into how the target object parameters effect the measured voltages at the electrodes. Our simulated tank is then set to be 30 inch by 30 inch. The tank is then divided into triangle elements and nodes. The number of nodes along each dimension of the tank is 40. With 40 by 40 elements the total number of elements 1600. To match the conductance of the ocean each element was set to 0.305 ohms $\cdot$ meter. This tank configuration will be used in our background, or the homogenous measurements. Figure 3.1 shows the simulated empty tank, before the introduction of an object and before excitation by an injected current. The term *voltage disturbance* is now introduced. In the

presence of only a homogenous tank, i.e. a tank without any object their will still be voltage measurements at the electrodes as the current flowing in the tank will still generate a spatial varying voltage pattern. A weakly electric fish placed in the tank at this point will sense the *background* voltage. It is only when an object enters the field that the fish senses the change, or a *disturbance* from the normal background voltages. The fish learns the background voltage pattern, and recognizes when it changes. This is equivalent to the ability of our skin to adapt to temperatures the temperature of the room, or the ability of our eyes to change the dynamic range when it becomes dark.

3.1.2 Electrode Configuration

Just as members of the *Elasmobranchii* use tiny adjacent pores leading to ampullae of lorenzini for sensing small voltage potentials we used adjacent stainless steel electrodes in our first physical experiments. In the simulation we set 10 electrodes each spaced apart by two elements or 1.5 inches. The electrode contact impedance will be neglected as unlike skin electrodes which tend to have poor connections we are nearly guaranteed to make a good connection with a submerged electrode.

3.1.3 Stimulation Pattern

The EIDORs tool suite provides a nearly infinite configurability in the applied stimulation pattern with a few limitations. As of the writing of this thesis EIDORs is only capable of stimulating with a current and measuring the potentials. This is acceptable for our linear electrode experiments, but will not be of use in the current measurement experiments. We will fix the ground electrode, or reference electrode as electrode 10. The first electrode, electrode 1 will be the current

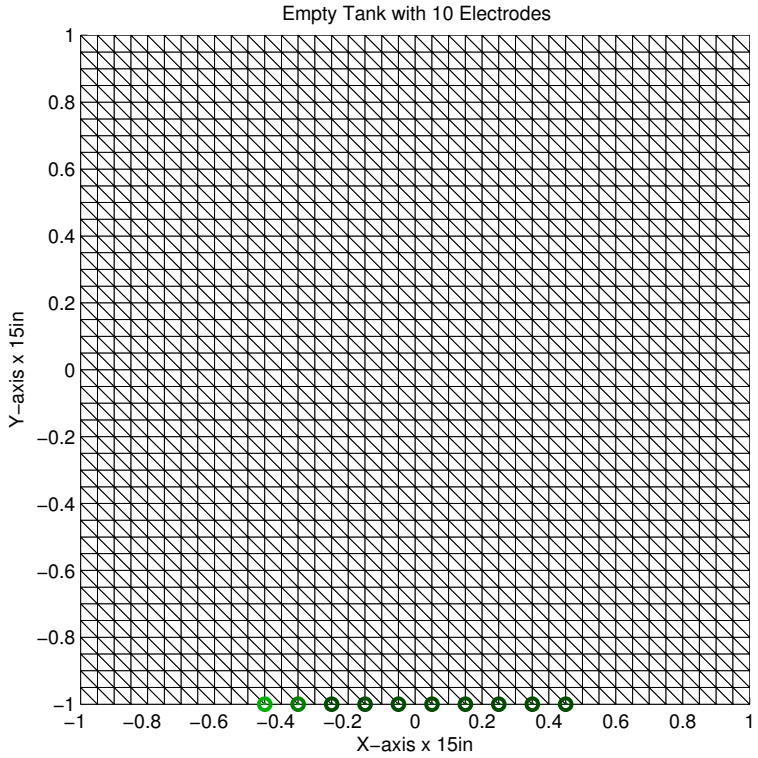

Figure 3.1: Image showing the simulated empty tank. For the simulations a 30 inch by 30 inch tank was divided in 40 by 40 elements. Each element was 0.75 inches^2. 10 electrodes were placed 0.75 inches apart along the front wall of the tank. Current was injected was done from electrode 1, while the electrode 10 was selected for a ground reference

injection electrode. The injection current can of course be varied, but for these simulations the current is fixed to 1mA. It is also possible to use more complicated stimulation patterns but to be biomimetic we chose to fix the location of the stimulation electrodes just as weakly fish have fixed locations for their electric organ. To obtain different views we would instead use motion.

Figure 3.2 shows the result of our stimulation pattern. Regions in red have high positive electric field intensities, while regions in blue have high negative

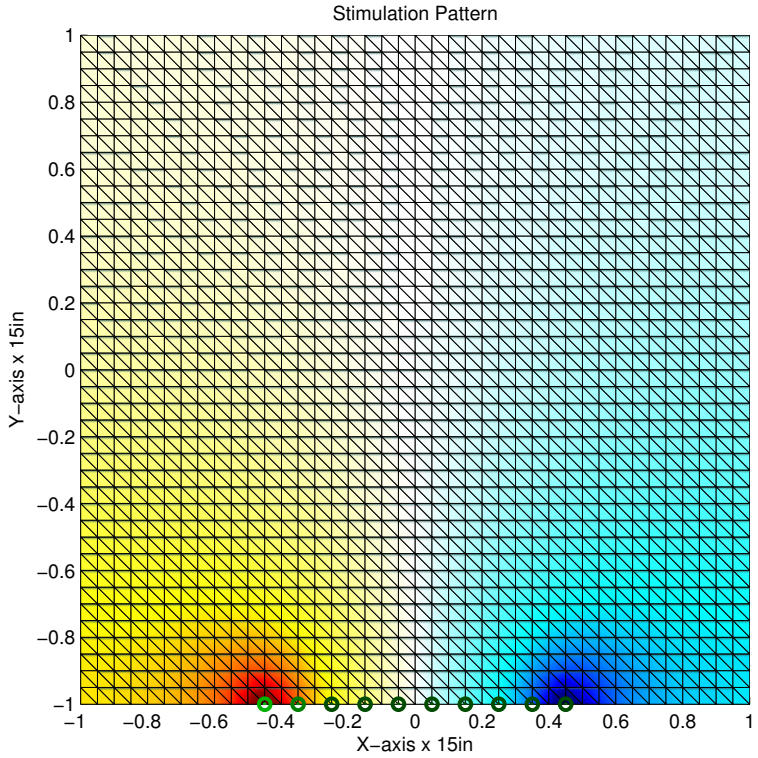

Figure 3.2: The tank was filled with simulated sea water with an impedance of 0.305 ohm $\cdot$ meters. The resistance of each element was approximately 16 ohms. The voltage pattern resulting from stimulation in a homogenous tank due to an injected current of 1mA is shown.

electric field intensities. The pattern resembles the pattern of figure 2.3 in section 2.3. As discussed in the previous chapter, the field due to a dipole falls of as a function of $\frac{1}{r^3}$. As distance from the generate dipole increase the intensity of the field falls off at a higher rate.

3.2 Effects of Object Distance

Many weakly electric fish use their electroreeceptors for electrolocation this allows them to hunt in conditions where light is obstructed. The distance to prey is then essential for the fish in predicting proper maneuvering. To explore the ability for electrolocation to predict the distance of an object from the electrode array a simulated object with a circular geometry was placed in the tank. This object had a radius of 1.5 inches, its conductivity was set to 500 ohm $\cdot$ meter, and was therefore of higher resistance than the surround fluid. This is equivalent to the plastic targets used in our the physical experiments. The object was positioned directly next the the electrode array with an offset of 0 inches from electrode 5. It was then moved way from the array, until it was directly on the other side of the tank.

Figure 3.3(a) shows the object at 18 inches from the array. The upper right subfigure shows the location of the object relative to the array. The upper center subfigure shows the vector field of the current in the tank. The upper-right subfigure shows the change in current that results from the placement of an object. Finally, the bottom subfigure shows the change in voltage that would be measured as a result of the object being place in the field. These voltages at each electrode represent the differential voltage between the adjacent electrodes. The voltage measured in the homogenous tank, that is the tank with out an object, have been subtracted away to accentuate the changes in voltage resulting purely from the existence of the object.

Comparisons should be done between figure 3.3(a) at 18 inches, figure 3.3(b) at 15 inches, figure 3.4(a) at 9 inch and figure 3.4(b) at 4 inches. Clearly the magnitude of the voltage *disturbances* increase as the object approaches the array. This is important since it shows that embedded in the signals for an object with a

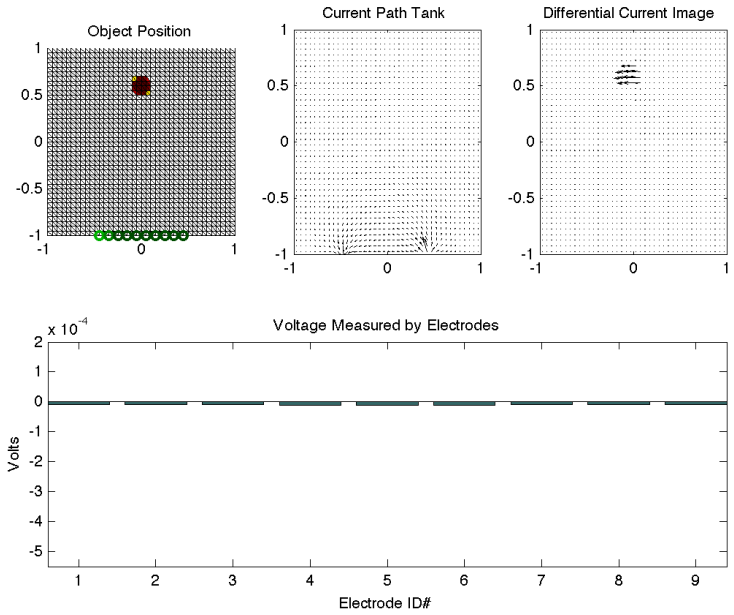

(a) Simulated changes in electrode voltage for an object 18 inches from the center of the electrode array.

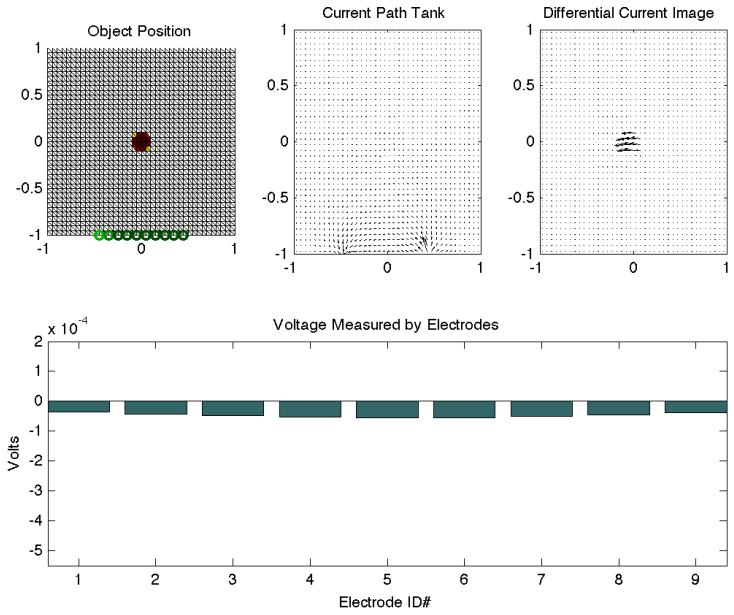

(b) Simulated changes in electrode voltage for an object 15 inches from the center of the electrode array.

Figure 3.3: An the object approachs the electrode array and the changes in voltage caused by the object become larger in magnitude.

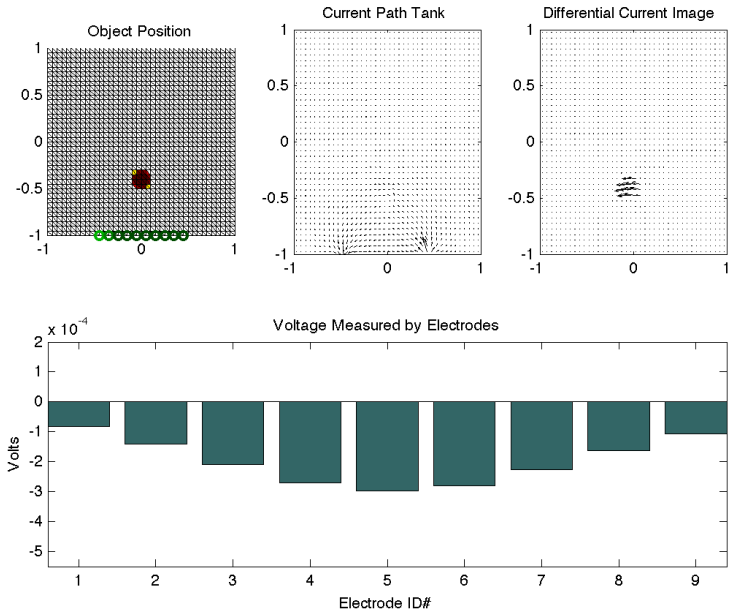

(a) Simulated changes in electrode voltage for an object 9 inches from the center of the electrode array.

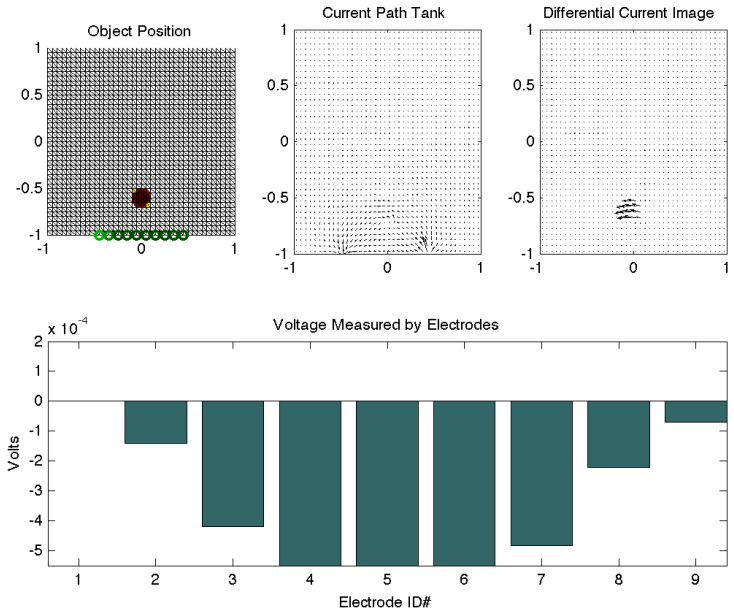

(b) Simulated changes in electrode voltage for an object 6 inches from the center of the electrode array.

Figure 3.4: An the object approachs the array and the changes in electrode voltage caused by the object become larger in magnitude.

fixed radius and fixed material is distance information. This of course is supported by natural evidence of weakly electric fish being able to detect obstacles and food sources [Fer96].

The plot in figure 3.5 shows the disturbance voltages as a function of the distance of the object from electrode array. The object is placed directly in front of electrode 5, and this small lateral offset from the center of the array can account for the small dip in disturbance below zero, until it rises back up an approaches zero. The target object is again the 1.5 in radius target. At a distance of approximately 10 inches the disturbance is very small, and probably in distinguishable from background. This agrees with some of our physical experiments, where at a certain distance the signals vanish. Figure 3.11 show a surface plot, relaying the same information as figure 3.5 only for all 9 differential voltages measurements.

3.3 Effects of Object Position

Weakly electric fish have the ability to localize an object and determine a heading; either by moving away from a dangerous object or towards an object of interest. To simulate this type of behavior the same tank configuration was used. A simulated 1.5 inch radius cylindrical object was used as the target. The object was composed of a material with a conductivity of 500 ohm $\cdot$ meter. By sweeping the object in front of the array at a constant distance the relationship between the disturbance voltage measurements and the object position can be determined. The homogenous tank measurements were subtracted from the measurements taken with the object in the tank.

These *disturbance voltages* are again shown in the bottom subfigure of figure 3.7(a), figure 3.7(b), figure 3.8(a), and figure 3.8(b). The light green elec-

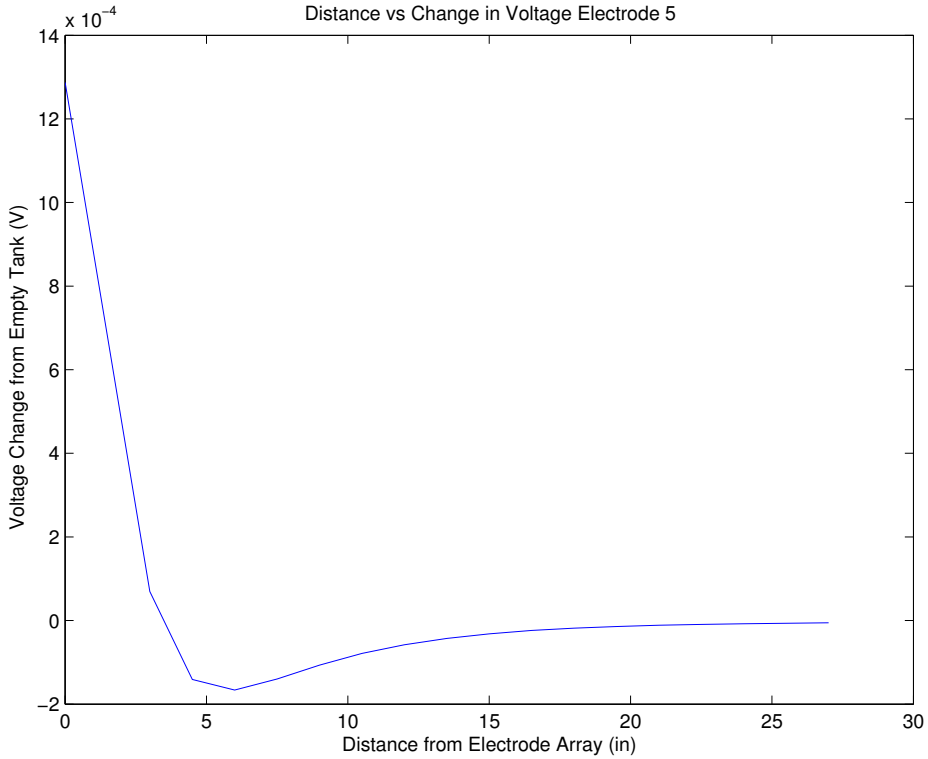

Figure 3.5: Voltage vs Distance relationship for center electrodes as object approaches .

trode represents electrode 10, the reference electrode. Notice the pattern, as the object moved close to an electrode pair the magnitude of the disturbance voltage measured increases. As the object is swept right to left the voltage measurements mirror this behavior. Predicting the direction to an object is fairly simple, and can be accomplished by choosing a heading towards the electrode with the largest amplitude. As we shall see heading is much easier to determine than distance, material, and shape since all three effect the amplitude of the signal, while heading information is contained in the relative magnitudes between different electrode pairs.

Figure 3.9 show the disturbance electrode field for electrode pair 5 and 6, at

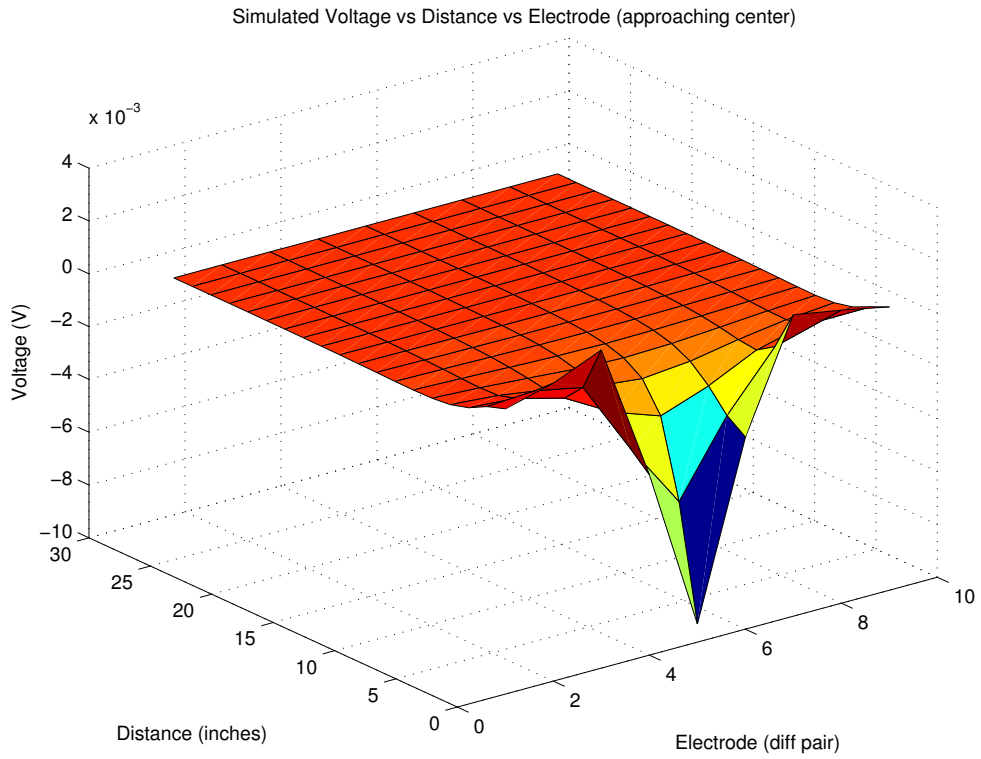

Figure 3.6: Simulated surface plot of voltage vs distance relationship for all electrodes .

a distance of 6 inches away from the wall. The peak voltage occurs when the object is directly in front of the pair. Figure 3.10 shows the same measurement only this time for a different electrode pair offset from the center. The peak again occurs when the object is directly in front of the pair. Finally, figure 3.11 shows a surface plot showing the measured voltage disturbance as a function of the target position and the electrode pair. The highest magnitudes form a nearly linear relationship between position and electrode pair, consequently, predicting object direction relative to the electrodes is possible.

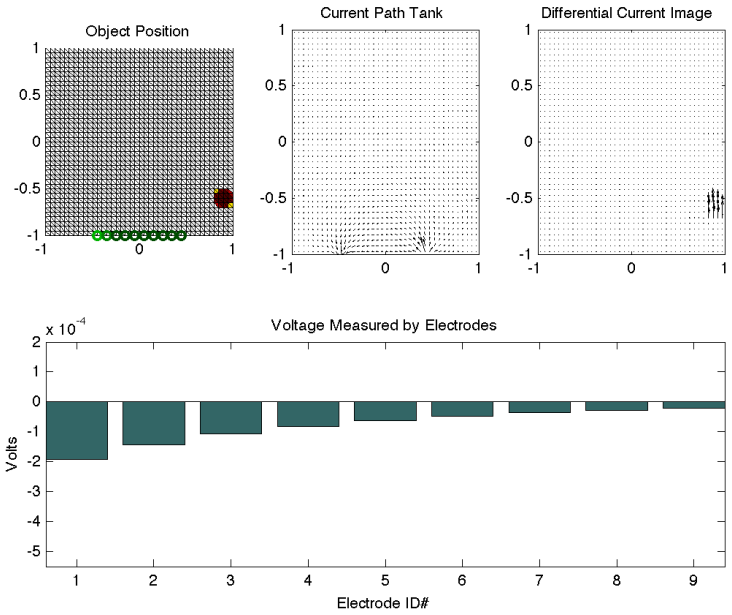

(a) Simulated changes in electrode voltage for an object offset to the right of the center of the array by 13.5 inches.

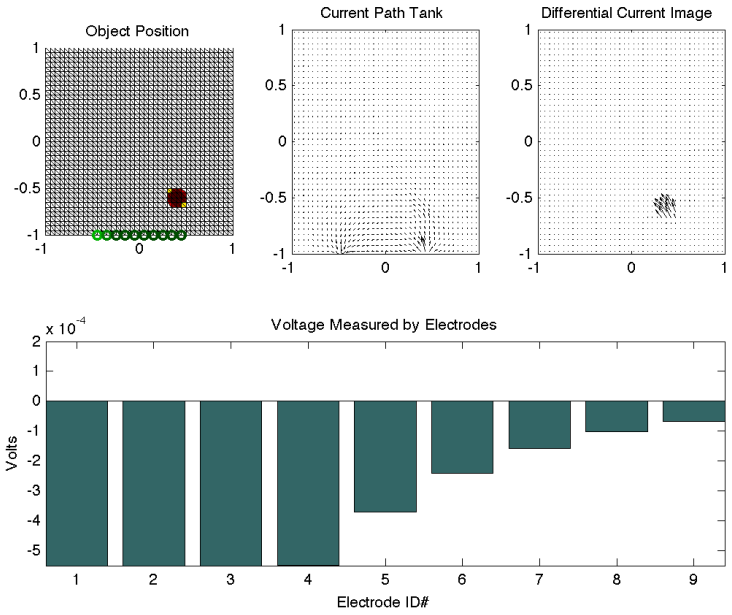

(b) Simulated changes in electrode voltage for an object offset to the right of the center of the array by 6 inches.

Figure 3.7: An the object is swept in right-front of the electrode array, a large voltage change is recorded in the electrode closest to the object.

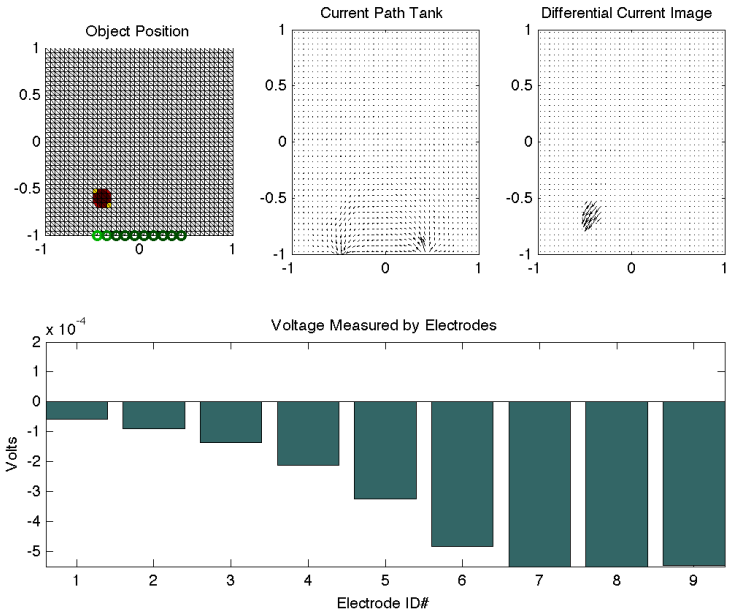

(a) Simulated changes in electrode voltage for an object offset to the left of the center of the array by 6 inches.

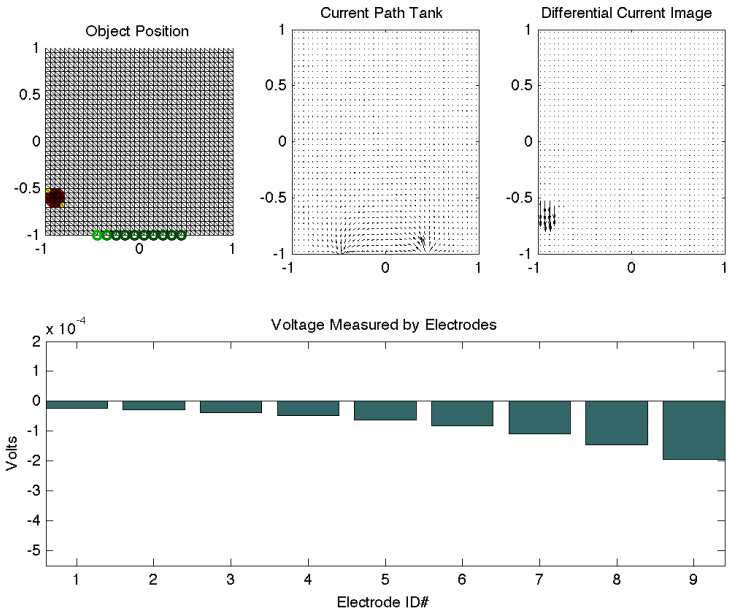

(b) Simulated changes in electrode voltage for an object offset to the left of the center of the array by 13.5 inches.

Figure 3.8: An the object is swept in left-front of the electrode array, a large voltage change is recorded in the electrode closest to the object.

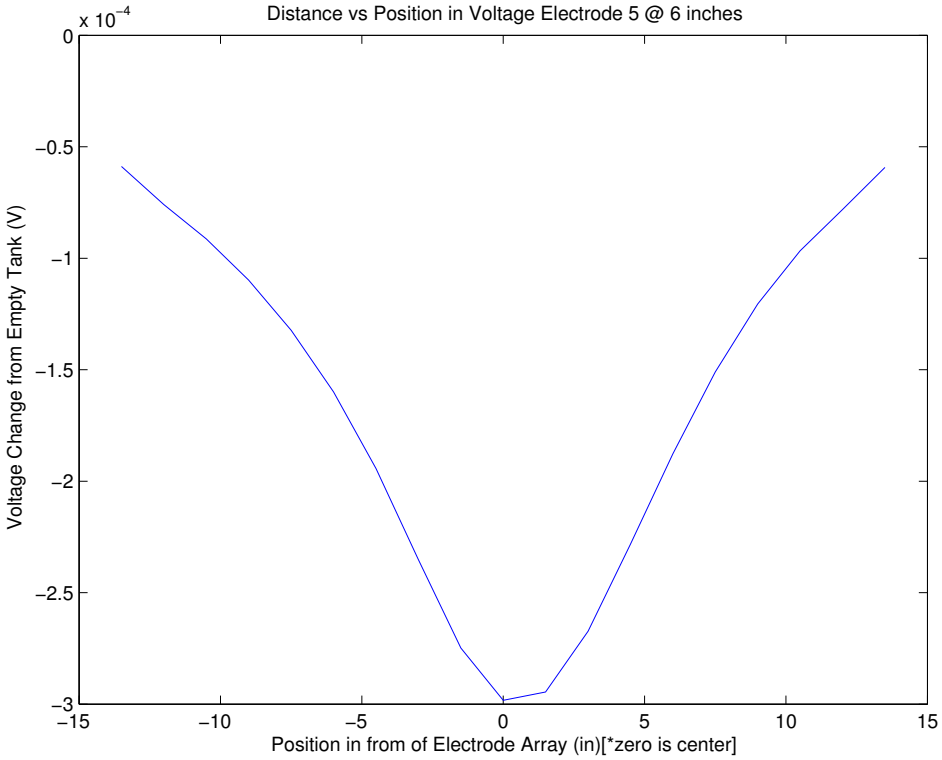

Figure 3.9: Position information is encode in the voltage signals. Here we see the voltage measured between electrode pair 5 in the center of the array. As the object passed the center of the array the magnitude of the voltage change reaches a maximum.

3.4 Effects of Object Material Composition

The electrical properties of object can vary wildly. From their bulk resistance to the capacitance of living tissue, weakly electric fish have the marvelous capability of identifying the difference between materials. The *contrast* between the the water and the target object is essential, an we will explore through simulation, the ability of different materials to cause a voltage disturbance between different electrode pairs.

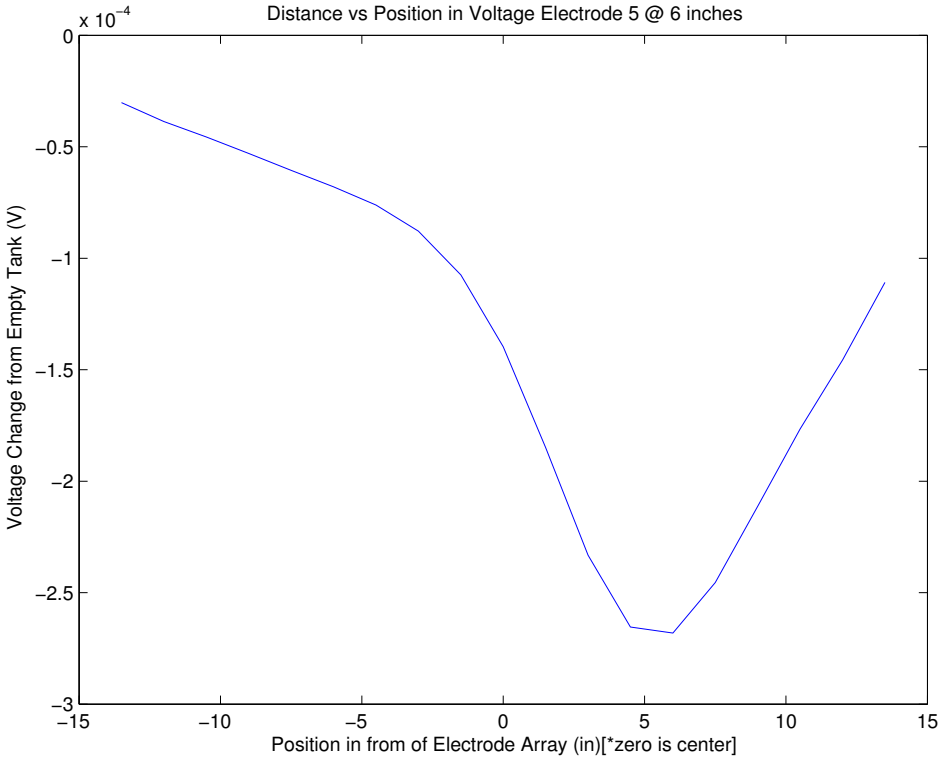

Figure 3.10: Position information is encode in the voltage signals. Here we see the voltage measured between electrode pair 2 in the center of the array. Similar to figure 3.9 the voltage peaks, since the position of the pair is to the right the peak occurs to the right of center. As the object passed the right of the array the magnitude of the voltage change reaches a maximum.

The simulated tank is filled with salt water with a conductivity of 0.305 ohm $\cdot$ meter. This is essential, since it the difference between the water conductivity and the object conductivity that will allow detection. A element conductive of 0.305 ohm $\cdot$ meter means the resistance of each individual element is approximately 16 ohms. We place a object with a fixed geometry and position in the tank and measure the resulting disturbance voltages as we vary it material properties, changing it resistance from 0 ohms to 60 kiloOhms.

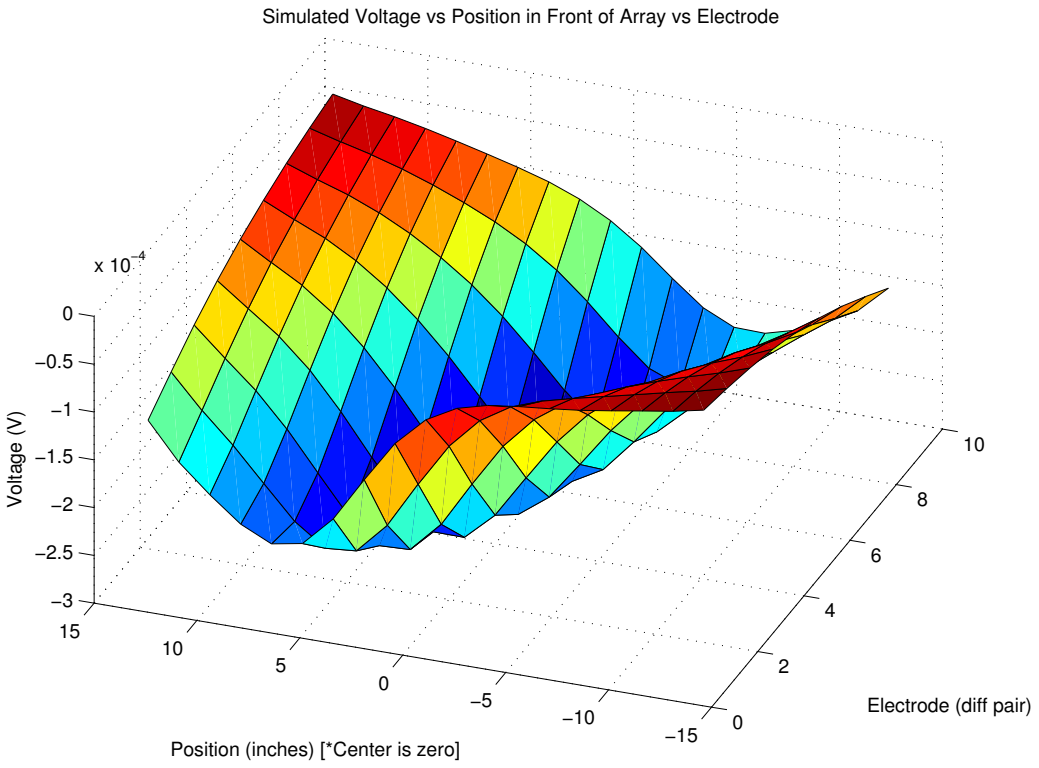

Figure 3.11: Simulated surface plot of voltage vs position relationship for all electrodes. For each electrode pair the largest magnitude change occurs as the object is closest. Direction information is encoded in the signals.

In EIDORs the material properties are shown by changing the color. Therefore in material variation figures with objects of impedance lower than the surrounding water the object appears blue, when the impedance is greater than the water the object appears red.

In figure 3.12(a), figure 3.12(b), figure 3.13(a), and figure 3.13(b) the effects of the object material is shown on the disturbance voltages measured at the electrodes. Figure 3.12(a) shows an object with element resistance of 1ohm. It is therefore more conductive than the surrounding water, the change in the voltage as compared to the homogenous tank condition is positive, this is clearly different

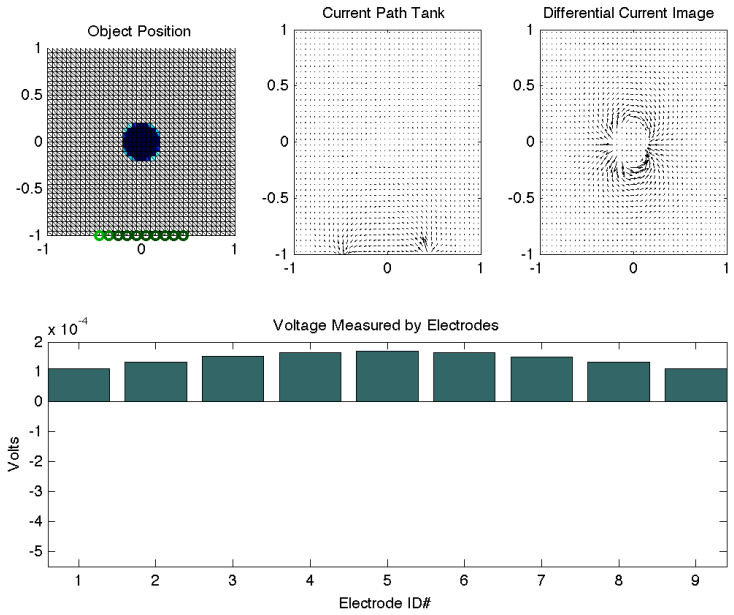

(a) Simulated changes in electrode voltage for an object with a resistance of 1 ohm, this is more conductive than the water.

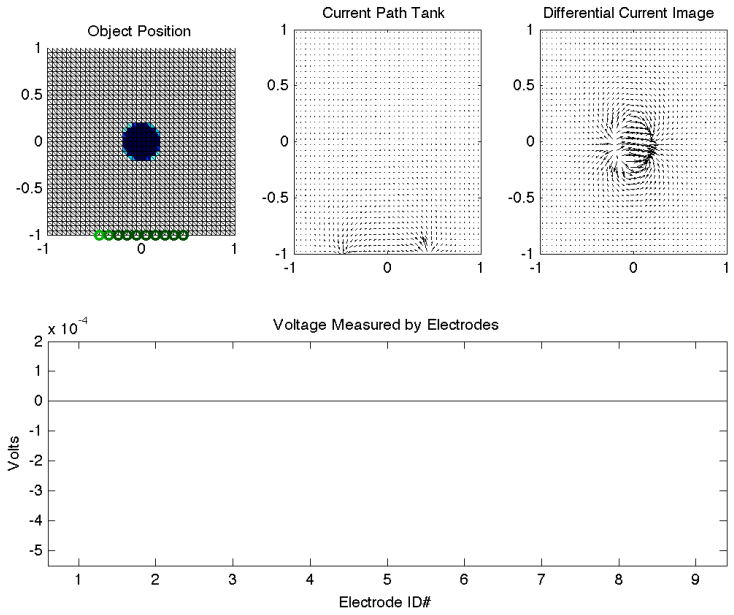

(b) Simulated changes in electrode voltage for an object with a resistance of 16 ohm, this is approximately the same as the water.

Figure 3.12: The electrical properties of the object effect the ability to detect it, an object with lower resistance is detectable, while an object with the same spatial resistance is completely hidden.[48]

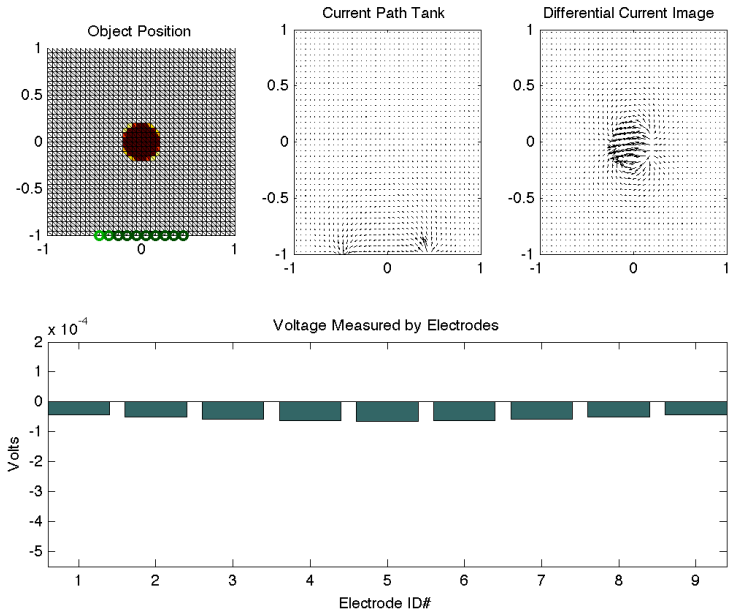

(a) Simulated changes in electrode voltage for an object with a resistance of 32 ohm, this is twice the resistance of the water.

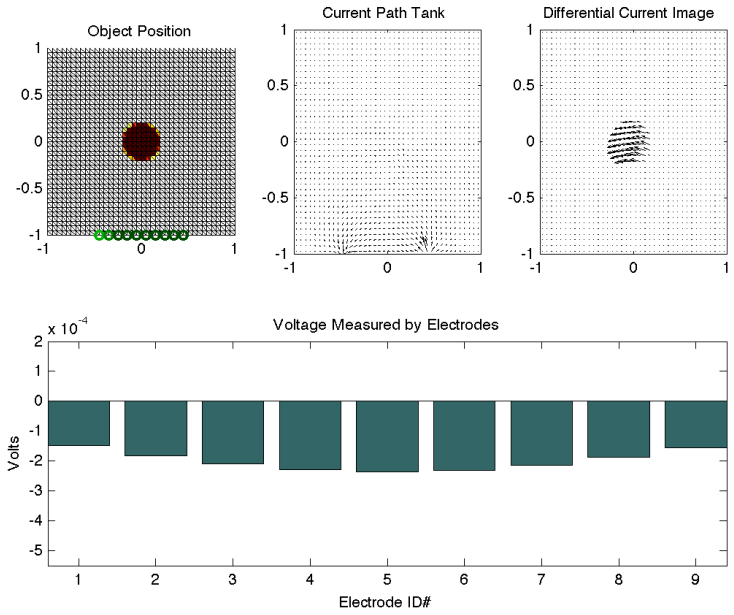

(b) Simulated changes in electrode voltage for an object with a resistance of 65k ohm, this is far less conductive than the water.

Figure 3.13: Object detectability is material dependent, in the case of a object that has higher resistance than the water, it is possible to locate it, the larger the difference in resistance from the water the greater in change in voltages at the electrodes.

than the case when an object is an insulator. Figure 3.12(b) shows the same result only the elements resistance of the object were set very close to element resistance of the water. Clearly if an object has similar electric properties to the surrounding it will be nearly impossible to identify. Figure 3.13(a), and figure 3.13(b) show the disturbance voltages simulated for objects with a conductance larger than the water. As the object resistance increases relative to the resistance of the water so does the simulated voltages.

The relationship between material resistance and the simulated disturbance voltages is plotted in figure 3.14. Resistance has a non-linear relationship, that appears to have a inverse power relation with the measured voltage. This makes it fairly difficult to identify the type of material an object consists of, as well as the distance and size of that object, as all three effect the amplitudes of the simulated disturbance voltages.

3.5 Effects of Objects Size on Simulated Voltage Pattern

The last parameter we explored in simulation is the effect of the size of the object on the measured voltages. As would be expected increasing the the size of the object does effect the the ability to sense the object. To simulate the effects of object size, we again place a circular object in the simulation environment. The radius of the object was increase slowly from 0.25 inches to 14 inches. Figures 3.15(a) 3.15(b) 3.16(a) and 3.16(b) show four of the simulations. The distance from the center of the array to the surface of the object was maintained. This prevents the proximity of the object from affecting the measured voltage pattern. For small objects on the same order of size as the array, the relationship between object size and voltage appears linear, this begins to deviate as the object size become much larger than the array size. Notice in figure 3.17, as the

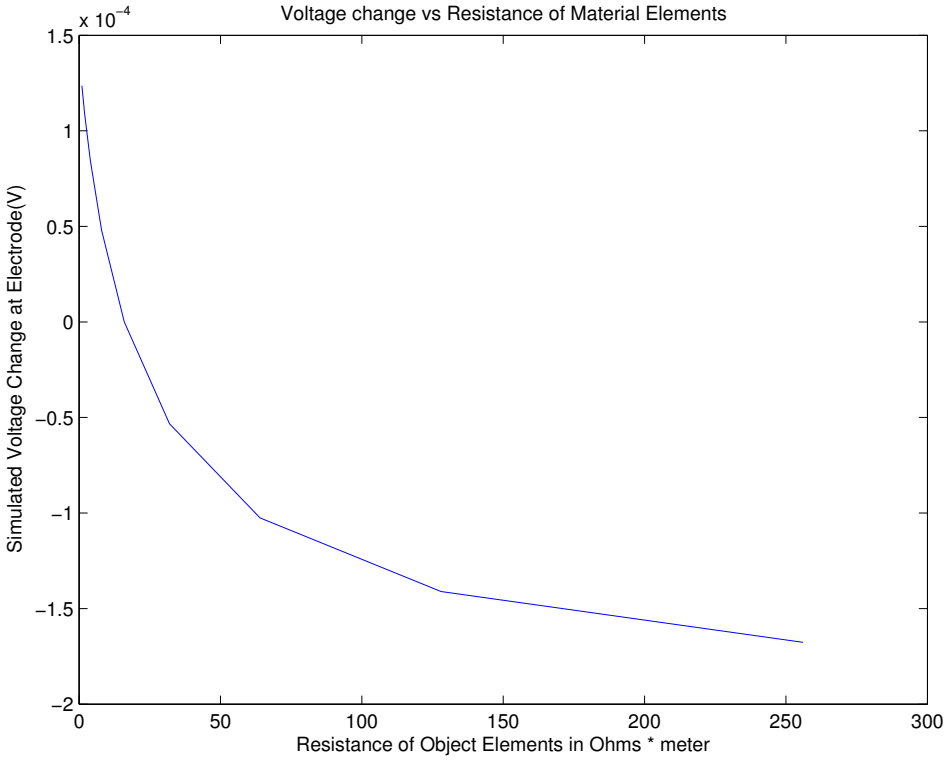

Figure 3.14: This figure shows the relationship between the resistance of the target objects elements and the voltage output at the electrodes for a fixed distance. The relationship is non-linear and looks to be exponential.

object grows to greater than 10 inches, at the length of the array, the marginal change in voltage becomes smaller. This makes intuitive sense, a large object should eventually approach a linear plane of infinite extent and the asymptotic behavior would suggest just such a behavior. The object size to measured voltage disturbance is plotted across all 9 differential pairs in figure 3.18, the same pattern is seen for all electrodes.

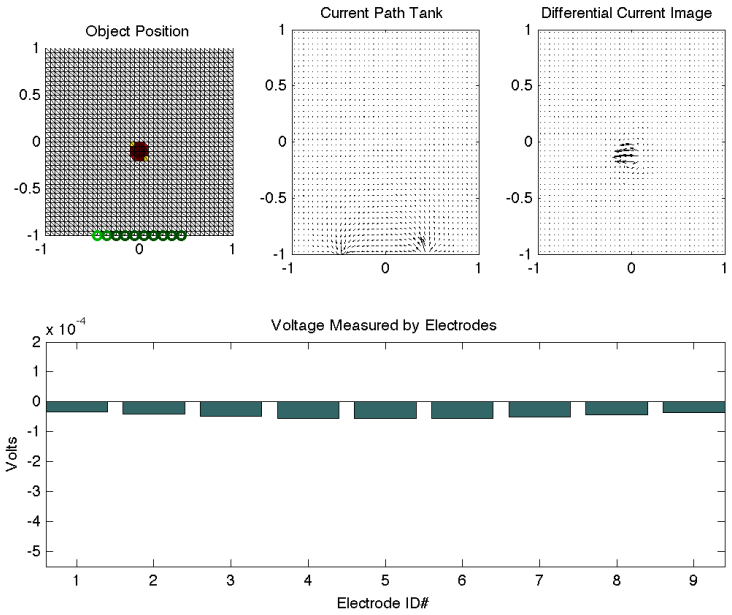

(a) Simulated changes in electrode voltage for an object of radius 1.5 inches .

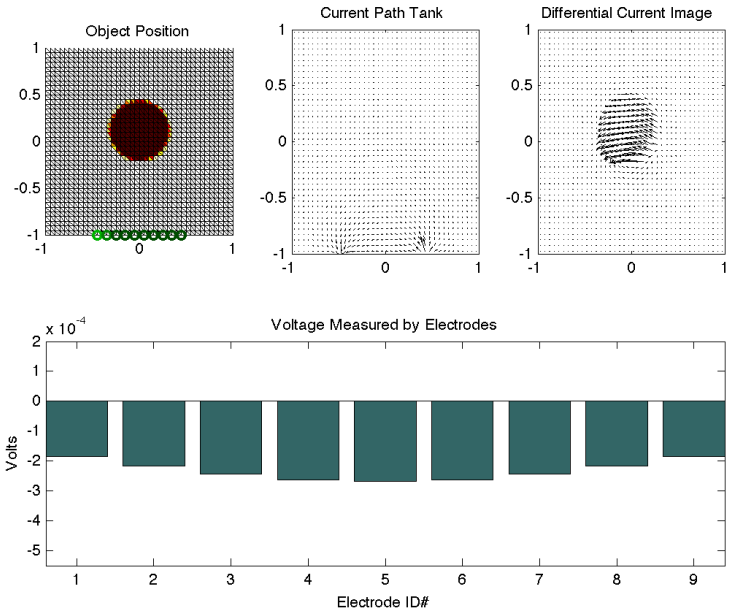

(b) Simulated changes in electrode voltage for an object of radius 4.8 inches .

Figure 3.15: Object detectability is target size dependent.

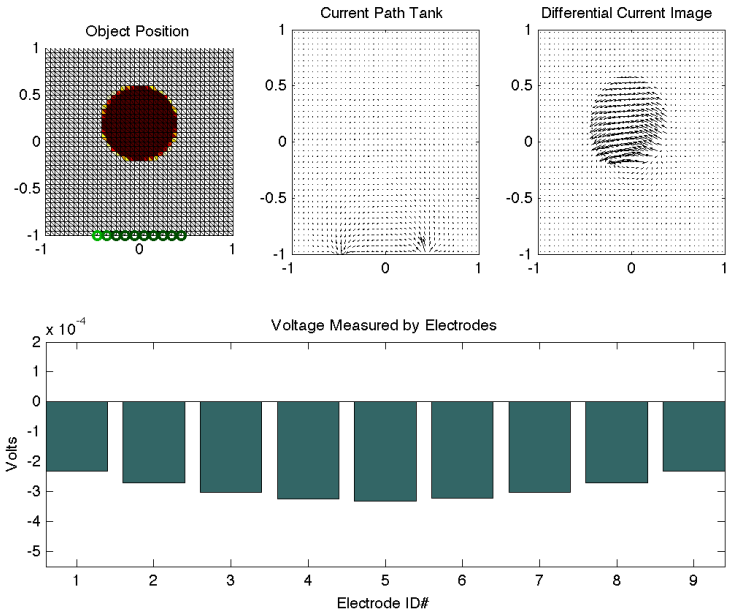

(a) Simulated changes in electrode voltage for an object of radius 6.0 inches .

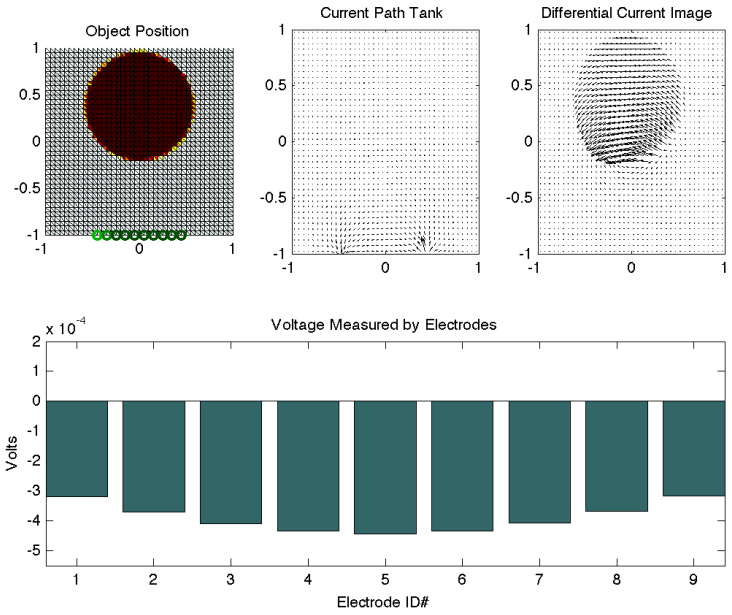

(b) Simulated changes in electrode voltage for an object of radius 8.7 inches .

Figure 3.16: Eventual the effect of increasing object size diminishes.

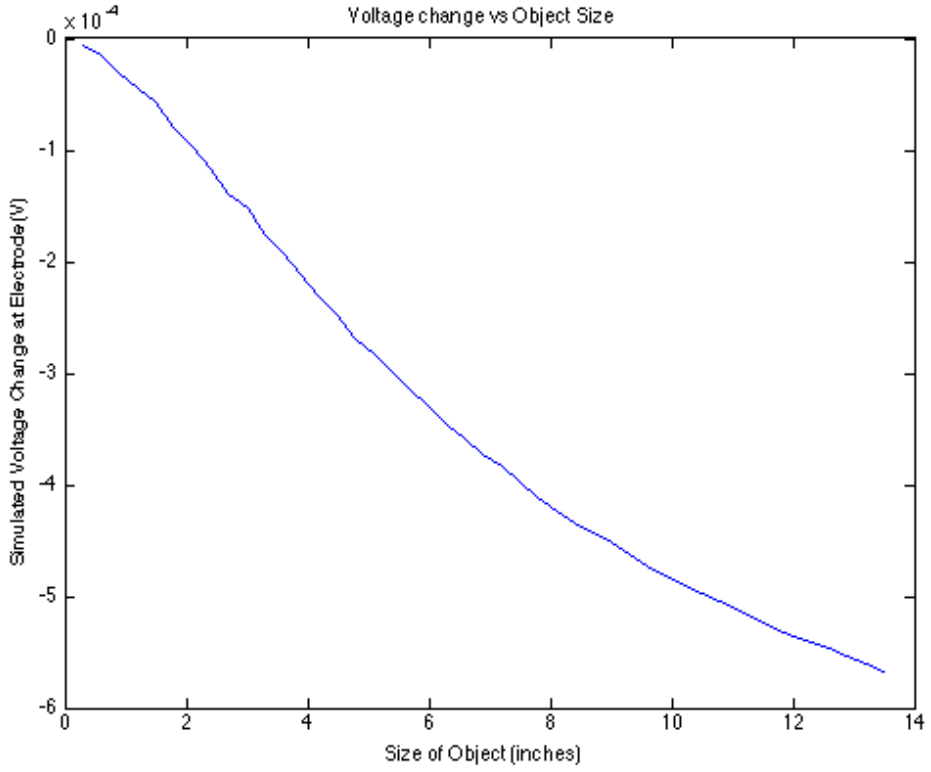

Figure 3.17: Object size has a similar non-linear relationship with measured voltages for large object. For small objects those only a few times larger than the electrode separation distance the object size versus measured voltage could be approximated with a linear curve. As the size of the object continues to increase the voltage changes measured at the electrodes reaches a plateau and a asymptotic behavior is present.

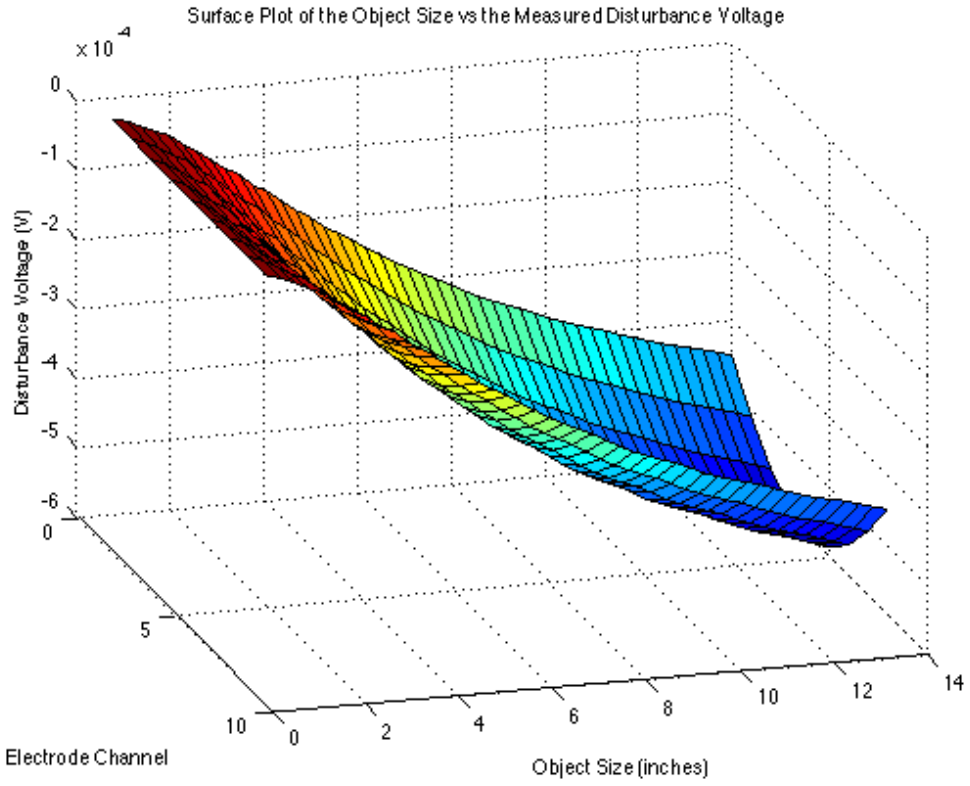

Figure 3.18: There is a similar relationship an all ten electrodes. The greatest disturbance voltage occurs at the electrode closet to the object, in this case channel 5. Smaller objects are consequently harder to detect than larger objects. There is a limit, when an object reaches large sizes greater than the extents of our electrode array, the change in measure voltage no longer increases as quickly.

CHAPTER 4

Design of A System for Differential Voltage Sensing

A 16-channel differential voltage sensor was developed to mimic the electrical sense abilities of marine sharks and skates. Unlike sharks and skates the system uses an active electric field, in this way it is similar to the weakly electric fresh water fish of the Teleostei family, who actively probe their environment. Active sensing gives the system the ability to sense passive objects with material properties different from the surrounding medium. The system measures adjacent voltages between 17 separate electrodes. All 17 electrodes were arranged in a linear fashion, exactly like the configuration used in the simulations of the previous chapter. The device is capable of sampling across all 16 channels simultaneously, this is somewhat inferior to fish, who contain several thousand electroreceptors, all woking in parallel [Fer96]. Custom analog front ends were designed and built for amplifying the voltage potentials and providing bandpass filtering. These printed circuit board (PCB) components were developed to be programmable. An additional motherboard was developed for interfacing with the analog front end cards. The entire system was designed to be portable, and was used to run tests in a salt water aquarium tank. Target objects of multiple materials were explored, along with the effects of position on the sensed voltage potentials [Fri12].

4.1 Electrode Array Design

The first difficulty in measuring a voltage in a marine like environment is the corrosiveness of salt water. Since we applied a voltage to the transmitter electrodes we accelerate this effect. Electrolysis occurs when a material experiences a redox reaction due to an applied voltage potential. The electric field causes ionization of the surface of the electrodes and a metal ions are attracted, covering or plating the surface with oxidized metal ions which are poor conductors. The salt water is an effective electrolyte and allows transport of the ions. A sinusoidal voltage potential was chosen over a direct current (DC) signal to help mitigate the electrolysis effect. DC current has a greater tendency to corrode electrodes because the anode and cathode remained fixed, electrons and therefore free ions will always leave one electrode and be attracted to the other. Alternating currents (AC), were used in all of the experiments. AC currents rapidly switches the anode and cathode, as a result, electrons leave and enter the electrodes equally, minimizing the electrolysis effect. In theory, if corrosion was not an issue and the system was not expected to measure reactive effects a DC current could be used for resistive measurements, but due to environmental limitations we chose to use a slow changing ($\tilde{1}$KHz) sinusoidal wave. Corrosion changes the impedance of the electrodes, and this can alter the measured voltages [BB84]. Our original experiments used bare copper wire [Fri12]. The copper was easily corroded within several hours of being placed in the tank the experiment became compromised Ċopper is fairly susceptible to corrosion and was quickly set aside in favor of stainless steel. Stainless steel is a common material used in the development of electrical impedance tomography systems. It has the advantage of being a decent conductor ($6.9 \cdot 10^{-7}$ohm $\cdot$ meter), resistant to corrosion in salt water and readily available for rapid prototyping.

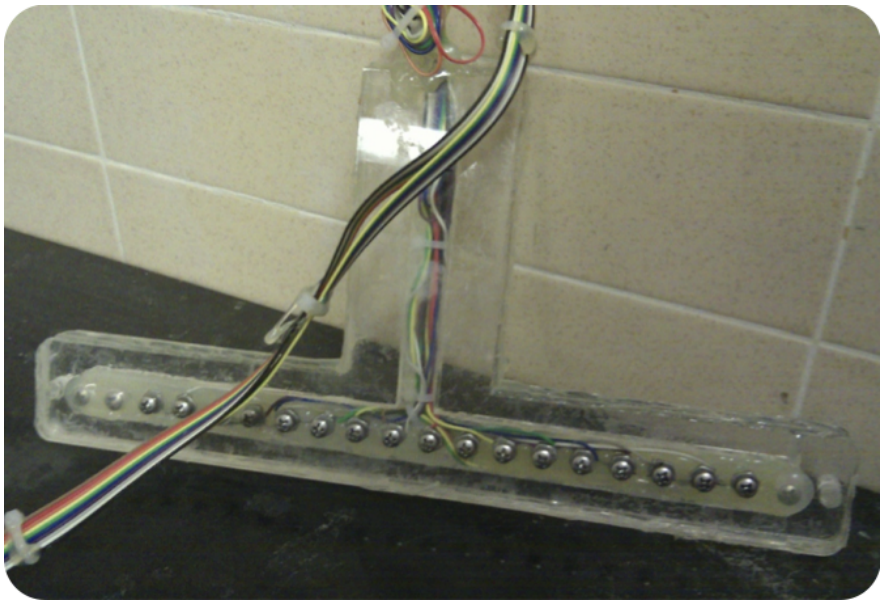

Figure 4.1: Stainless steel electrode array, consisting of 17 electrode with $\frac{1}{2}$ inch spacing.

Our first linear electrode array using stainless steel hardware is shown in figure 4.1. It consists of 20 stainless 6-32 screws arranged in a linear array with 0.50 inch spacing. Since the analog front end was only capable of processing 16 channels, only 17 of the electrodes were used, the remaining electrodes were insulated with hot melt adhesive. The housing for the electrode array was rapid prototyped using an Epilog Mini 18 laser cutter. Laminate construction was used, it consists of 3 layers, a top plate with holes for screws, a middle section with a cutout for the the wires and connectors, and finally a solid back plate. The entire assembly was held together using industrial adhesive. For material inspiration, we again look to the weakly electric fresh water fish, who have a non-conducting, high impedance skin surface. The mechanical components of the electrode assembly were machined from a non-conductive polymer, polymethyl methacrylate, PMMA, or as it is known in industry as plexiglass. During testing it was found to have several leaks. To prevent current flow between electrodes

inside the sensor array the leaks were stopped by injecting hot melt adhesive into the assembly filling all the voids. Hot melt adhesive is itself another polymer, in this case a thermoplastic with a low transition point, it also happens to be non-conductive. The electrodes were each individually connected to a single conductor of a 20 conductor ribbon cable. The ribbon cable was terminated with a high density connector, and connected to an analog from end board.

4.2 Analog Front End for Amplification and Bandpass Filtering

Weakly electric fish evolved tuberous electroreceptors that are sensitive to the frequency output of their own electric organ. The fish have a sort of bandpass filter, allowing it to tune out extraneous signals and focus on only the signal it emits [Fer96]. Figure 4.2 show output from a pair of electrodes placed in ocean at a marina. The trace was recorded on an expedition we took to explore electric fields in the ocean [Fri12]. We used an AC excitation voltage, with a amplitude of 1Volt peak to peak, the frequency was set to 1kHz, the signal was generated by a Agilent 33401A arbitrary wave form signal generator with a 50 Ohm output impedance. The transmit electrodes were separated by 1in. The receive electrodes were also separated by 1in and placed perpendicular to the transmit electrodes. The voltages between the receive electrodes were amplified by a Analog devices instrumentation amplifier, the AD623.

There are clearly two dominant frequencies in the signal, the smaller amplitude signal is the 1kHz signal we introduced, the low frequency, high amplitude signal, is the noise present in the water and created by AC power supplies of the nearby boats. It has a frequency of 60Hz. The *noise* signal limits our ability to

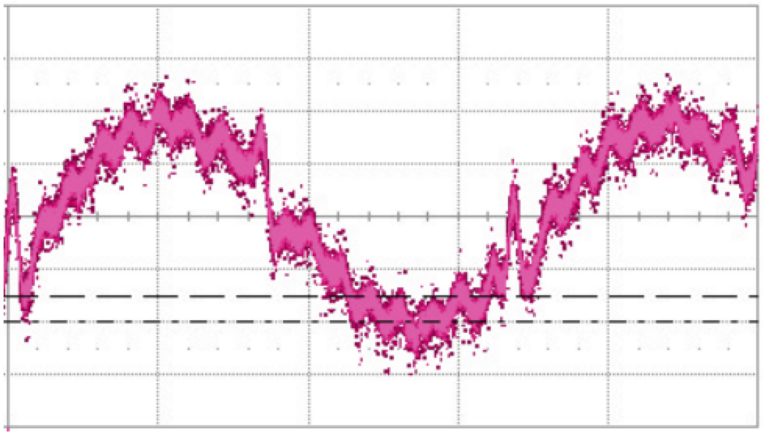

Figure 4.2: Oscilloscope capture of noise present at the marina del ray site of our ocean deployment[Fri12].

sense the voltages resulting from from the applied AC voltage, as the ability to sample using an ADC is limited by the dynamic range of the signal. To improve these results it was necessary to construct a preamplifier with a band pass filter tuned to the transmit frequency. Gain could then be applied to the filtered signal to match the dynamic range of our ADC. The addition of the filter allowed us to attenuate extraneous out of band signals.

Figure 4.3 shows the first prototype for the analog front end used in the adjacent electrode sensing experiments. It is composed of a instrumentation amplifier and two cascaded fliege bandpass filters. The gain, bias, and center frequency were all tuned by hand using potentiometers. The amplitude of the resulting signal was sampled using a bench top multimeter, configured for RMS voltage measurements. A python script accesses the samples over an ethernet interface. During a second ocean expedition, the revised circuity significantly improved our results and a similar topology was implemented in the revised analog front end for the adjacent electrode array experiments.

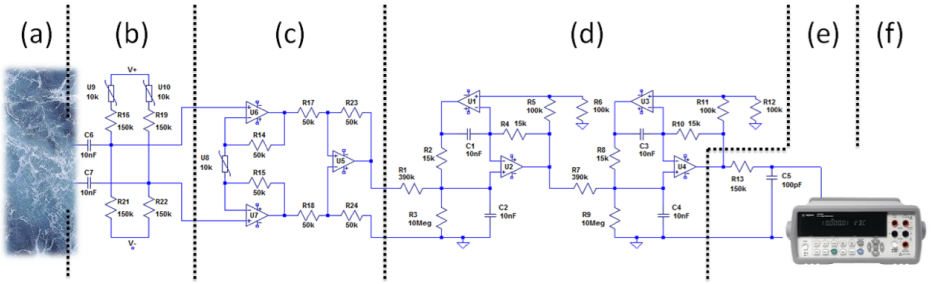

Figure 4.3: The first version of the analog front end used is voltage sensing. Signal is first amplified by a instrumentation amplifier in (c). Section (d) is a narrow bandpass filter tuned to the excitation frequency. Sampling was accomplished using a bench Agilent digital multimeter with RMS sensing capabilities[Fri12].

For the adjacent voltage measurement system the circuit used in the prototype was repeated 16 times, the through hole components were converted to surface mount components to reduce its size. Each channel required 8 digital potentiometers to control the bias and gain of the instrumentation amplifiers and the center frequency of the fliege bandpass filters. To allow for scaling the device to more channels a motherboard was developed to provide the regulated bipolar voltage supplies for the analog components, and voltage rails for the digital components. Figure 4.4 show the analog frontend card as it was assembled.

The mother board provided 4 slots, each slot could be populated with a different analog card, allowing the system to sample across a total of 64 channels. Configured as four linear arrays, this would allow a total of 68 electrodes and 64 adjacent differential voltage measurements. A dual digital potentiometer IC was chosen to minimize board surface area, and each card has 64 digital potentiometers just for tuning bias, gain, and center frequency. Once fully assembled, with 4 analog front end cards, a total of 256 digital potentiometers require programming. Figure 4.5 shows a fully assembled system with all four daughter

Figure 4.4: Each of the analog from end card contains 16 channels. Each channel has a programmable gain instrumentation amplifier and a programmable band-pass filter[Fri12]..

Figure 4.5: Fully assembled BEI-68 system[Fri12]..

card populated[Fri12]. To set the the potentiometers a microcontroller with a USB interface was selected. An NXP ARM Cortex-M3 LPC1768 microcontroller was placed on the motherboard and custom firmware was developed to allow the microcontroller to be flashed with a new program, and set the configuration parameter of the digital potentiometers over a SPI bus. The firmware was developed using the mbed online compiler.

The analog signals are fed out the back of the motherboard to shielded cables and digitized using a National Instruments PCIe-6323. The NI PCIe-6323 is capable of sampling across 64 different channels simultaneously at a sampling rate of 6400kSPS. Since we never exceed 1KHz exception frequency, we are well

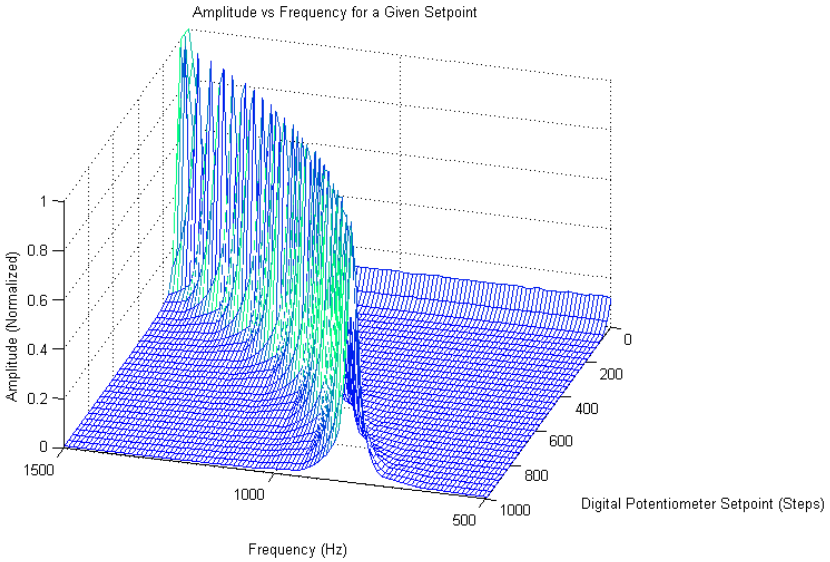

Figure 4.6: The analog front end on the BEI system has programmable bandpass filters. The frequency for each channel can be selected using the 128 programmable dual digital potentiometers. Each individual potentiometer can be programmed by the embedded microcontroller[Fri12]..

below the nyquist limit. The analog bandpass filters on the card prevent aliasing. Matlab drivers provide an interface to the data acquisition system. The host PC accessed the embedded microcontroller as a virtual serial port and the feedback from the sampled signals was used to tune the center frequencies of the bandpass filters. The schematic for the BEI-68 system as it came to be called is provided in appendix.

Since each of the 64 individual bandpass filters has a fairly high quality factor, and passive component tolerance can vary significantly, tuning the system was an essential part of getting the system to function correctly. Since the transmitter only outputs a single frequency, variations in the center frequencies between channels can result in significant attenuation. The different measured amplitudes in each channel before proper tuning are shown in figure 4.7.

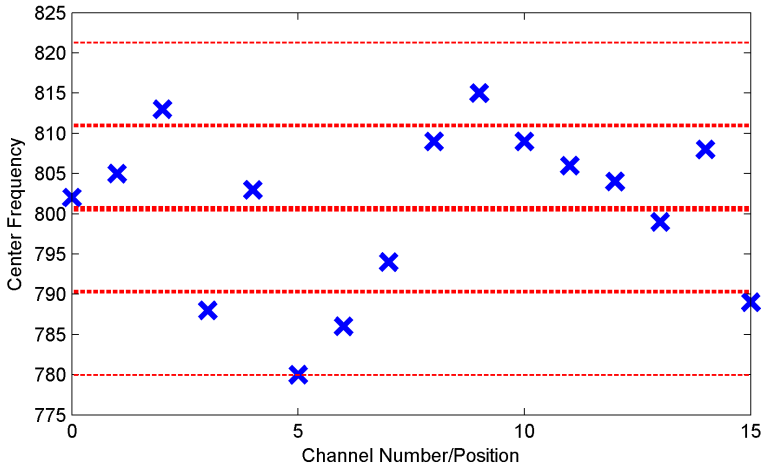

Figure 4.7: Variations in components results in different center frequencies for each channel[Fri12]..

Figure 4.6 shows the results from tuning one channel of an analog front end card. The process of tuning the system takes several minutes. The transmitter is set to a amplitude that does not saturate the analog front end. The gain is lowered on the instrumentation amplifier so that all channels have the sample gain. The digital potentiometer set point is then swept across all available steps and the amplitude of the signal is recorded. The set point that maximizes the amplitude is stored as the properly tuned value. The set points are stored on the host system so that on future tests they can be restored. A binary search algorithm was later developed to reduce the number of set points the microcontroller was required to scan.

4.3 Experimental Setup for Linear Array

A schematic of the experimental setup is shown in figure 4.8. For our linear adjacent array electrode array experiments we fixed the position of the sensor on the wall of our 30 inch long by 30 wide inch by 24 inch deep aquarium tank.

The transmit electrode and its reference electrode were placed to the left and right of the array of electrode sensors. They were placed approximately 1 inch away from each of the outer most electrodes. The distance between the transmit electrode and it reference was 14 inches. Driving the transmitter electrodes was an arbitrary wave form generator. The electrode array was placed approximately 8 inches down from the surface of the tank, this distance reduces the effect of the surface, which itself acts like a large high impedance object. To introduce a disturbance an object was attached to a 2 axis gantry. During the differential sensor experiments we used a custom built motion controller capable of moving the object around the tank to any coordinate desired. MATLAB code was written to send commands to this gantry system via a virtual serial port connection. The object used was a chrome plated steel rod with a 1.5 inch diameter. The object was scanned over the entire tank and the voltages were sampled at 6400kSPS. The amplitude of the signal was extracted for each of the 16 electrodes and stored for further processing. An image taken before data collection is show in figure 4.9.

4.4 Signal Processing

The NI PCIe-6323 were configured to sample segments of length 64. At the sampling rate of 6400 kSPS, a measurement across all 16 channels can be computed 100 times per second. Figure 4.10 shows all 16 sampled sine waves. The maximum value was extracted by doing a 64 point FFT on the signal and extracting the amplitude at the transmit frequency. Mathematically, this is equivalent to a digital lock-in amplifier. The result is the passed through an FIR filter. The FIR filter was designed to remove the DC component of the amplitudes. Figure 4.11 shows a block diagram of the moving average filter implemented in MATLAB as an FIR filter. The amplitudes are stored in a shift register, and an average

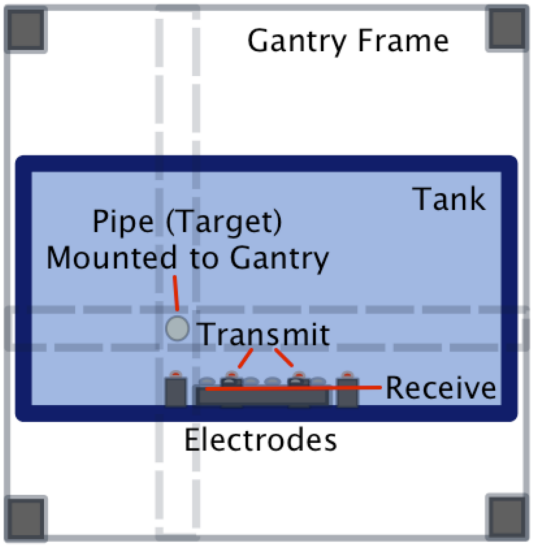

Figure 4.8: Schematic of experimental setup as viewed from top for differential sensing experiments.

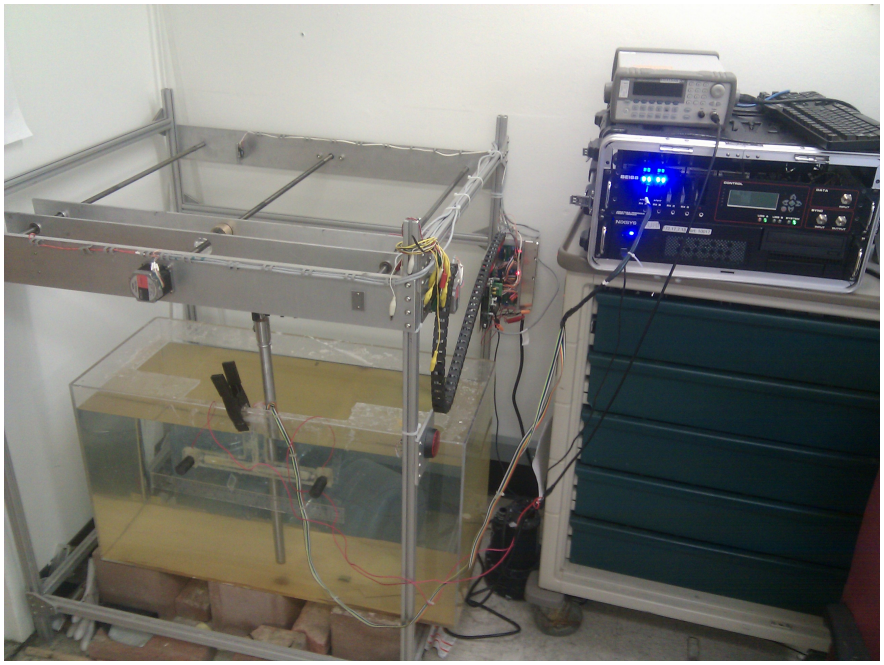

Figure 4.9: Image of front of experimental setup.

is calculated across all stored values, the *long* rolling average. A *short* rolling average is computed on only the most recent samples. The long average is then

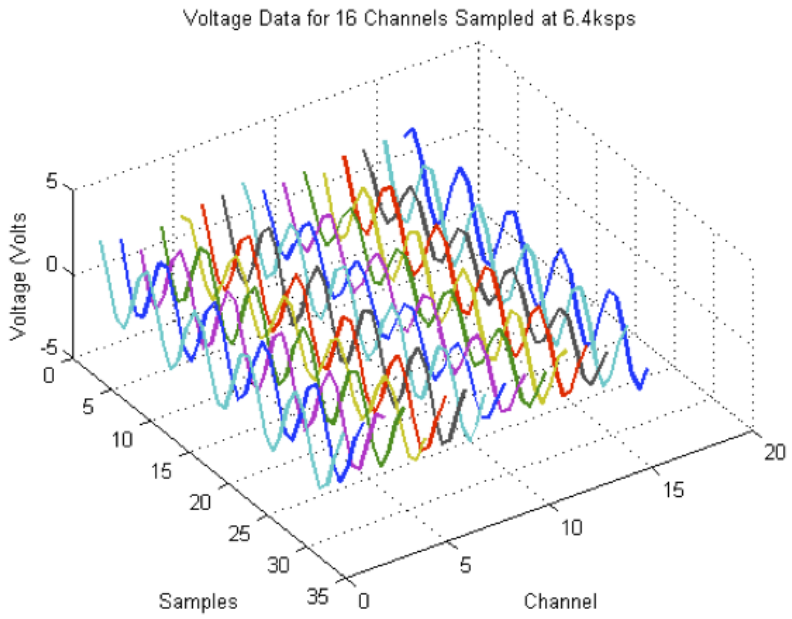

Figure 4.10: 16 Channels simultaneously sampled by the BEI system before processing.

subtracted from the short average. This filter acts on the data by removing the background and allowing our system to become *accustom* to the tank. Recent disturbances are accentuated, such as the movement of the target in the vicinity of the electrodes. By plotting a heat map of these disturbances as a function of time and electrode number you can generate images like figure 4.12. Using the *heads-up display*, a user is able to clearly differentiating when an object enters, and leaves the area nearest the electrodes. It also provides information on the location of the object, with the disturbance being strongest at the electrode closet to the target object.

By moving the object over the entire tank and recording the amplitude of each channel is is possible to build a map of the voltages versus object position. Figure 4.13 show one of the maps, plotted as a surface for the electrode pair associated with channel 8. It is interesting to note how the shape of this plot

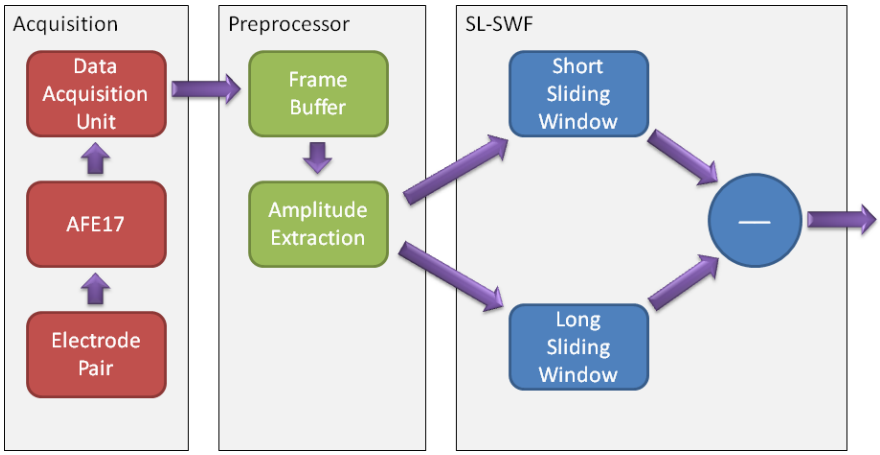

Figure 4.11: Digital signal processing flow graph for the BEI system.

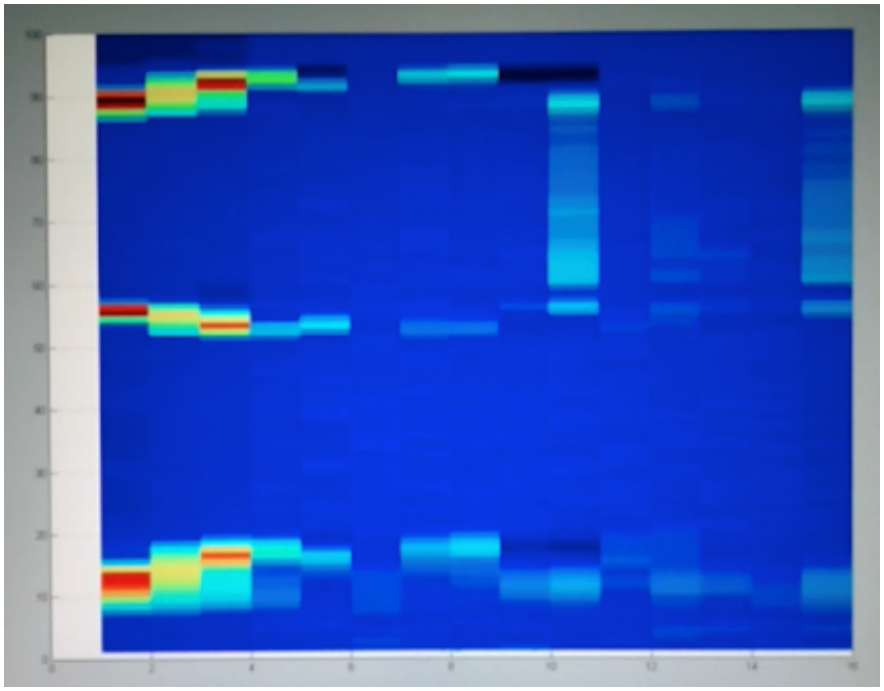

Figure 4.12: The target is swept in front of the sensor array. The vertical axis represents time. Voltage intensity is encoded in color intensity. The horizontal axis is electrode pair.

agrees with simulation. Figure 3.11 shows the same sort of inverse power relationship between amplitude and object distance from the fixed array. The left

and right lobes in simulation also appear in the measured voltage field. Changing our perspective, figure 4.14, looks down the tank perpendicular to the array, the perspective makes it easier to see the reduction in the disturbance voltage measured as the object moved farther from the array(from right to left). Applying a spacial filter removes the voltage drift that occurs with time, a high pass filter is applied to the surface plot from on electrode, figure 4.15.

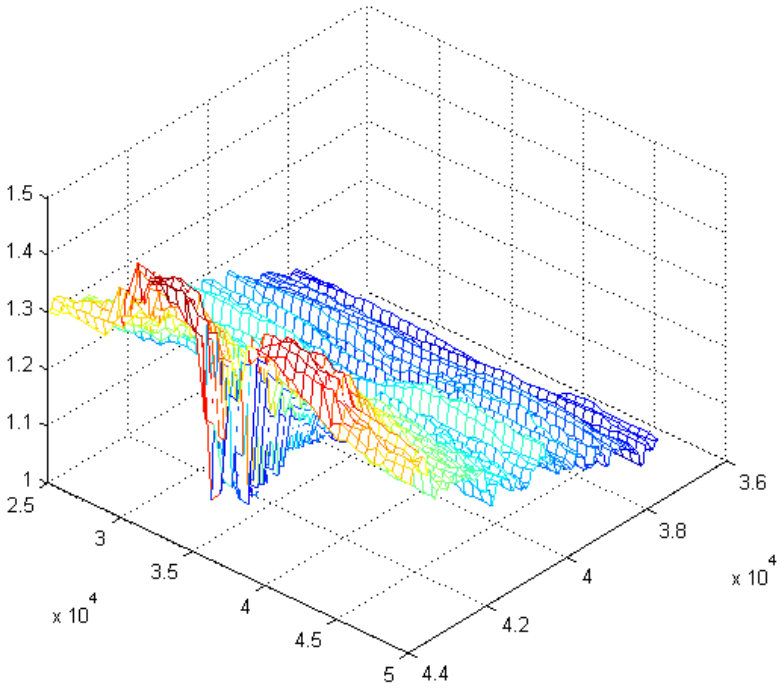

Figure 4.13: Voltage on channel 8 plotted as a function of the position of the target.

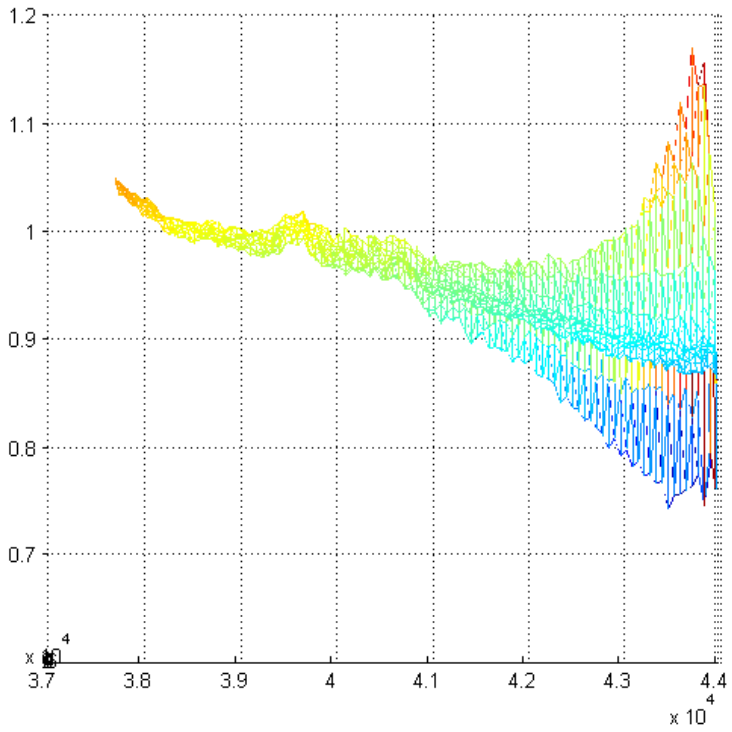

Figure 4.14: Amplitude plotted as a function of the distance between electrode channel 15 and the target object.

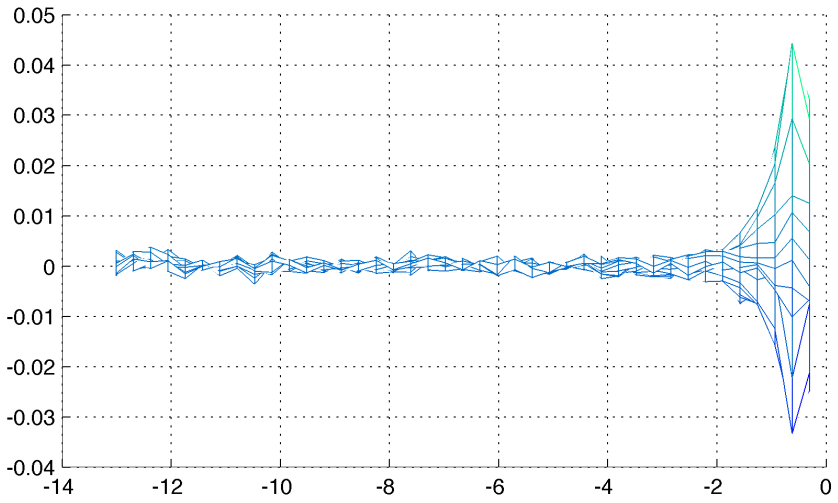

Figure 4.15: Measured amplitude of voltage at electrode pair as a function of distance.

CHAPTER 5

Design of a System for Low-side Current Sensing

In the previous chapter we discussed the results and design of a system consisting of a linear electrode array, measuring adjacent voltages in the water. The source of the voltages was an arbitrary voltage signal generator. The linear array, with its tightly packed electrodes and adjacent voltage measurements in many ways resembled the configuration of ampullae lorenzini organelles on marine predators. One major difference is that the ampullae lorenzini are normally only sensitive to DC and low frequency voltages. Looking to our discussion about electrical resistive tomography, it was recognized the maximum depth at which a geological structure could be *imaged* was a function of the distance between the electrodes [Fri]. For our linear array it is possible to compute the voltage between the outermost electrodes by summing the individual voltages between each electrode pair. Mathematically this is acceptable, since voltage is a path integral and is the same regardless of the path taken, equation 2.9. The limitation with the adjacent electrode approach is the requirement for an entire array of electrodes to sense objects at a maximum distance. Additionally, our configuration was nearly identical to the modern four electrode configurations, where one pair of electrodes is delegated to supplying current, while the others sense voltage. All of this increases the required electrode count.

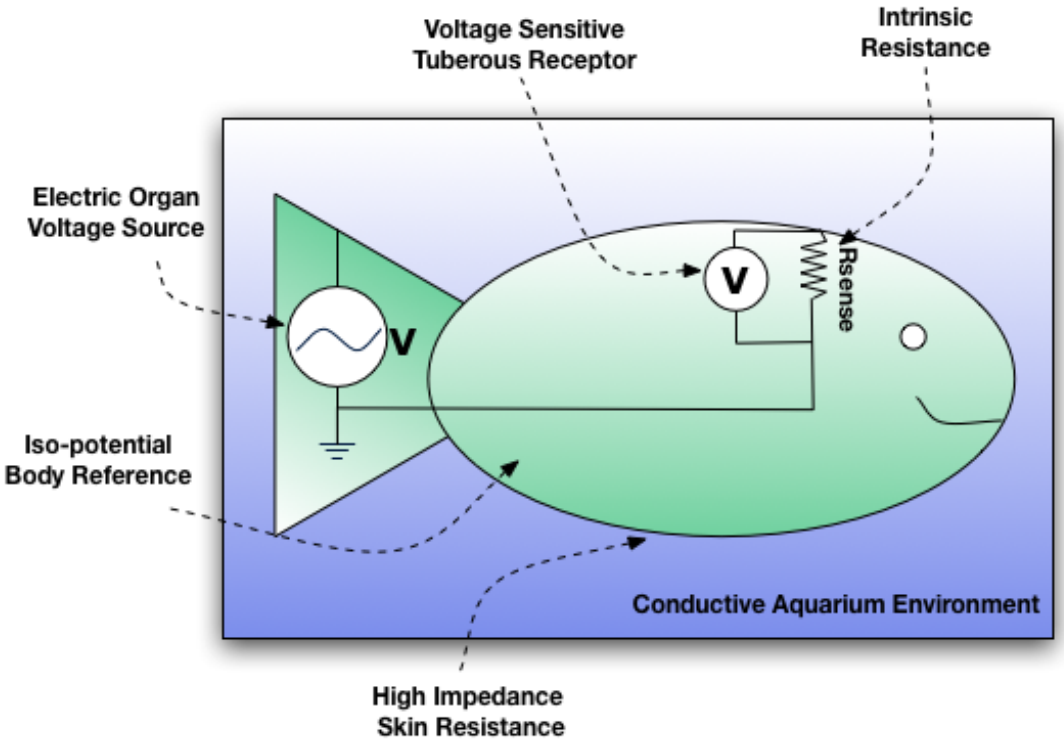

Figure 5.1: Schematic configuration of the sensory system of a weakly electric fish using lump sum circuit components.

5.1 Current Sensing in Nature

In an attempt to reduce the electrode count, and provides useful obstacle information to our robot jellyfish we again looked to biology for inspiration. It is recognized that weakly electric fish, of the assorted species that actually actively generates voltages for electrolocation, do not measure tiny adjacent voltages across the surface of their skin, instead they measure the transdermal potential that exists between their iso-potential internal body and the outside surface. These transdermal voltages are the result of the current supplied by the electric organ returning through the tuberous electroreceptors embedded along the surface of the animal in the head region.

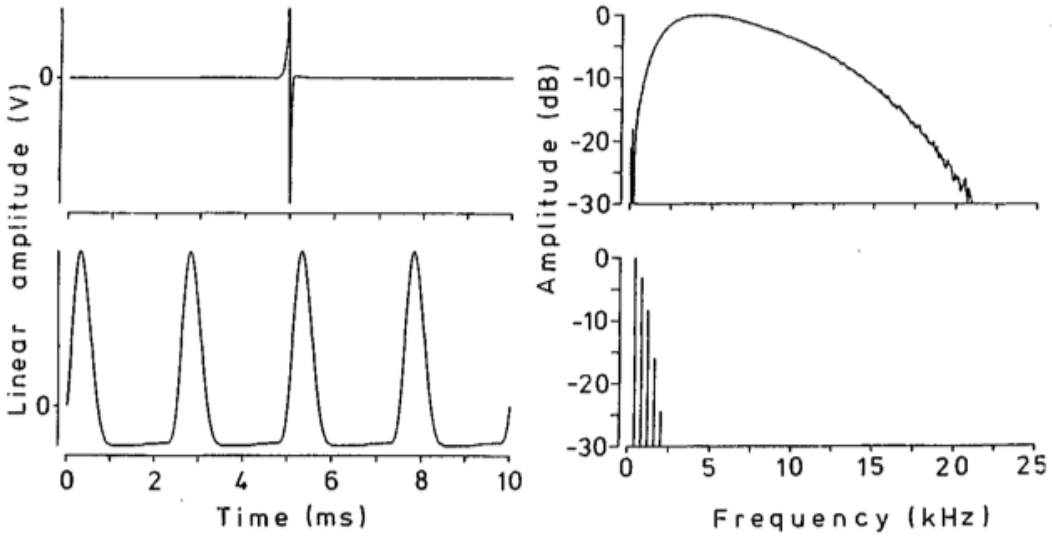

Figure 5.2: Different species of weakly electric fish can have drastically different electric organ discharge waveforms. *Top.* A pulsatile waveform the frequency response has a wide bandwidth. *Bottom.* A continuous waveform, this signal has a much narrower bandwidth. [Fer96].

While the fish and its tiny electroreceptors , along with the 3 dimensional space they inhabit would best be modeled by using a continuum, we make some assumptions to assist us in the design of a device. First we modeled the entire system using a lumped element model, which assumse the voltage sources, resistances and capacitances are confined to perfect circuit elements like resistors and voltage sources. Our simple model is shown in figure 5.1.

5.2 Continuous Voltage Source

The fish themselves do not generate perfect sine waveforms, and their signals vary among individuals and species. This variation is clear in figure 5.2 where two different waveforms from separate species of fish are depicted. The upper-left signal is from a pulsatile species, and this is clear in the fourier transform, as the

signal fills a fairly wide bandwidth, just as would be expected from the pulse source. We instead chose to build a system that closer resemble the signal in the lower-left. These continuous waveform species, have a narrow bandwidth in the frequency domain, this is seen in the lower-right spectrum narrower bandwidth. The lump circuit model was chosen to be a sinusoidal signal generator. This signal generator is placed in the tail, to model the fishes electric organ. The generator, outputs a voltage that is in direct contact with its environment through a submerged electrode.

5.3 Lump Circuit Model of an Electric Fish

We modeled the tank as some *unknown* conductive load. The reference ground is placed inside the body of the fish, this again agrees with the animals physiology, whose internal body is maintained at an isopotential. To maintain an isopotential body, the skin of the fish must be of a higher resistance.

To model the electroreceptors, we used a simple resistive element. This resistive elements is of lower value than the skin of the animal and therefore allows current to return through the skin only at this point. The action potentials themselves are generated by the voltage across the sensory cells, so in our model we placed a voltage probe across the leads of the resistor.

5.4 Low-side Current Sensing Comparison

The lump circuit model schematic depicted in figure 5.1 looks suspiciously like a classic circuit used in power management for monitoring the current usage for a system, the low-side current sensing configuration [PS12]. In power management, it is often essential to record current usage to monitor battery depletion.

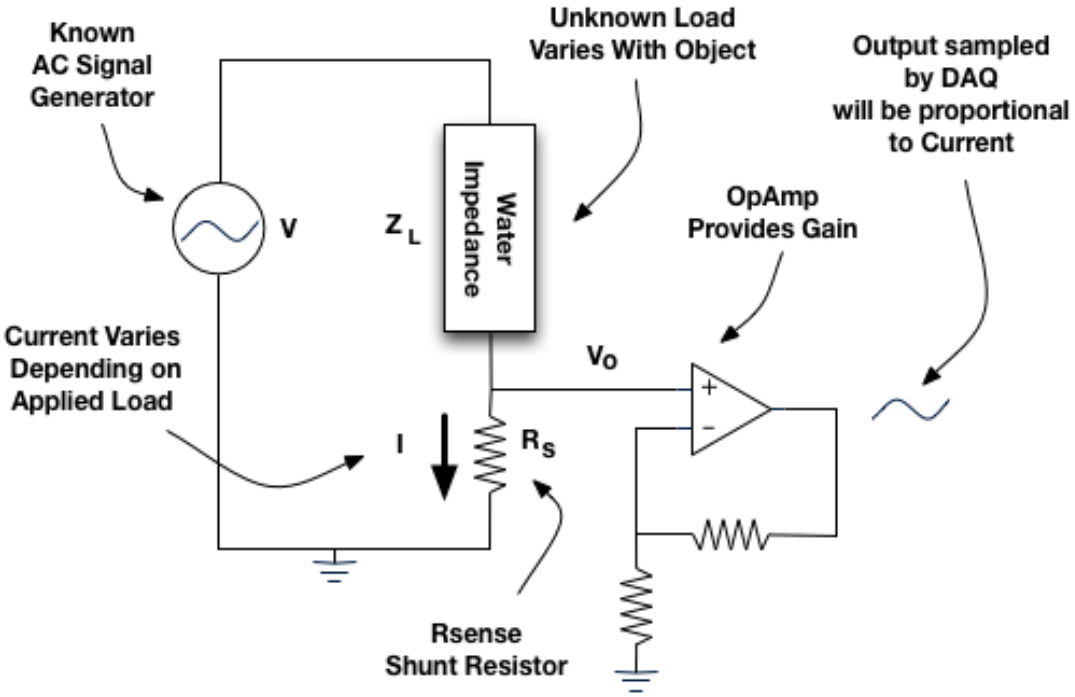

Figure 5.3: Schematic for a simple low side current sensor using only a single operational amplifier and a current shunt resistior.

Rearranging the circuit in figure 5.1 and adding a non-inverting amplifier to provide signal gain to match the dynamic range of the ADC you arrive the circuit in figure 5.4. The non-inverting amplifier also has very high input impedance preventing the sense circuit from loading the unknown load circuit.

The equation for the output voltage V_o can be generated from the classic voltage divider equation.

$$V_o = V \cdot \frac{R_{\text{sense}}}{R_{\text{sense}} + Z_L} \tag{5.1}$$

The voltage at the input of our non-inverting amplifier is V_o, while values for the input voltage V and the shunt resistor R_{sense} are selected. Setting the value

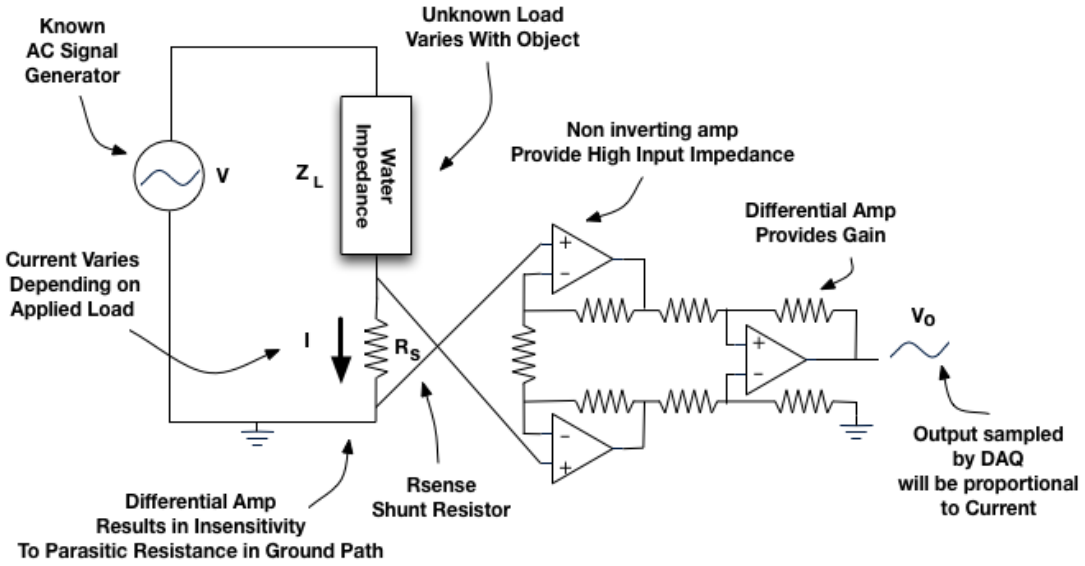

Figure 5.4: Schematic for a simple low side current sensor using only a differential amplifier and a current shunt resistior.

of the shunt resistor where $R_{\text{sense}} << Z_L$ leads the the relationship below:

$$V_o = V \cdot \frac{R_{\text{sense}}}{Z_L} \tag{5.2}$$

Rearranging and solving for Z_L:

$$Z_L = R_{\text{sense}} \cdot \frac{V}{V_o} \tag{5.3}$$

The impedance of the *load* ends up being the quantity we are interested in measuring. The voltage at the output V_o is inversely related to the impedance Z_L. From ohm's law, $V = I \cdot Z_L$, we know that the current through the circuit is a function of the impedance given a fixed voltage. Therefore by using the current sense circuit, with a known voltage, we can determine the impedance of our load, in this case the water in the aquarium and any object placed nearby our sensor.

The circuit in figure 5.4 can be improved. Notice the the sense resistor and the non-inverting amplifier use the same ground. The voltage generated by current

traveling through the sense resistor is amplified along with any residual voltage present between the lower terminal of the resistor and ground. This offset in the voltage between the ground and the lower terminal on the sense resistor is called the parasitic resistance. This resistance could be present in the traces in in PCB or any other paths that exist between the resistor and the ground on the signal generator.

To solve this problem instead of a simple operational amplifier a instrumentation amplifier was used. The instrumentation amplifier has the advantage of two non-inverting amplifiers on the input terminals giving it a very high input impedance, and therefore not loading the circuit under investigation. In addition to the two input buffers, the second stage of a instrumentation is a differential amplifier, that performs a subtraction on the inputs providing a good common mode rejection ratio. While an instrumentation amplifiers offers the advantage over ordinary differential amplifiers of having nearly infinite input impedance they have the disadvantage of not being able to deal with signals with a high common mode voltage, this is due to the limits of the power supply on the two input buffer operational amplifiers. Since we are using a transmit voltage no greater than 5 volts and most of the time less than 2 volts peak to peak, this limitation is unimportant. The power rail used for our the analog from end were +9 and -9. The configuration used in for current sense is shown in figure 5.4.

5.5 Design of a Flexible Instrumentation Amplifier Platform For Current Sensing

A second flexible analog front end was developed that allowed multiple modes of operation. Figure 5.5 shows one channel of the HammerHead amplifier board.

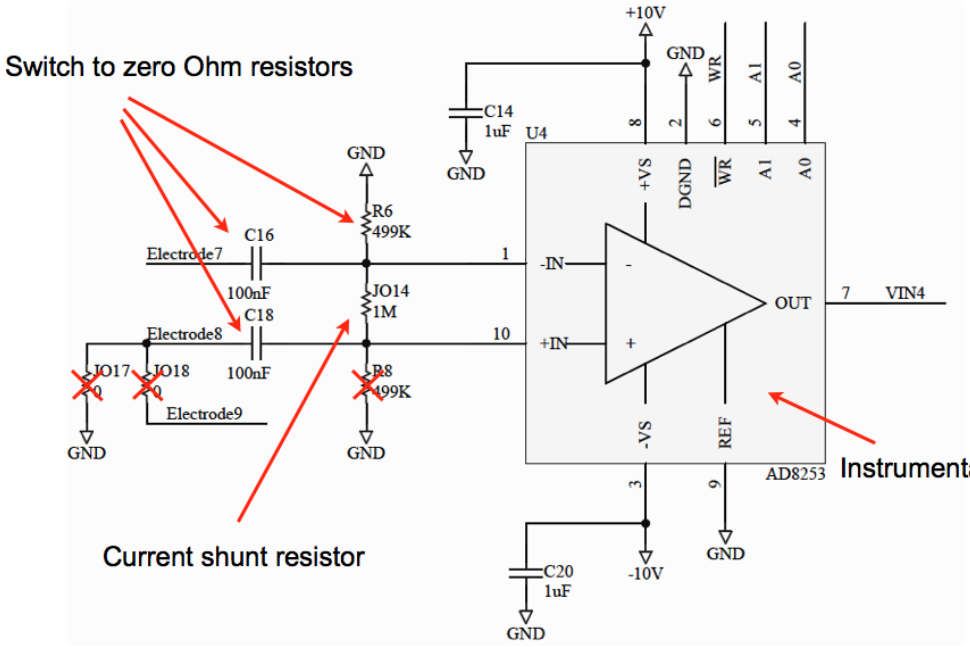

Figure 5.5: Current sense amplifier implementation on the hammerhead AFE.

This device was originally developed to duplicate the abilities of the AFE16, but with simple modifications it could be configured to act as a low-side current measurement amplifier. The modifications to allow current sensing are shown in red. The AC coupling capacitors were converted to zero ohm resistors, the 1M Ohm resistor between the inverting and non-inverting input was swapped for a 200Ohm current shunt resistor. Looking at equation 5.2 this sense resistor, controls the current to voltage gain. It should be significantly smaller than the bulk resistance of the water, measured to be approximately 60kOhms but large enough so the the voltage drop across is can be amplified adequately to be sampled. Using sense resistor that is too large can result in non-linearities in the measured impedance. A 200 Ohms resistor was selected as an adequate compromise. Resistors connecting the individual electrodes were removed as we were no longer measuring adjacent voltages.

The HammerHead amplifier board, contained 8 separate channels, the total

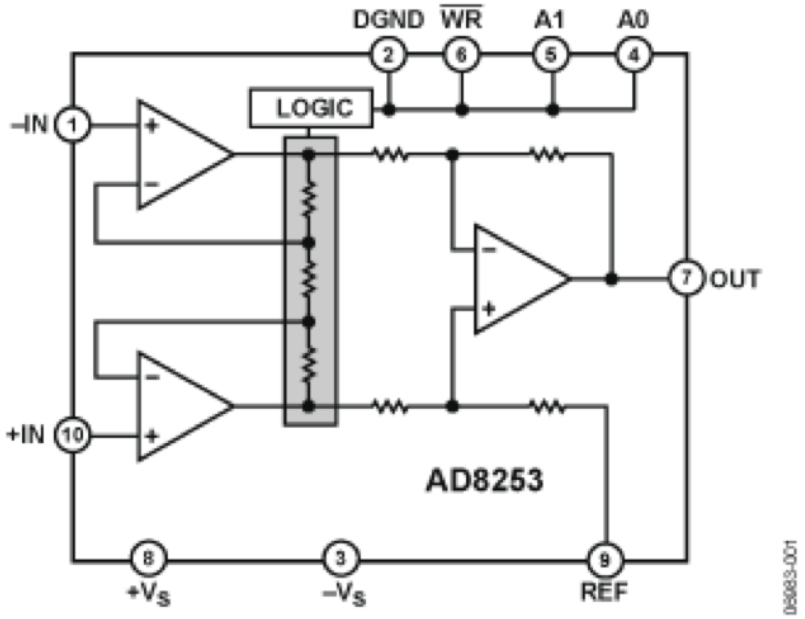

Figure 5.6: Analog devices AD8253 programmable gain instrumentation amplifier was used as a current sense amplifier on the HammerHead AFE.

board size was very small, 0.75 inch by 3 inch. Significantly smaller than the previous generation analog front end. The bandpass filter was not included since the purpose of this board was to be used in the tank and less spurious noise was present. Instead we explored the use of a digital lock-in amplifier for filtering at the transmit frequency. An Analog Devices AD8253 instrumentation amplifier was selected, figure 5.6. It has an extremely high input impedance of over a GigaOhm. The gain bandwidth product is 10MHz, this bandwidth was essential as the device has digital programmable gain of 1,10,100 or 1000. At the highest gain setting it is capable of passing a 20kHz signal, desirable as we wished to explore frequency division multiplexing, allowing multiple devices to sense in the same physical space. The previous generation system used a very high density Serial ATA data connector for connecting the device to the submerged electrodes. This made working with it more difficult, especially during early prototyping.

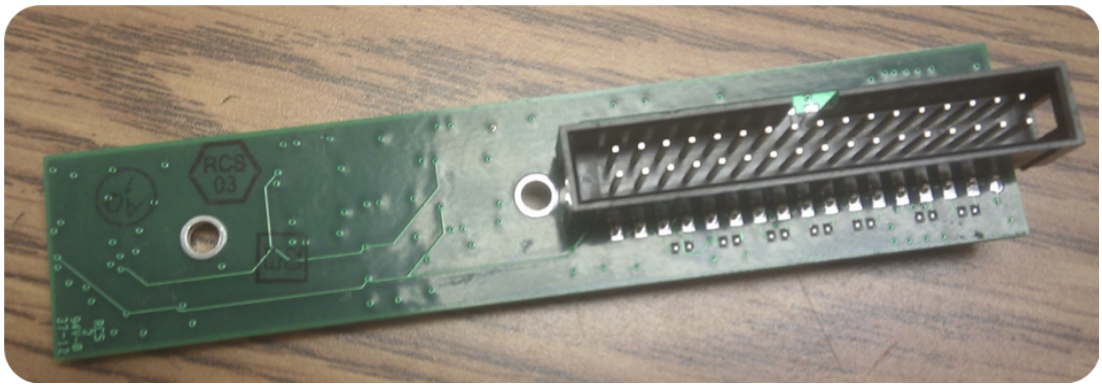

Figure 5.7: Hammerhead AFE from back, showing male header connector for electrode signals from electrode array.

Figure 5.7 shows the back-side of the HammerHead amplifier board. A standard 34 pin 0.100 inch connector was used for connecting to the electrodes. A shielded ribbon cable connected the amplifier board to the water.

A second, amplifier breakout board was designed, allowing rapid access to analog signals, and quick configuration of the gain. A smaller 0.050 pitch 24 pin connector was used to access the gain signals and the outputs of the amplifiers. The breakout board for these signals is shown in figure 5.8. A dual rail switching DC-DC regulator power supply was prototyped and used to power the analog components. The entire device could be run off of a single 9 volt battery. This 9V input power was then used to generate the +10 and -10 volt rails as well as the 3.3V digital rail.

The complete system is shown in figure 5.9. Here the we see the shielded ribbon cable, the HammerHead amplifier board, the amplifier breakout board and the DC-DC regulator. The eight current sense channels are fed through number wires to a USB based data acquisition board.

A Measurement computing USB-1608FS data acquisition device was selected. It has the capability to sample across all eight channels simultaneously. The max

Figure 5.8: Hammerhead breakout board, providing access to amplifier outputs and allows for programming of gain.

sample rate while using all eight channels is 100kSPS. This is well above the 3dB rolloff of the amplifiers when they are set to a max gain of 1000. The data acquisition system has a 16bit resolution and can have programmable range of +5 volts to -5 volts or +10 volts to -10 volts. For our purposes the range was always set to +5 volts to -5 volts.

Figure 5.10 shows the sampled signals from the 8 current sensors. The sample rate was set to the maximum of 100kSPS and a 1000 sample point window was taken. All eight channels were sampled concurrently. The amplitude of each channel was extracted using a the fast Fourier transform, figure 5.11 and then multiplying the result by a very narrow band pass signal. Before testing in the water fixed resistors were placed across each channel to ensure the each channel was functioning as expected.

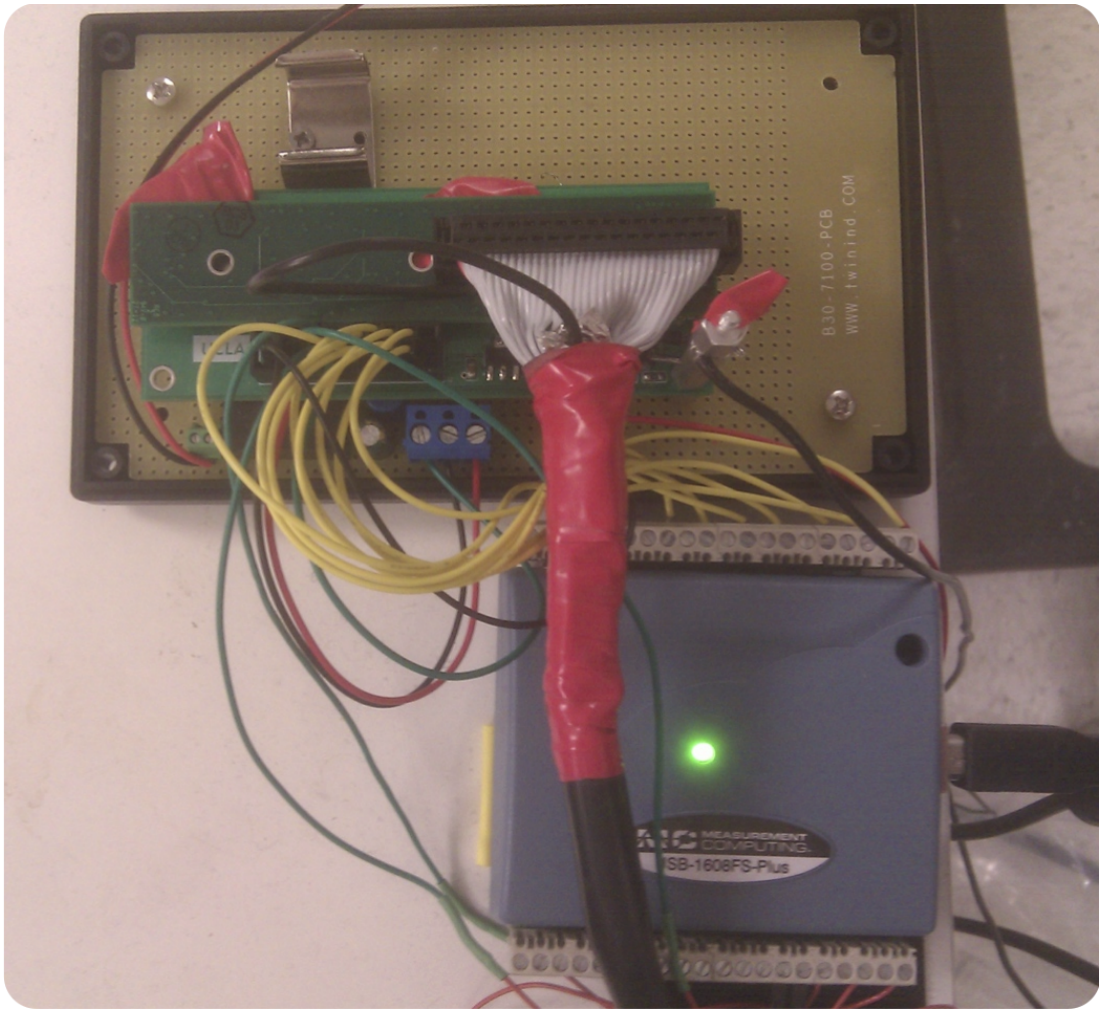

Figure 5.9: The hammerhead AFE, power supply and USB data acquisition system.

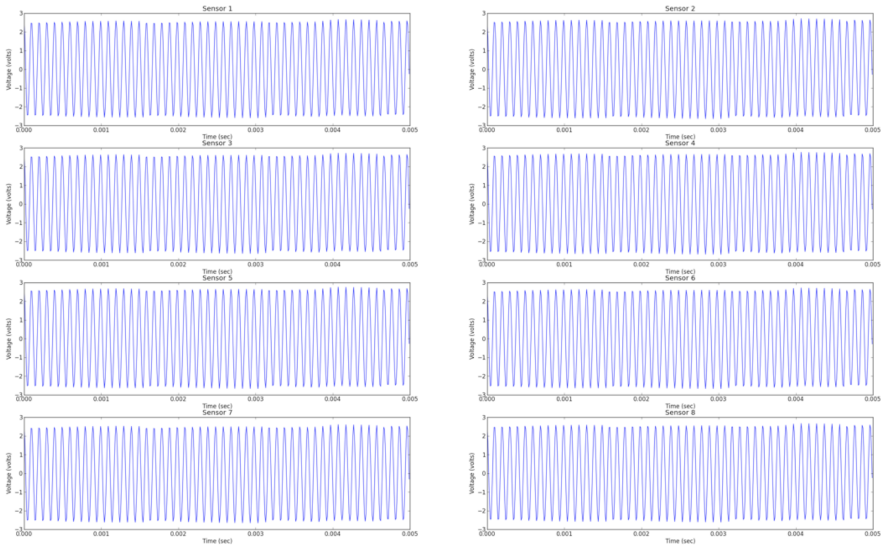

Figure 5.10: Raw sampled and unfiltered sine waveforms from all 8 current sensors. Sampled at 100kSps. Signal generator excitation voltage amplitude was set to 2Vpp, with a frequency of 10kHz.

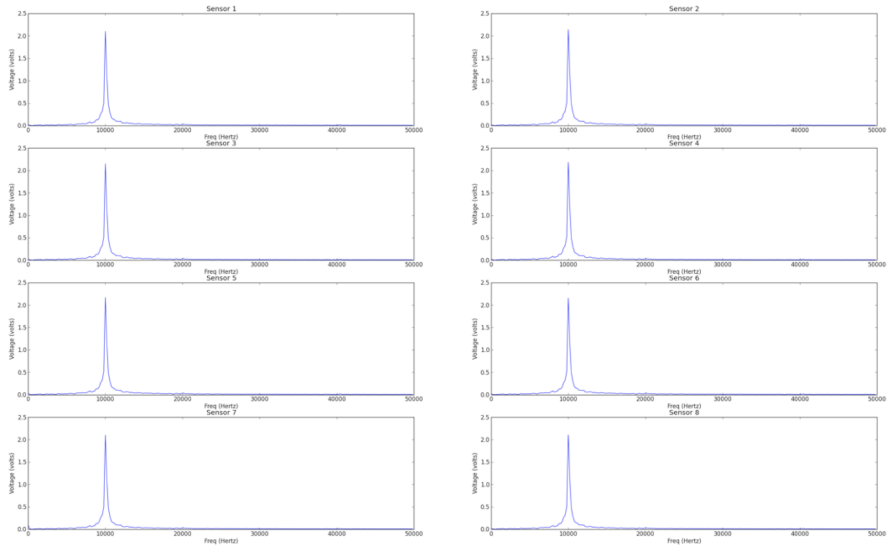

Figure 5.11: Fast fourier transform of capture signal from 8 current sensors of the hammerhead analog from end. Sampled at 100kSps with signal amplitude of 2Vpp and frequency of 10kHz.

CHAPTER 6

Design of Robot to Mimic Electric Sense of Fish

Jellyfish school in the ocean, forming enormous colonies. These colonies can be thousands strong, and yet they are able to avoid directly contacting each other. To produce a network of robots that have this type of capability would require a sensor capable of determining a direction and distance to and object, a kind of short range low power proximity sensor. We proposed using our impedance sensor strategy to sense spatial changes in the space immediately surrounding our robot and using this information to map its environment, providing feedback for manuevering. Extending this type of simple technology to allowing a sensor network of robotic jellyfish to swim in formation similar to their natural counterparts in figure 6.1 is a natural progression.

6.1 Sensor Design

Jellyfish are members of the family *Cnidarians*. These species have a natural radial symmetry. We exploited this symmetry in the design of radial sensor array. Our current-based impedance sensor is a natural fit for this type of array. Figure 6.2 shows a rendering of the Virgina Tech large Cyano jellyfish robot[ASY09]. The imagined system would have a transmitter producing a sinusoidal voltage below in the tentacle structure, shown in blue. A ring of electrosensors would be part of the construction of the device, using stainless steel hardaware, they would

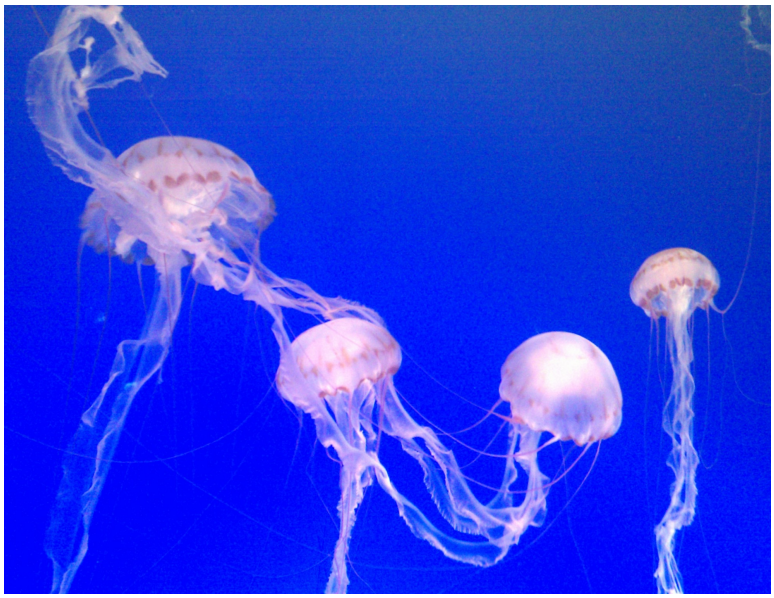

Figure 6.1: Jellyfish schooling. Jellyfish often form huge colonies and rarely collide, electrolocation is one method by which we could give artificial jellyfish robots the sensing and obstacle avoidance behavior.

be positioned around the artificial bell of the robot, shown in red. Changes in current due to spatial change in impedance cause changes in sensor readings that can be processed by our robot.

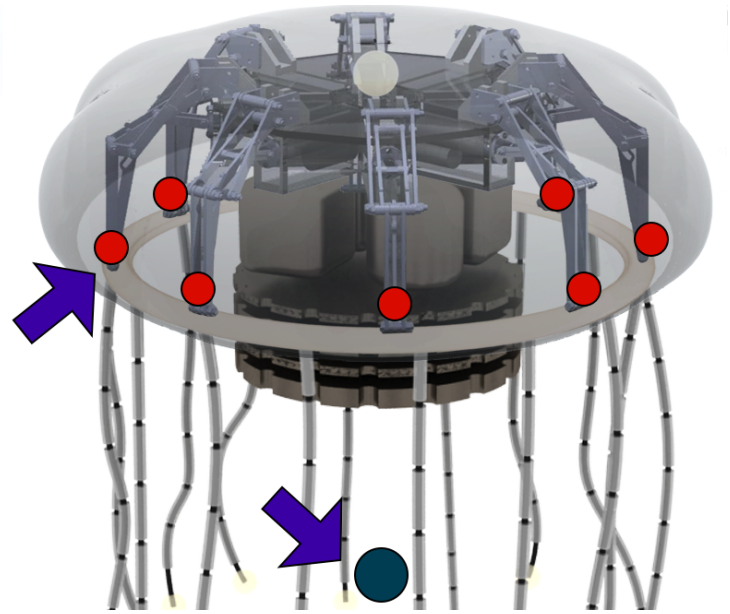

Figure 6.2: Rendering of a jellyfish robot with current sensors arranged around bell (*red*). The voltage generator sits below in the tentacles (*blue*). The configuration closely resembles the configuration of a weakly electric fish, where the electric organ is normally located on the tail, while electroreceptors are placed around the head.

The actual sensor array as it was implemented is shown in figure 6.3. It was constructed from a long PVC structural member. This vertically mounted support has the transmit electrode mounted on the lower end. The transmit electrode is internally connected to a wire that is insulated on the inside using hot melt adhesive. One end of the wire connects directly to the signal generator. The PVC support member is wrapped with a neoprene jacked that acts as a high impedance skin. It also provides a compressible material to maintain the position of the current sensor electrodes. The radial electrode array was prototyped using acrylic plastic and a laminate design, shown in figure 6.3. It has a 3 inch diameter.

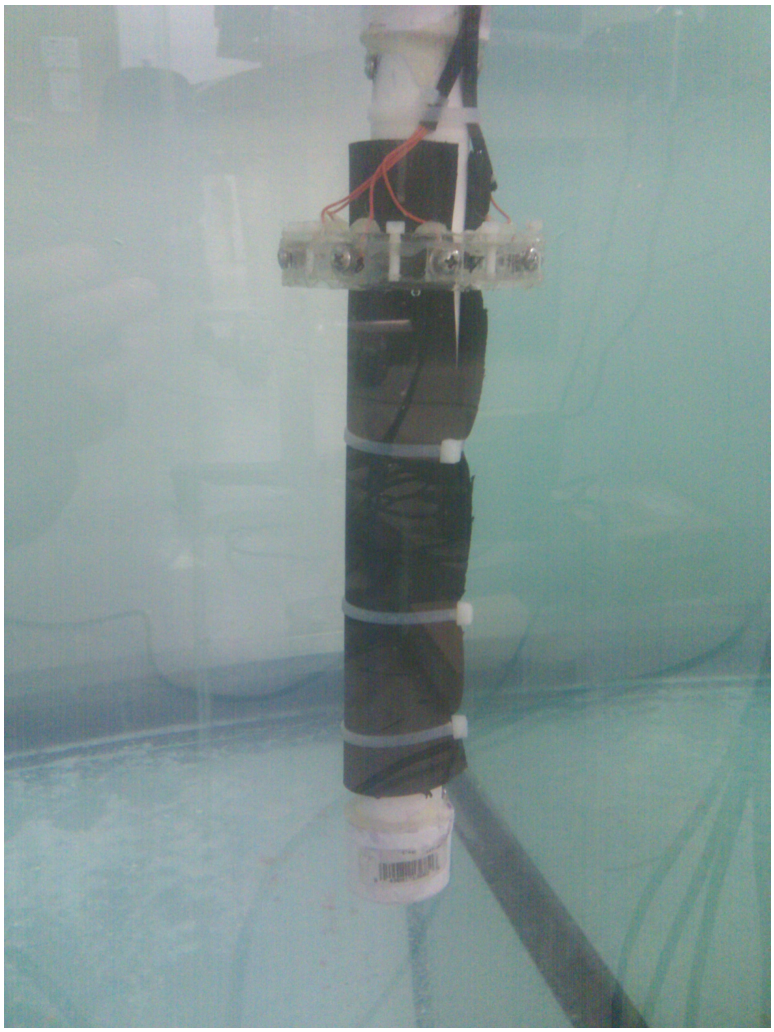

Figure 6.3: The electrode current sensor arranged to provide object detection and proximity sensing to a jellyfish robot.

Eight stainless steel screws protrude from the radial array. These stainless steel screws act as the electrodes, and are equally spaced around the circumference of the electrode array. Each electrode then connects to an insulated cable bus that comes out of the water and interfaces with a custom electrode breakout PCB. These eight wires connect to the the 34-pin 100 mil shielded cable and then connet directly to the current sensor amplifiers and current sense shunt

resistors.

The voltage from the signal generator is applied to the conducting water via the transmit electrode in the analog tentacle structure, the resulting current returns through each of the 8 shunt resistors which produces a sampled voltage that is proportional to impedance of the environment near each electrode.

6.2 System Architecture

The software architecture is a shown as a block diagram in figure 6.4.

Figure 6.4: System block diagram showing the flow of information through the system. Current reading are read by the electrodes in the tank and conditioned by the hammerhead AFE. The analog signals are then digitized a measurement computing USB-1608FS. A server streams the data to clients who can access the samples over the network and provide feedback to the motion control unit, powered by another server running LinuxCNC.

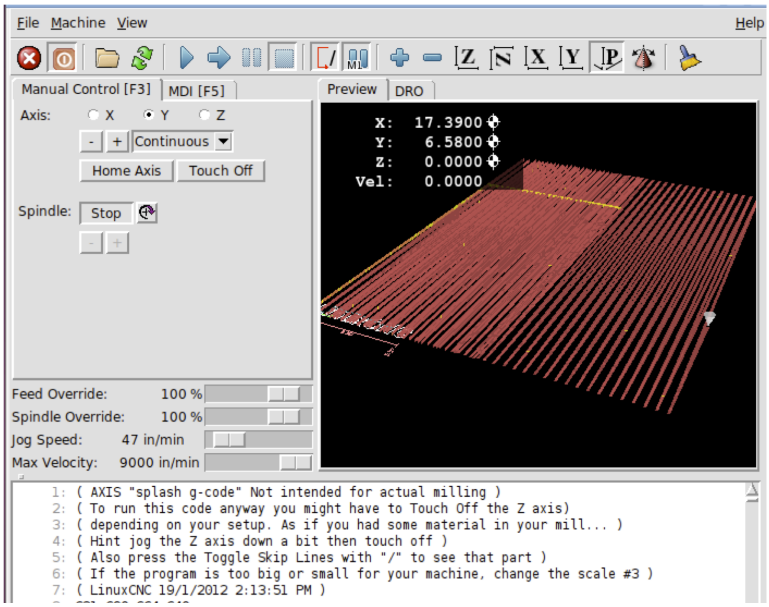

Figure 6.5: LinuxCNC allows for complex motion control. Commands for the robot are sent via a python module communicating with the emc linux telnet shell.

A voltage source is applied to the tank, and the resulting signals are sensed and amplified by the HammerHead amplifier board. The USB-1608FS data acquisition device (DAQ) from Measurement computing samples the data at the maximum sampling rate. Data is read from the DAQ using a custom C++ program written using the LibUSB user space USB library. This software runs on a host computer, and puts the sampled data into a linear matrix for further processing. Additional matrix operations are run on the data using the EIGEN linear algebra library. The data can also be run through a FFT should the user decide to do this on the host server PC. Once the data is preprocessed it is sent to clients using the ZeroMQ message passing library. Any number of client PCs running a python script can subscribe to the ZeroMQ message server and receive the packets of data in near realtime for further processing. It is on this client that

the amplitude of the signal is extracted, but there is an option to do this on the server where the process is more optimized. The ability to read the raw sample on the client allows for easier modifications to the signal processing algorithms. The processed signal can then be used to make decisions about probe trajectories. The original motion controller used in the adjacent voltage measurement experiments was inadequate for doing complex maneuvers. It was replaced with a Gecko g540 4 axis stepper motor controller of which only two channels were used. Motion of the gantry system was controlled by a x86 pc running LinuxCNC, figure 6.5. This software made it possible to send commands over the network using a socket interface. The client then send G-codes directly to the controller PC to request maneuvers.

6.3 Proximity Detection

An overhead schematic of the tank shows the radial sensor in the center of the tank, figure 6.6 The gantry is placed over the top of the tank and can move the sensor anywhere in the 2D space.

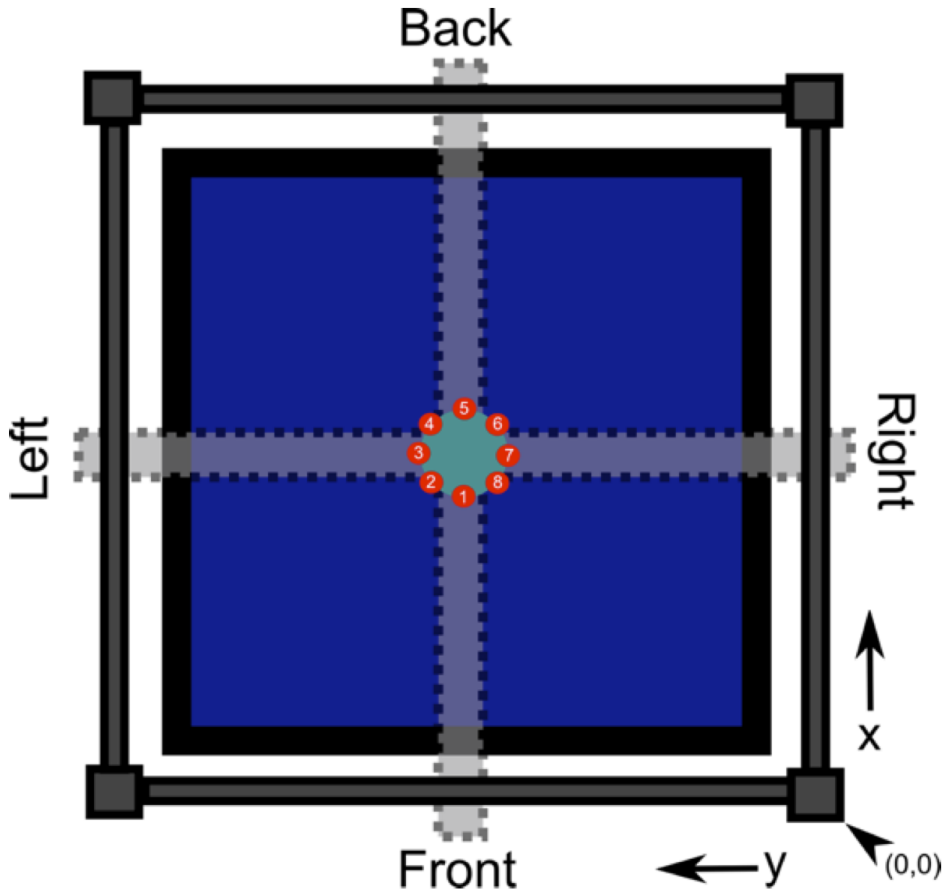

Figure 6.6: Schematic showing experimental setup from top. Gantry allows movement of radial sensor array in tank.

At the beginning of an experiment the sensor acquires information about the background, it does this by first moving to the center of the tank at the farthest point from any of the walls. A total of 200 samples were taken during the acquisition of the homogenous environment. Each sample involves taking a 500 point window of data and extracting the amplitude of the sampled sine wave. The average of all 200 amplitudes is computed for each channel. These eight background data points are then subtracted from all subsequent measurements. Figure 6.7 shows an acquired sample at the center of the tank after background

subtraction results. The schematic on the right of the image shows the probe placement. The left plot is a radar plot, the positive amplitude of each sensor is shown in the direction of each sensor. The result is that for each sensor the center of the tank has a near zero amplitude.

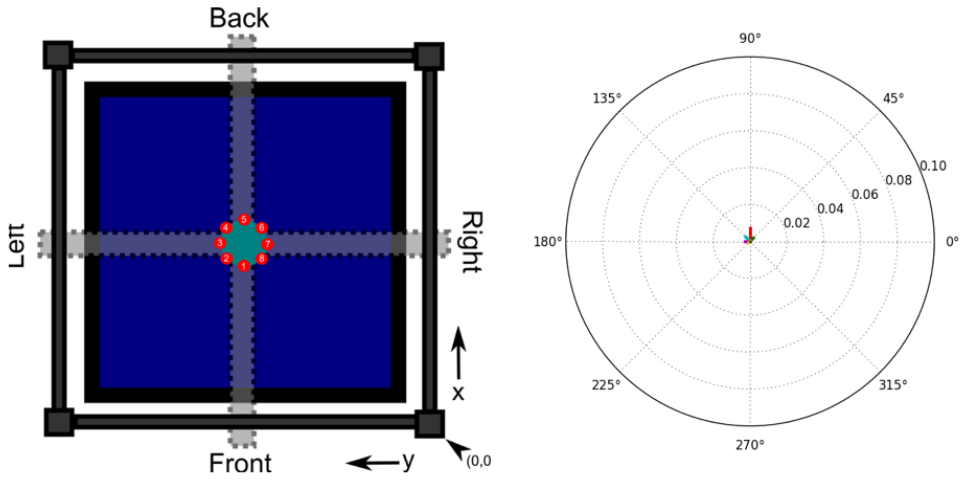

Figure 6.7: Radar plot showing magnitude of sensor reading at center of tank, with no nearby objects.

The sensor readings change when we move around the extents of the tank. In the front right corner we are near two walls, the front wall and the right wall. The objects are located at 0 deg and 270 deg These walls are very large, non-conductive glass objects. As we move close to the wall, current can not flow as easily in the space between the wall and the sensor and instead more current flows to the sensors farther away from the non-conducting objects, in this case to the sensor at 135 deg, figure 6.8.

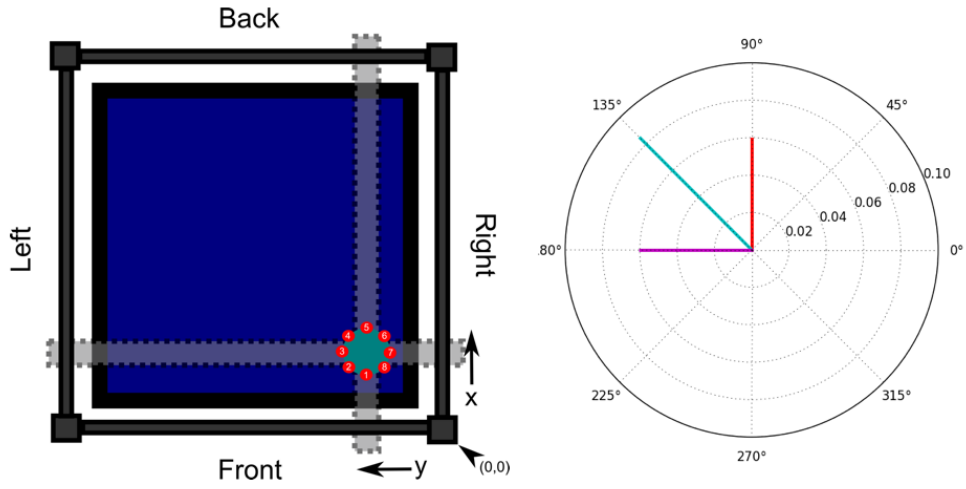

Figure 6.8: Radar plot showing sensor near right-front corner of tank. Note the directional magnitude of the reading, clearly showing the effectiveness of the sensor for proximity sensing and obstacle avoidance.

In the left-back corner of the tank, the non-conducting objects are now placed at 90 deg and 180 deg. Moving close to the wall limits the current that can flow to sensors, 3, 4 and 5. Instead more current flows into sensors, 1, 7 and 8, in the 315 deg direction,. figure 6.9.

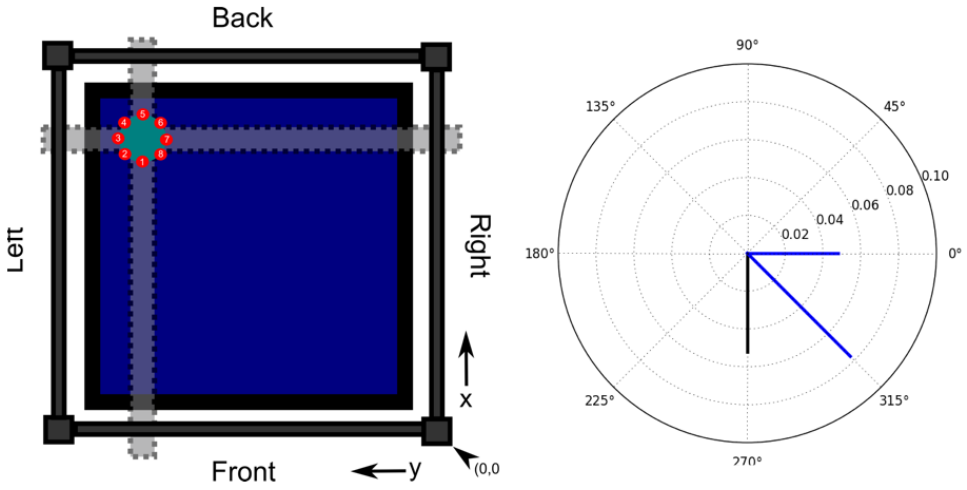

Figure 6.9: Radar plot showing sensor near left-back corner of tank. Note the directional magnitude of the reading, clearly showing a different direction than in .

The sensor has the ability to identify the direction of an approaching object. Geometry, material and distance are encoded in the amplitudes of the resulting signals, while direction is encoded in the relative amplitudes between electrodes.

6.4 Equivalent Resistance and Object Detection

For robotic jellyfish robot, the ability to avoid an obstacle, is an expected behavior, a collision could damage instrumentation and lead to a non-operational state. The detection limit of the system was explored by approaching a very large object, in this case the wall of the tank. The wall is composed of glass, a material with a low conductivity, and therefore an obstacle of high impedance. Since the voltage sampled in every channel is proportional to the current returning through the corresponding electrode, and therefore according to Ohm's law a measurement of the resistance of the region between the electrode and transmitter, we can

call the measured impedance the *equivalent impedance*. The *equivalent impedance* refers to replacing the water and space between electrodes with lump circuit of the same impedance value.

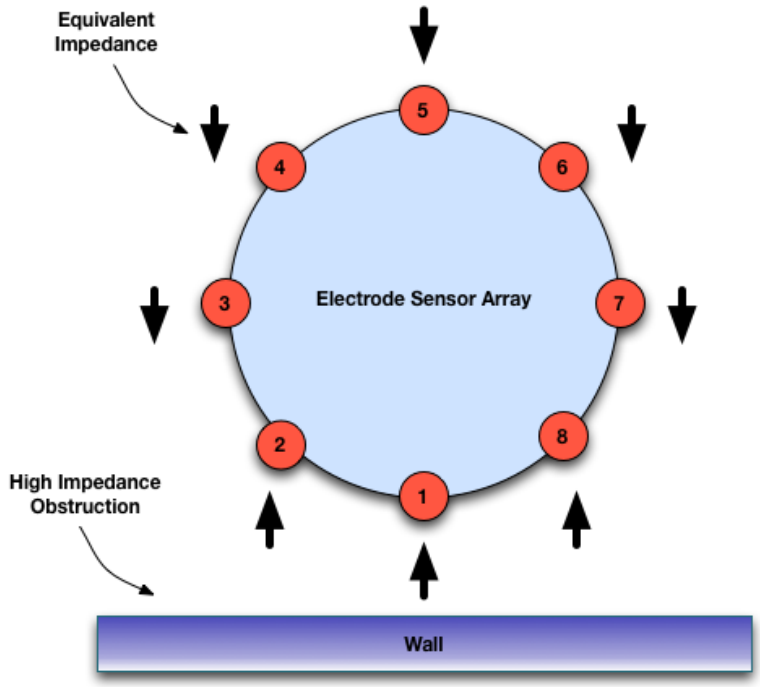

Figure 6.10: Schematic showing the expected change in equivalent impedance as the sensor array approaches a non-conductive (high impedance) object.

Looking at figure 6.10, the electrode array is approaching a wall. The water has a resistance less than the wall. As we approach the wall, the wall causes a reduction in the regions conductivity, and therefore an increase in the resistance. Electrodes closest to the approaching wall will have a marked increase in the equivalent resistance, while those away, will have a reduction, as more current flows away from the wall. Note that the voltage remains constant, since the signal generator outputs a continuous voltage of the same amplitude.

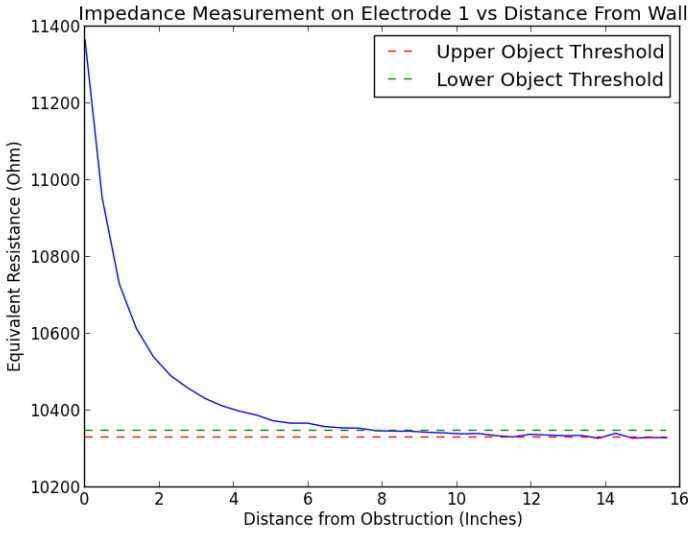

Figure 6.11: Measured equivalent impedance by electrode 1 versus distance from a large non-conducting object.

In figure 6.10 electrodes 1, 2 and 8 are closest to the wall during an approach and so see an increase in the impedance. Electrode 1 is the *near* electrode and therefore see the largest increase in equivalent impedance, this increase is visible in figure 6.11. As discussed previously, the magnitude follows an inverse power law with the distance. Figures 6.11, 6.12 and 6.18 all experience a decrease in returning current due to the rising equivalent resistance.

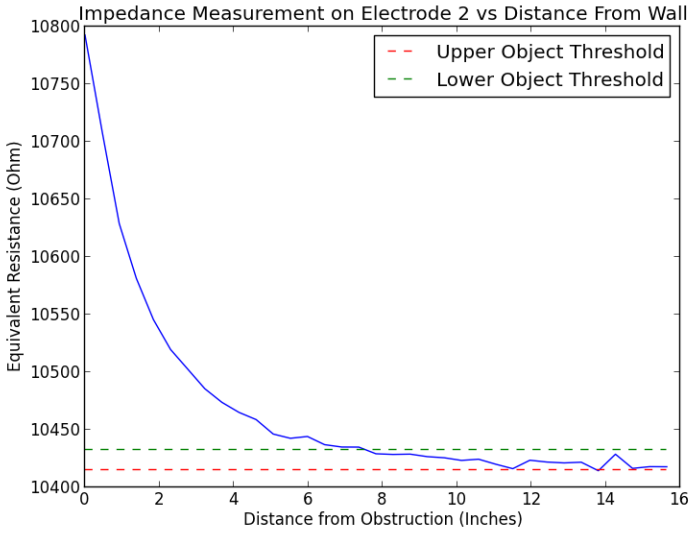

Figure 6.12: Measured equivalent impedance by electrode 2 versus distance from a large non-conducting object.

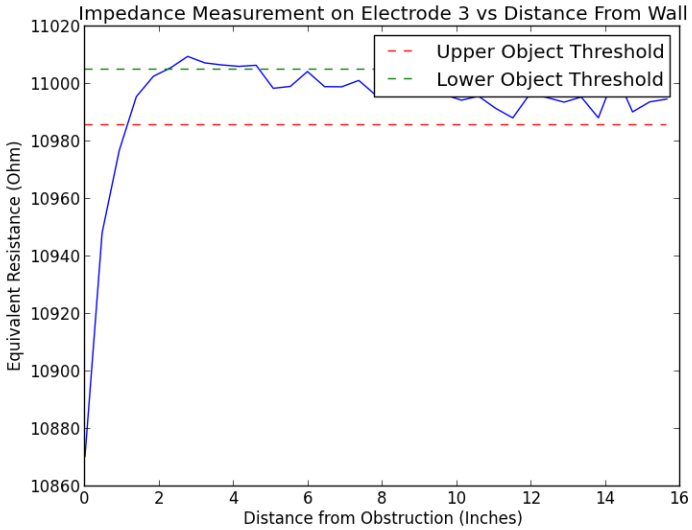

Figure 6.13: Measured equivalent impedance by electrode 3 versus distance from a large non-conducting object.

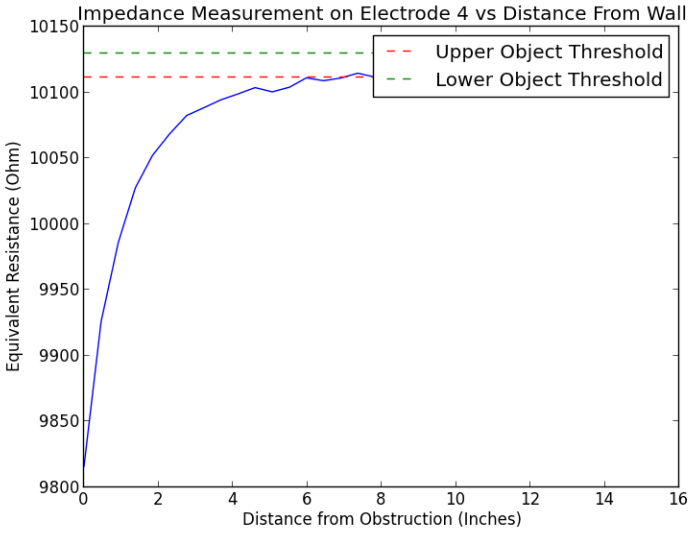

Figure 6.14: Measured equivalent impedance by electrode 4 versus distance from a large non-conducting object.

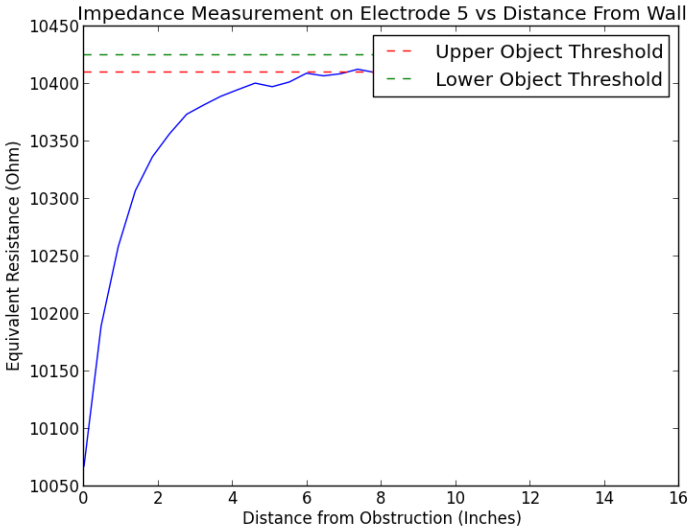

Figure 6.15: Measured equivalent impedance by electrode 5 versus distance from a large non-conducting object.

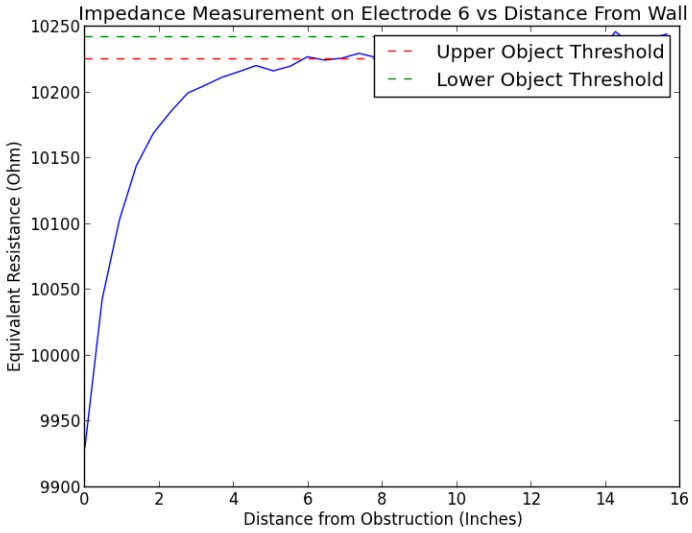

Figure 6.16: Measured equivalent impedance by electrode 6 versus distance from a large non-conducting object.

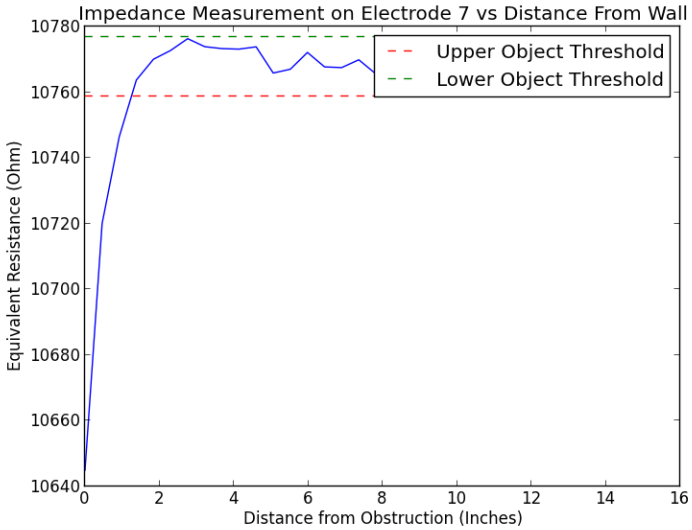

Figure 6.17: Measured Equivalent impedance by electrode 7 versus distance from a large non-conducting object.

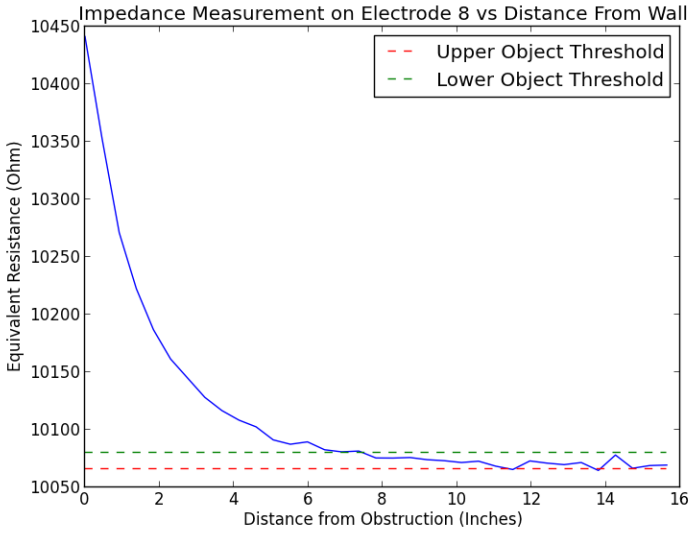

Figure 6.18: Measured Equivalent impedance by electrode 8 versus distance from a large non-conducting object.

The remaining electrodes 3, 4, 5, 6, and 7 are located away from the wall and see a reduction in the equivalent resistance. These reductions are clear in the figures 6.13, 6.14, 6.15, 6.16 and 6.17. Electrode 5 in figure 6.15 deserves additional scrutiny as it shows a very signifiant increase in current, as current flows in a direction away from the wall.

A nearly identical pattern is seen as we approach target on the right. Electrode 6, 7, and 8, shown in fugues 6.25, 6.26 and 6.27 now see a marked increase in equivalent resistance, while the remaining electrodes see a decrease as in figures 6.20, 6.21, 6.22, 6.23,and 6.24.

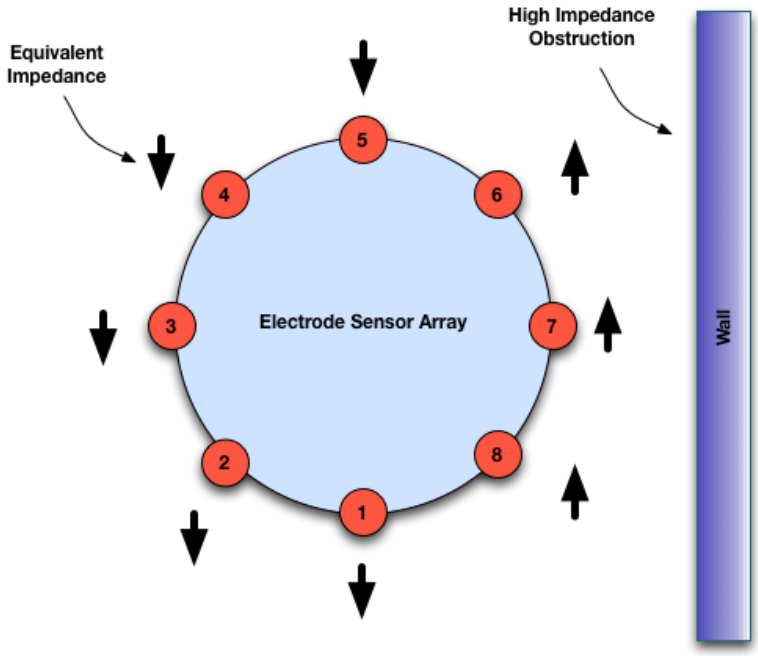

Figure 6.19: Schematic showing the expected change in equivalent impedance as the sensor array approaches a non-conductive (high impedance) object, this the object is on the left.

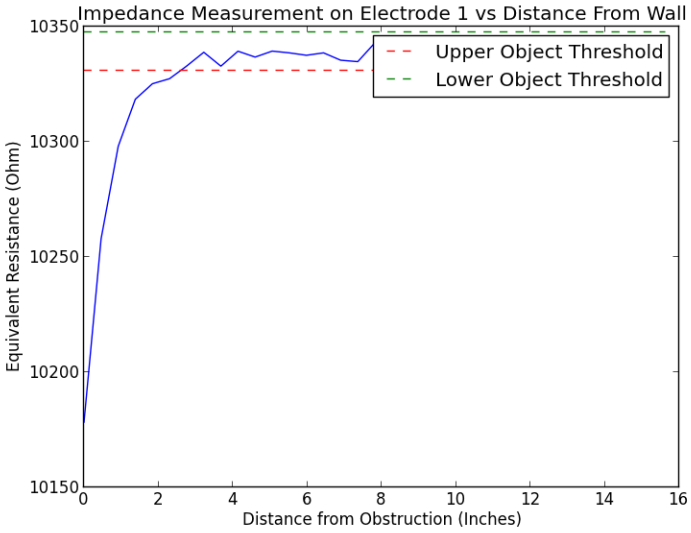

Figure 6.20: Measured equivalent impedance by electrode 1 versus distance from a large non-conducting object approaching on right.

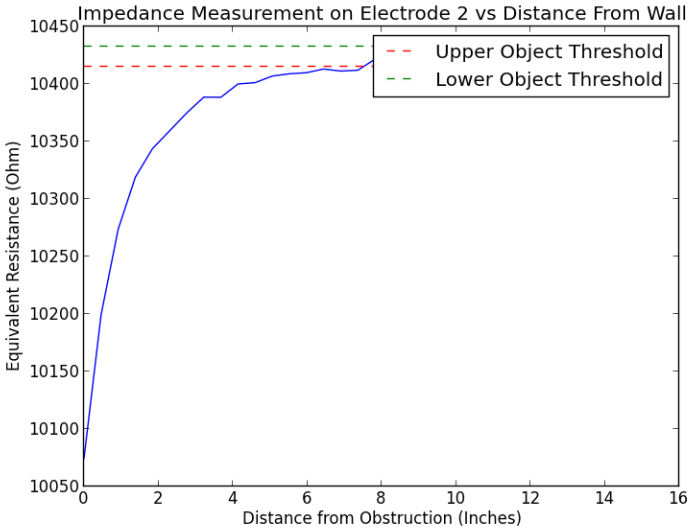

Figure 6.21: Measured equivalent impedance by electrode 2 versus distance from a large non-conducting object approaching on right.

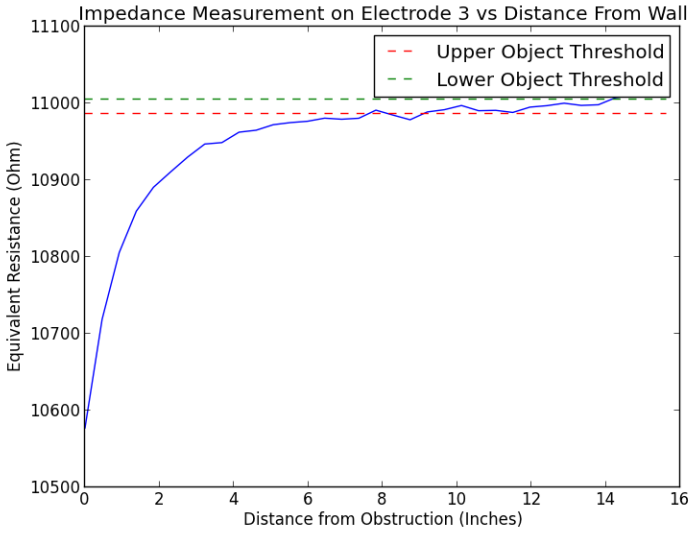

Figure 6.22: Measured equivalent impedance by electrode 3 versus distance from a large non-conducting object approaching on right.

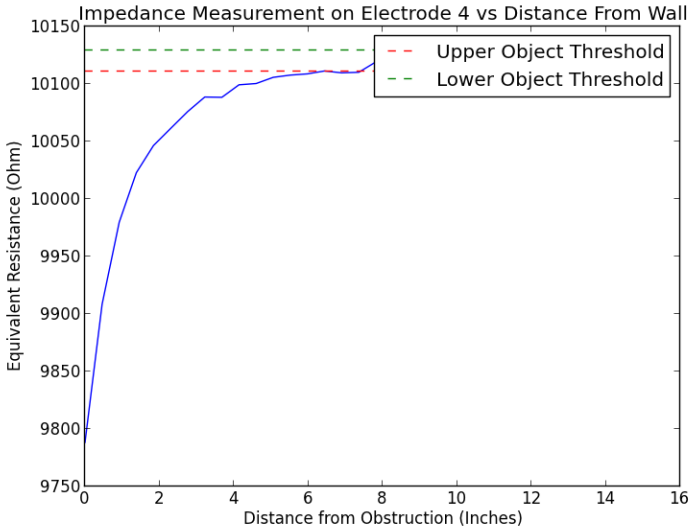

Figure 6.23: Measured equivalent impedance by electrode 4 versus distance from a large non-conducting object approaching on right.

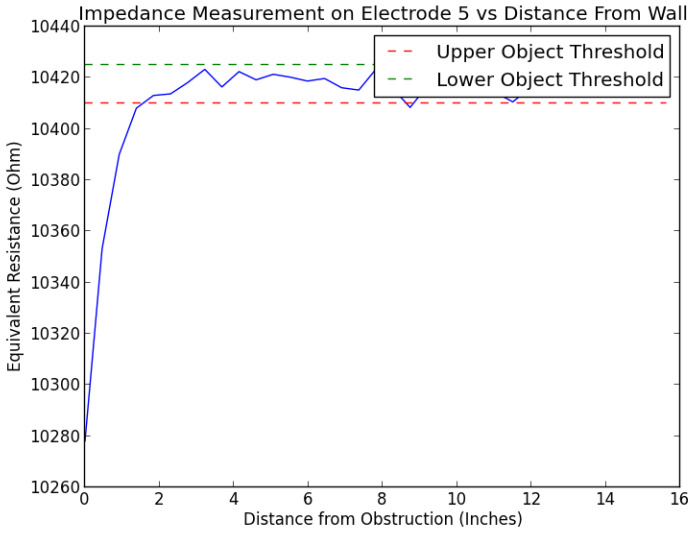

Figure 6.24: Measured equivalent impedance by electrode 5 versus distance from a large non-conducting object approaching on right.

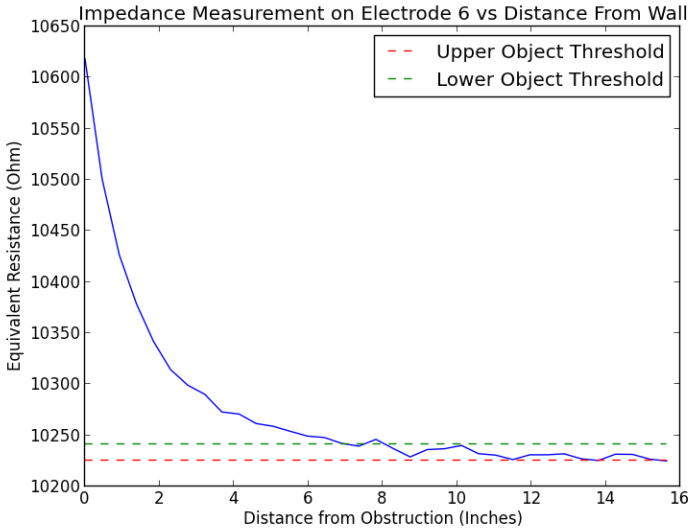

Figure 6.25: Measured equivalent impedance by electrode 6 versus distance from a large non-conducting object approaching on right.

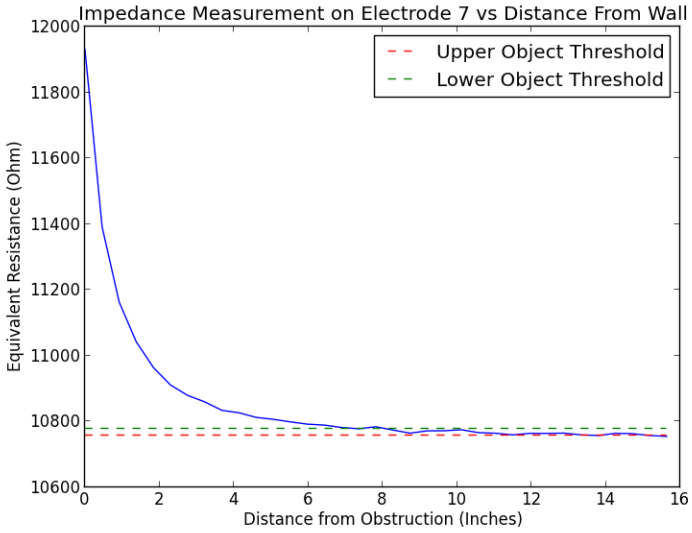

Figure 6.26: Measured Equivalent impedance by electrode 7 versus distance from a large non-conducting object approaching on right.

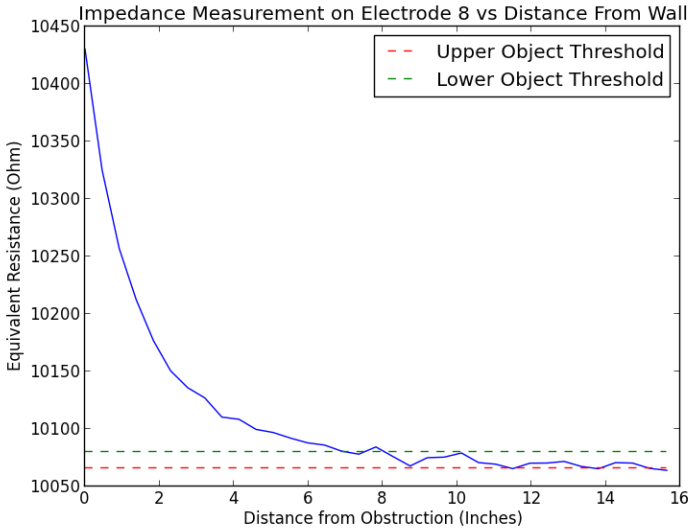

Figure 6.27: Measured equivalent impedance by electrode 8 versus distance from a large non-conducting object approaching on right.

Electrode	Mean	Standard Deviation
Electrode 1	10339.01 Ohms	4.13 Ohms
Electrode 2	10423.59 Ohms	4.31 Ohms
Electrode 3	10995.47 Ohms	4.82 Ohms
Electrode 4	10120.23 Ohms	4.58 Ohms
Electrode 5	10417.50 Ohms	3.77 Ohms
Electrode 6	10233.49 Ohms	4.08 Ohms
Electrode 7	10767.74 Ohms	4.51 Ohms
Electrode 8	10072.97 Ohms	3.70 Ohms

Table 6.1: Statistics on 800 samples taken in the center of the tank, at least 9 inches from the walls, with no object or nearby obstructions.

6.5 Maximum Range of Sensor

When computing the maximum detection range of our sensor first it was important to compute a noise floor for each of the individual channels. The sensor was scanned in the center of the tank in a 6 inch area. Each impedance measurement consisted of 1000 samples taken at 100,000 kSPS. The amplitude was computed on each sampled waveform. A total of 100 impedance measurements were taken at each position, consequently each sample took 1sec to complete. A total of 800 samples were taken in the middle of the tank, at a minimum distance of 9 inches from the walls. In this way the effects of objects and obstructions were minimized. Table 6.1 show the results from computing statistics on the all eight channels.

Electrode ID	Maximum Detectable Range
Electrode 1	8.28 inches
Electrode 2	7.82 inches
Electrode 3	1.38 inches
Electrode 4	5.98 inches
Electrode 5	7.36 inches
Electrode 6	5.98 inches
Electrode 7	1.38 inches
Electrode 8	7.82 inches

Table 6.2: Range of detection for the radial electrode sensor as it approaches a very large object such as a wall. The distance between transmit electrode and the receive electrodes is 12 inches. Closest electrode is electrode 1.

Upper and lower thresholds were set using the measured standard deviations, calculated from the previous experiment. Thresholds were set at 2 standard deviations from the mean *background* measurements. In each of the above figures, a green *upper threshold* and red *lower threshold* are plotted. In this way it is possible to say that with 95% certainty the measured impedance is different from the background measurement, suggesting that an object has entered the vicinity.

From these thresholds it is possible to measure maximum detectable range with 95% certainty. These ranges are shown in table 6.2.

This assumes the sensor array approaches the wall with electrode 1 oriented so that it is closest. The results differ slightly if the electrode array approaches a wall with a different sensor. Table 6.3 shows the results if we rotate the sensor and approach the wall with electrode 7 closest.

Electrode ID	Maximum Detectable Range
Electrode 1	2.76 inches
Electrode 2	7.82 inches
Electrode 3	7.82 inches
Electrode 4	6.44 inches
Electrode 5	1.84 inches
Electrode 6	7.36 inches
Electrode 7	8.82 inches
Electrode 8	7.36 inches

Table 6.3: Range of detection for the radial electrode sensor as it approaches a very large object such as a wall. The distance between transmit electrode and the receive electrodes is 12 inches. Closest electrode is electrode 7.

There are a couple of interesting results to take note of, including the fact that the electrodes orthogonal to the closest electrodes always give the worst detection range. This is because the current distribution is altered the least in the orthogonal direction. The maximum detectable range for the sensor configuration, was approximately 8 inches. Even sensors away from the converging object provide information about its existence. The ability to sense a object is dependent on its material properties and size. In the case where we have a near perfect insulator and a very large size, the detectable range was on the same order as the separation distance between the electrodes. This agrees with observations that fish are able to detect distant objects up to their body length[Fer96].

CHAPTER 7

Conclusion and Future Work

In this thesis we explored the use of electrostatics for object and proximity detection, by developing a biomimetic sensor. This was complicated by the nature of electrostatics, as the phenomenon is described by a second order differential equation involving the applied voltage, current injected, and the varying spatial impedance properties of the material and space under inspection. While many uses have been found for electrical impedance sensing including use as a real-time lung volume monitoring, as in electrical impedance tomography or geological prospecting as in electrical resistive tomography, we proposed a novel sensor arrangement using a radially arranged current sensing electrodes that mimics the structure and function of weakly electric fish, and a linear sensor array comparable to sharks and skates.

For the linear sensor, we could identify the approximate position of the object laterally. While distance was difficult to predict, we showed that size, distance and material were all encoded in the output of the sensor. This sensor structure resembled the structure of the ampullae lorenzini, a tiny organelle that is sensitive to tiny adjacent voltage differences. We combined this ability with a signal generator to create an active form of adjacent voltage monitoring.

For the radial sensor array, each individual electrode was able to measure the *effective resistance* of its immediate environment, and from that information, when combined with other readings determine a vector towards the oncoming

object. The sensor itself was designed to act like the tuberous electroreceptors along the surface of the fish, and record the voltage potential arising *trans*-dermal, or in our case *trans*-shunt resistor. The entire sensor was built to be mobile and capable of exploring its environments via use of a robotic gantry.

We explored the modeling of our system using finite element analysis. Our modeling gave us insight into the effects of object size, object material composition, object distance and lateral position. This modeling then informed us of the expected capabilities of the sensor once implemented.

Finally, we showed that objects could be detected at a range on the same order as the separation distance between transmitter and electrode as we could sense on object at a distance of approximately 8 inches. The sensor separation was 12 inches.

In the future the platform can be used for exploring sensor fusion, that is combining the multiple channels to make more informed decisions about the environment. Additionally it is possible to use motion as a means of generating additional *views* of the environment, making mapping for easier navigation possible.

.1

Matlab Source for Electrostatic Tank Simulation Using Eidors

```
function [vd, vo1, vh1, electrode_nodes] = tanksim(c,r,x,y, name)
% tanksim utilized the Eidors tool set to simulate
% the voltage measurements for a rectangular tank
% with a 10 electride linear array

ELEC_COUNT = 10;
GND_ELEC_IDX = 10;
meter_per_in = 0.0254; % meters per inch
salt_water_conductivity = 0.305; % ohms_meter
tank_dims = [40,40]; % elements

tank_mdl =  mk_common_model('f2s',ELEC_COUNT);
e = size(tank_mdl.fwd_model.elems,1);

for ii = 1:length(tank_mdl.fwd_model.electrode)
    tank_mdl.fwd_model.electrode(ii).nodes = ii*2 + 10;
end

tank_mdl.fwd_model.gnd_node = ii*2 + 10;

tank_shape = [30,30]; % in
tank_shape = tank_shape * meter_per_in; % convert to meter

single_element_dim = tank_shape./tank_dims;
element_conductivity = salt_water_conductivity / single_element_dim(1);
bkgnd = element_conductivity;
fprintf('Conductivity of Water: %f', bkgnd);

img = mk_image(tank_mdl.fwd_model, bkgnd);


stim = mk_stim_patterns(ELEC_COUNT,1,'{mono}','{mono}',{},1);
img.fwd_model.stimulation = stim;
```

```
for i=1:ELEC_COUNT
    img.fwd_model.stimulation(i).stim_pattern = [1,zeros(1,ELEC_COUNT-2),-1]';
end
img.fwd_model.meas_select = [0 1];

img_h = img;
img_o = img;

select_fcn = inline(sprintf('(x+%f).^2+(y+%f).^2<%f^2', x, y, r),'x','y','z');
img_o.elem_data = (bkgnd*1+(c-bkgnd)*elem_select(img.fwd_model, select_fcn));

winsize = [ 0 0 800 600];
f = figure('Position',winsize);
axis tight

img_h.fwd_solve.get_all_meas = 1;
vh= fwd_solve(img_h);

img_o.fwd_solve.get_all_meas = 1;
vo= fwd_solve(img_o);

img_v = rmfield(img_o, 'elem_data');

% Show homoeneous image
a = subplot(231);
title(a,'Object Position');
show_fem(img_o);
axis tight

% Show inhomoeneous image
b = subplot(232);
show_current(img_o,vo.volt(:,1));
axis tight
title(b,'Current Path Tank');
axis([-1,1,-1,1]);

% Show difference image
b = subplot(233);
img_v.node_data = vh.volt(:,1) - vo.volt(:,1);
img_v.calc_colours.cb_shrink_move = [0.3,0.6,+0.03];
```

```
show_current(img_o,vh.volt(:,1)-vo.volt(:,1));
axis tight
title(b,'Change in Current Path');
axis([-1,1,-1,1]);
electrode_nodes = [img.fwd_model.electrode.nodes];
vd = abs(vh.volt(electrode_nodes,1) - vo.volt(electrode_nodes,1));
vh1 = vh.volt(electrode_nodes,1);
vh1d = diff(flipud(vh1));
vo1 = diff(flipud(vo.volt(electrode_nodes,1)));
title('Differential Current Image');
d= subplot(2,3,[4,5,6]);

bar(vo1-vh1d);
axis tight

vd = vo1-vh1d;

title(d,'Voltage Measured by Electrodes');
ylabel('Volts');
xlabel('Electrode ID#')
ylim([-5.5e-4 2.0e-4]);

fname = sprintf('%s-%dohm_m-rod%.2f-x%1.1f-y%1.1f',name,c,r,x,y);
fname = strrep(fname, '.', '_');
saveas(f,sprintf('%s.png',fname),'png');
end
```

.2 Hammer Head AFE

.2.1 Hammer Head Schematic

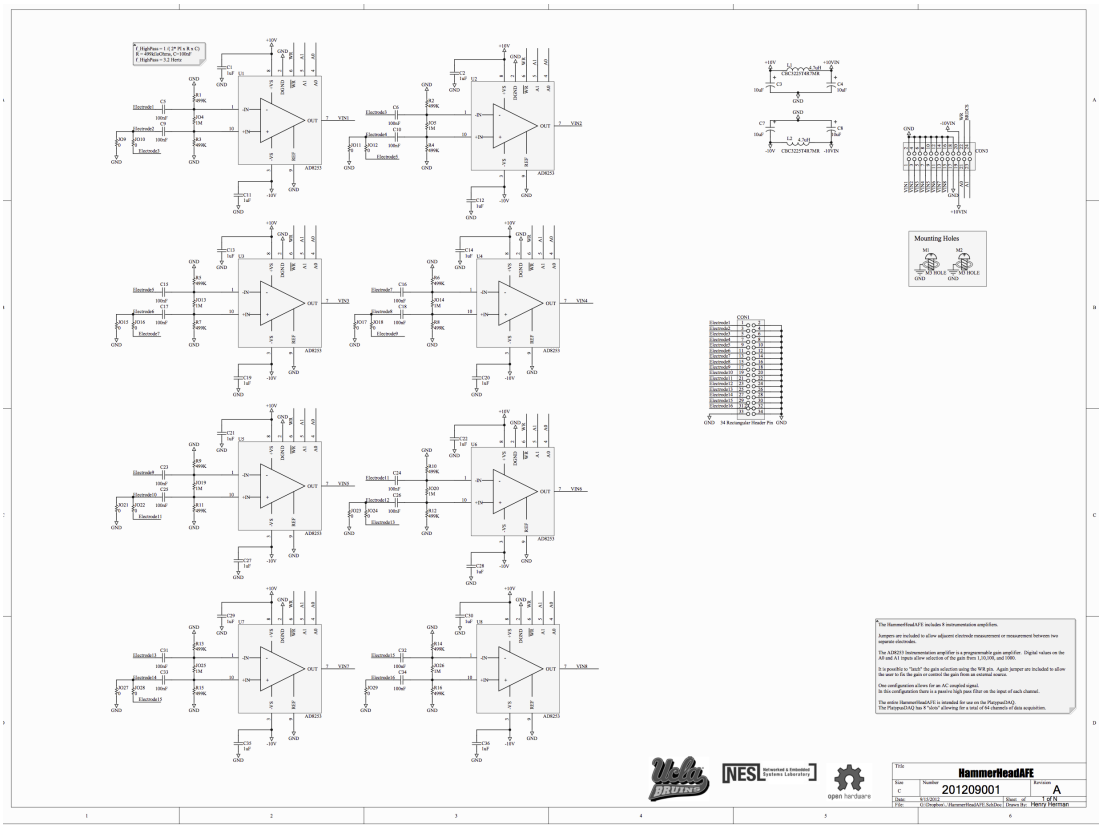

.2.2 Hammer Head Board Layout

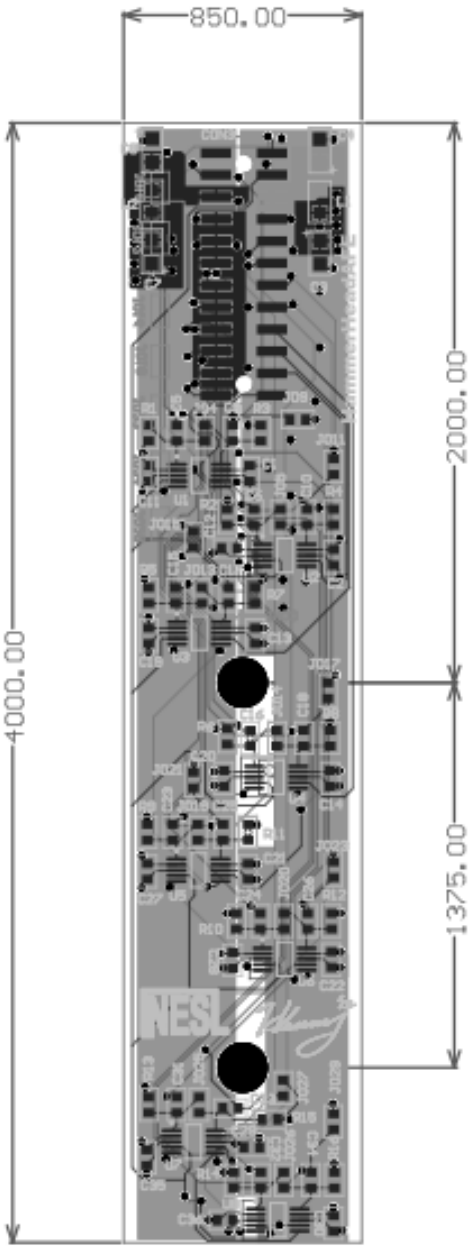

.3 BEI-68 Motherboard

.3.1 Back Plane

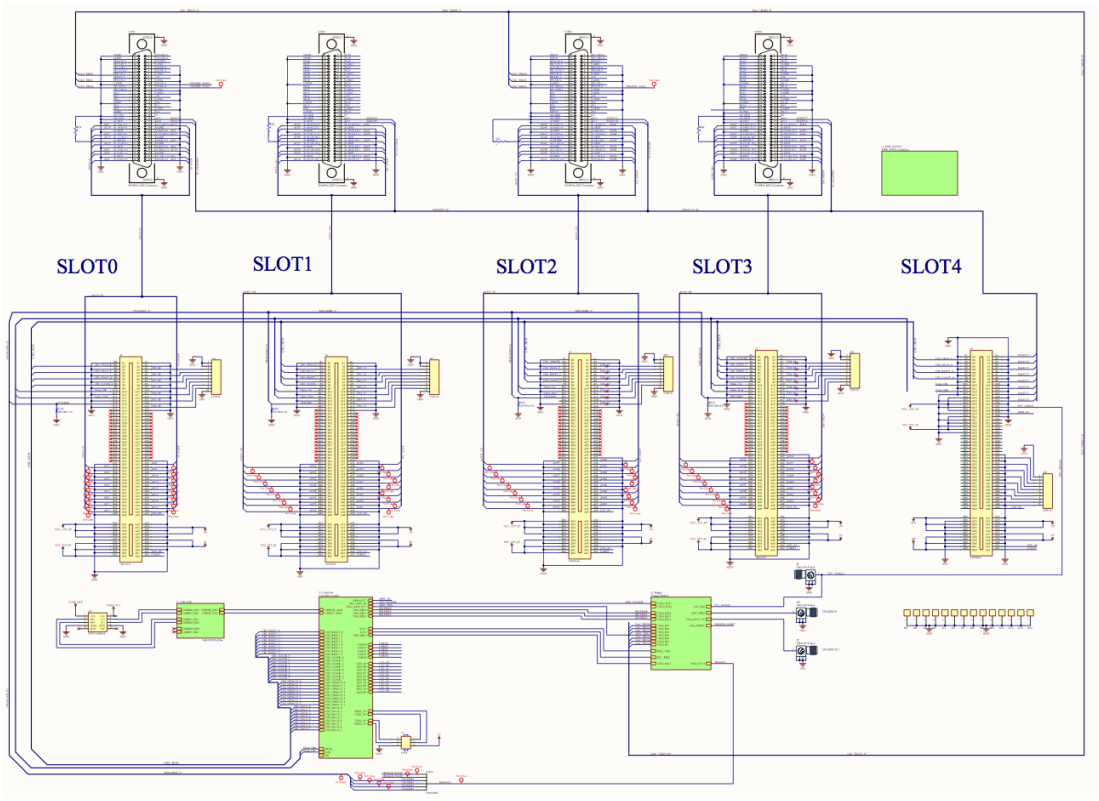

.3.2 Power Supply

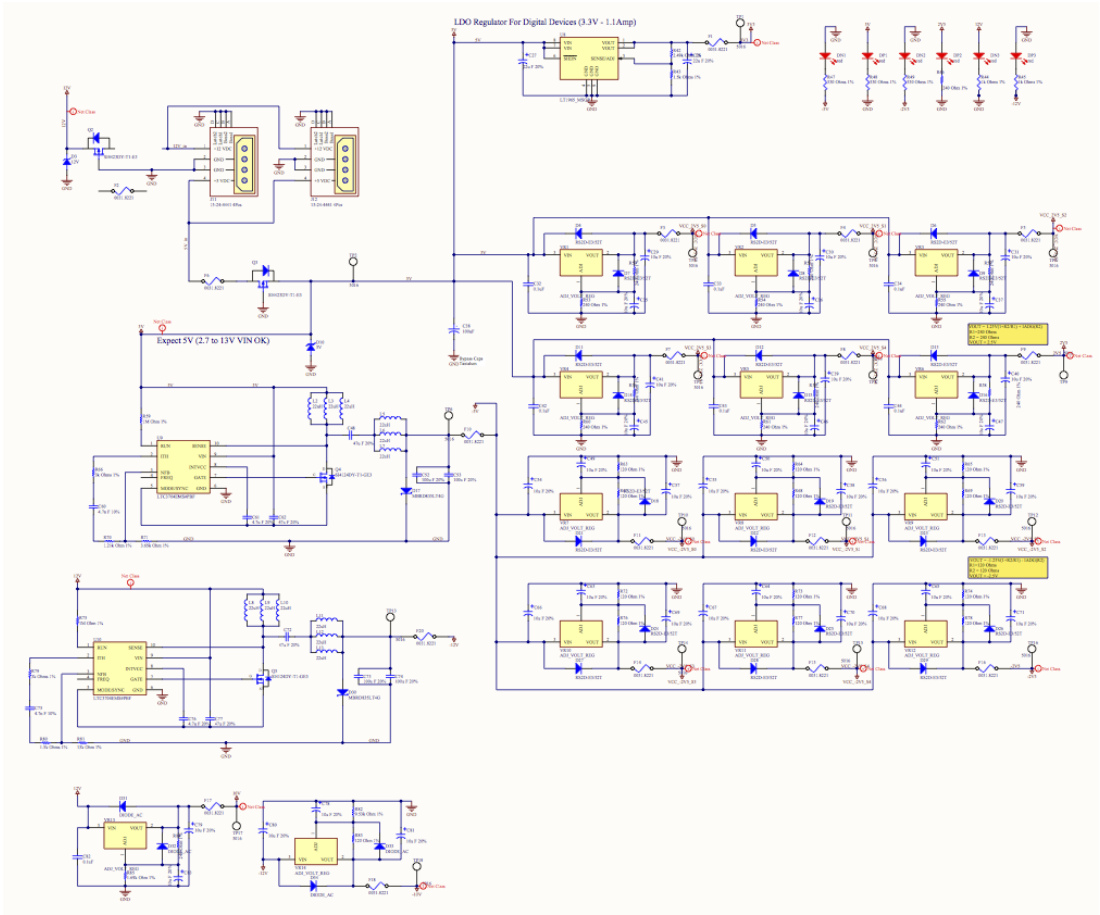

.3.3 Controller

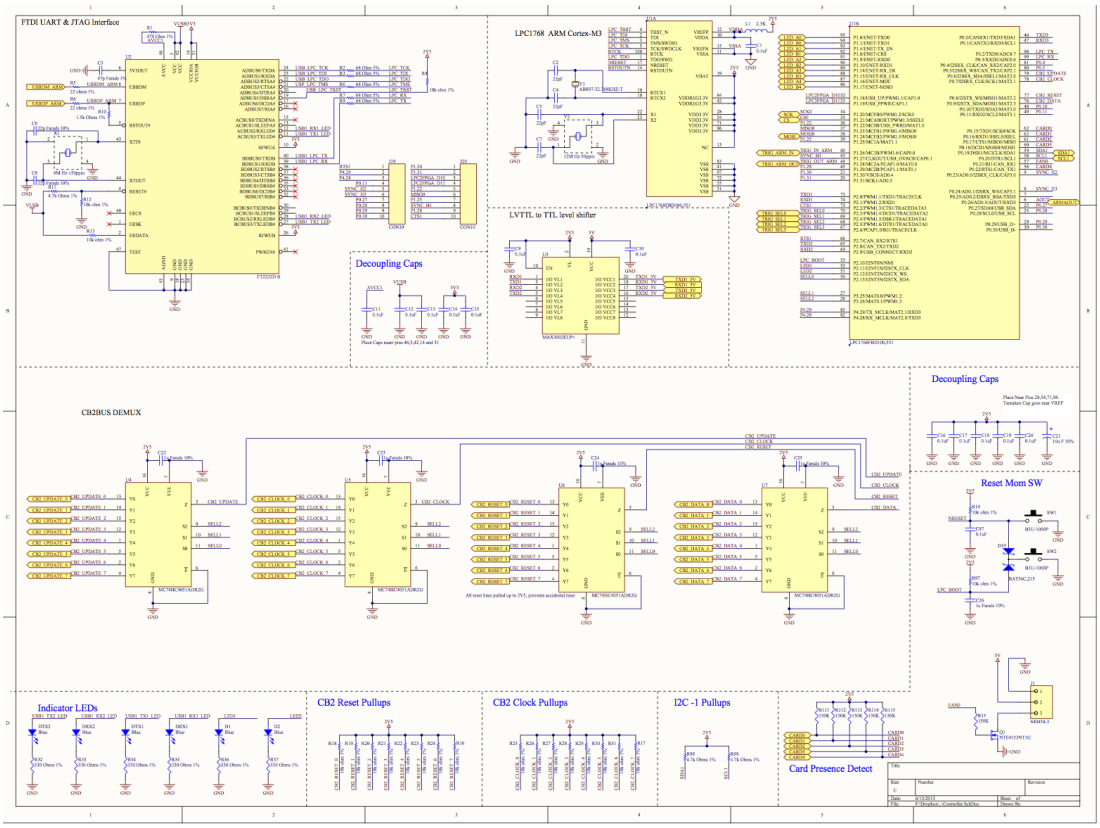

.3.4 USB Hub

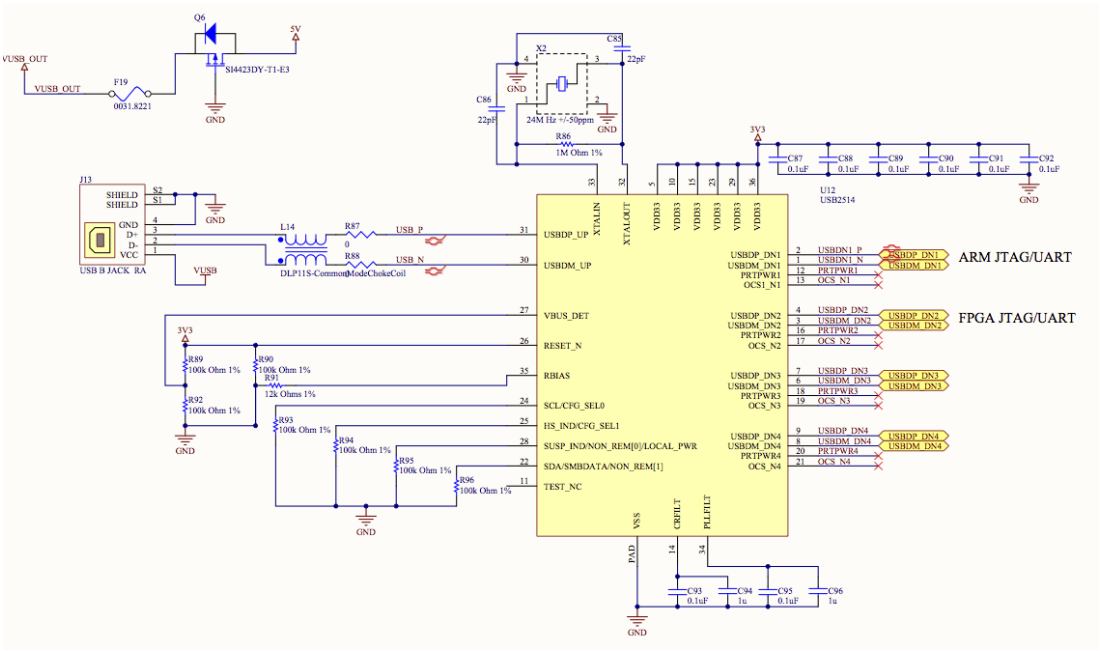
Q6
5V
SI4423DY-T1-E3
VUSB_OUT
F19
0031.8221
GND
X2
C85
22pF
C86
22pF
24M Hz +/-50ppm
R86
1M Ohm 1%
3V3
C87 0.1uF
C88 0.1uF
C89 0.1uF
C90 0.1uF
C91 0.1uF
C92 0.1uF
U12
USB2514
J13
SHIELD
SHIELD
GND
D+
D-
VCC
USB B JACK_RA
VUSB
L14
DLP11S-CommonModeChokeCoil
R87
0
R88
USB_P
USB_N
USBDP_UP
USBDM_UP
XTALIN
XTALOUT
VDD33
VBUS_DET
RESET_N
RBIAS
SCL/CFG_SEL0
HS_IND/CFG_SEL1
SUSP_IND/NON_REM[0]/LOCAL_PWR
SDA/SMBDATA/NON_REM[1]
TEST_NC
VSS
CRFILT
PLLFILT
PAD
R89 100k Ohm 1%
R90 100k Ohm 1%
R91 12k Ohms 1%
R92 100k Ohm 1%
R93 100k Ohm 1%
R94 100k Ohm 1%
R95 100k Ohm 1%
R96 100k Ohm 1%
C93 0.1uF
C94 1u
C95 0.1uF
C96 1u
USBDP_DN1
USBDM_DN1
PRTPWR1
OCS_N1
USBDN1_P
USBDN1_N
PRTPWR1
OCS_N1
USBDP_DN1
USBDM_DN1
ARM JTAG/UART
USBDP_DN2
USBDM_DN2
PRTPWR2
OCS_N2
FPGA JTAG/UART
USBDP_DN3
USBDM_DN3
PRTPWR3
OCS_N3
USBDP_DN4
USBDM_DN4
PRTPWR4
OCS_N4

References

[ASY09] Villanueva A., Bressers S., Tadesse Y., and Priya S. "Jellyfish inspired underwater unmanned vehicle." *Proc. SPIE*, p. 7287, 2009.

[BB84] D.C. Barber and Brown B.H. "Applied potential tomography." *J. Phys. E: Sci. Instrum*, **17**:723, 1984.

[Ben71] M.V.L. Bennett. "Electroreception." *W. S. Hoar and D. J. Randall: Fish Physiology*, **5**:493–574, 1971.

[Bla75] R Blakemore. "Magnetotactic bacteria." *Science*, **190**:377–379, 1975.

[Da92] W. Daily and et al. "Electrical resistivity tomography of vadose water movement." *Water Resources Research*, **28**(5):1429–1442, 1992.

[Fer96] C.J. Ferraris. *J.R. and Eschmeyer, W.N. Encyclopedia of Fishes*. Academic Press, San Diego, CA, 1996.

[Fie] S.Q. Field. "Listening to electric fish." `http://sci-toys.com/scitoys/scitoys/biology/electric_fish/electric_fish.html`. Accessed: 2013-05-10.

[Fri] J. Friedmann. "Locked in Rock: Sequestering Carbon Dioxide Underground." `https://www.llnl.gov/str/May05/Friedmann.html`. Accessed: 2013-05-10.

[Fri12] J Friedman. *Biomimetic Electrostatics for Submerged Oceanic Sensing, Communication, and Coordination*. PhD thesis, Universtiy of California, Los Angeles, June 2012.

[HW78] R.P. Hendersen and J.G. Webster. "An Impedance Camera for Spatially Specific Measurements of theThorax." *IEEE Transcations on Biomedical Engineering*, **25**:250–254, 1978.

[Kal58] A.J. Kalmjin. "Detection of weak electric fields." *Sensory Biology of Animals*, **9**:154–189, 1958.

[Kra96] B Kramer. *Electroreception and Communication in Fishes*. Gustav Fischer, Stuttgart, Germany, 1996.

[LM58] H.W Lissman and K.E. Machin. "The mechanism of object location in emphGymnarchus Niloticus and similar fish." *Journal of Experimental Biology*, **35**:451–486, 1958.

[MB81] J.G. Mather and R. R. Baker. "Magnetic sense of direction in woodmice for route-based navigation." *Nature*, **291**:152–155, 1981.

[Nee86] J Needham. *The Shorter Science and Civilisation in China*. Cambridge University Press, New York, 1986.

[Pa76] TJ Pitcher and et al. "A blind fish can school." *Science*, **194**:963–965, 1976.

[Pa12] S Philip and et al. "Fish Lateral Line Innovation Insights into the Evolutionary Genomic Dynamics of a Unique Mechanosensory Organ." *Molecular Biology and Evolution*, **29**:963–965, 2012.

[PL02] N Polydorides and WRB Lionheart. "A Matlab toolkit for three-dimensional electrical impedance tomography: a contribution to the Electrical Impedance and Diffuse Optical Reconstruction Software project." *Meas. Sci. Technol*, **13**:1871–1883, 2002.

[PS12] Semig P. and Wells S. "A Current Sensing Tutorial." *EE Times: Power Management*, 2012.

[SB00] RA Serway and RJ Beichner. *Physics for Scientist and Engineers*. Saunders College Publishing, Orlando, Florida, 2000.

[SB01] RA Serway and RJ Beichner. *Elementary Differential Equations and Boundary Value Problems*. John Wiley & Sons, Inc, New York, 2001.

[Smy89] WR Smythe. *Static and Dynamic Electricity*. Hemisphere Publishing Corp., New York, 1989.

[SS09] R Smith and D Sjogen. "An evaluation of electrical resistivity imaging (ERI) in Quaternary sediments, southern Alberta, Canada." *Geological Society of America Bulletin*, **121**:1570–1583, 2009.

[Tik63] A. N. Tikhonov. "Solution of incorrectly formulated problems and the regularization method." *Soviet Mathematics*, **4**:10351038, 1963.

[Wal96] C Walcott. "Pigeon homing: observations, experiments and confusions." *The Journal of experimental biology*, **199**:21–27, 1996.